



401 N. Lindbergh Blvd.  
St. Louis, MO 63141  
Tel.: 314.993.1700, #546  
Toll Free: 800.424.2841, #546  
Fax: 800.708.1364  
Cell: 314.283.1983

Send via email to: [jbode@aaortho.org](mailto:jbode@aaortho.org) and [cyoung@aaortho.org](mailto:cyoung@aaortho.org)

## AAO Foundation Final Report Form (a/o 6/30/2022)

Type of Award: Biomedical Research Award (Burstone-Indiana Biomechanics Award)

Name(s) of Principal Investigator(s): Do-Gyoon Kim

Institution: The Ohio State University

Title of Project: Site-specific postmenopausal characteristics of jaw bone

Period of AAOF Support: 07-01-20 to 06-30-22

Amount of Funding: \$30000

Summary/Abstract

**The work has been published and the pdfs of 3 manuscripts are attached.**

Respond to the following questions:

1. Were the original, specific aims of the proposal realized? Yes
2. Were the results published? Yes. 3 full peer reviewed papers
  - a. If so, cite reference/s for publication/s including titles, dates, author or co-authors, journal, issue and page numbers:

Jie Liu, Keiichiro Watanabe, Shareef Dabdoub, Beth S. Lee, **Do-Gyoon Kim**. Site-specific characteristics of bone and progenitor cells in control and ovariectomized rats. *Bone*. 2022 Jul 21;116501

Liu J, Kim EK, Ni A, Kim YR, Zheng F, Lee BS, **Kim DG**. Multiscale characterization of ovariectomized rat femur. *Journal of Biomechanics*. 2021 Jun 9;122:110462

Keiichiro Watanabe, Samantha Lewis, Xiaohan Guo, Ai Ni, Beth S. Lee, Toru Deguchi, **Do-Gyoon Kim**. "Regional variations of jaw bone characteristics in an ovariectomized rat model." *Journal of the Mechanical Behavior of Biomedical Materials*. 2020 Oct;110:103952.

- b. Was AAOF support acknowledged? Yes
  - c. If not, are there plans to publish? If not, why not? N/A
3. Have the results of this proposal been presented? Yes
- a. If so, list titles, author or co-authors of these presentation/s, year and locations

Jie Liu, Keiichiro Watanabe, Ching-Chang Ko, Beth S. Lee, Myon Hee Lee, **Do-Gyoon Kim**, “Effects of Estrogen Deficiency on Jaw and Limb Bones in a Rat Model.” *Trans. of Orthopaedic Res. Society, Vol. 46, p.1587LB, 2021.*

Keiichiro Watanabe, Samantha Lewis, Ai Ni, Toru Deguchi, Beth Lee, **Do-Gyoon Kim**, “Masticatory Effects on Regional Variation of Estrogen Deficient Rat Jaw Bone Density.” *Trans. of Orthopaedic Res. Society, Vol. 45, p.1678, 2020.*

- b. Was AAOF support acknowledged? Yes
  - c. If not, are there plans to do so? If not, why not?
4. To what extent have you used, or how do you intend to use, AAOF funding to further your career?

The results from this project will be used as the preliminary results to submit multiple NIH proposals.

Accounting for Project; i.e., any leftover funds, etc.

Object Class	Budget	Expended	Committed	Balance
Salaries and Wages	\$6,640.00	\$6,204.90	\$0.00	\$435.10
Fringe Benefits	\$2,360.00	\$1,703.37	\$0.00	\$656.63
Materials and Supplies	\$10,000.00	\$5,630.00	\$39.13	\$4,330.87
Purchased Services	\$0.00	\$12,061.69	\$0.00	(\$12,061.69)
Animal Expenditures	\$0.00	\$2,877.28	\$0.00	(\$2,877.28)
Other Direct Costs	\$11,000.00	\$369.05	\$0.00	\$10,630.95
Facilities & Administration	\$0.00	\$0.00	\$0.00	\$0.00
<b>Direct Total</b>	<b>\$30,000.00</b>	<b>\$28,855.84</b>	<b>\$39.13</b>	<b>\$1,105.03</b>
<b>Direct + Indirect Total</b>	<b>\$30,000.00</b>	<b>\$28,855.84</b>	<b>\$39.13</b>	<b>\$1,105.03</b>

## Journal Pre-proof

Site-specific characteristics of bone and progenitor cells in control and ovariectomized rats

Jie Liu, Keiichiro Watanabe, Shareef Dabdoub, Beth S. Lee, Do-Gyoon Kim



PII: S8756-3282(22)00178-8

DOI: <https://doi.org/10.1016/j.bone.2022.116501>

Reference: BON 116501

To appear in: *Bone*

Received date: 18 March 2022

Revised date: 11 July 2022

Accepted date: 18 July 2022

Please cite this article as: J. Liu, K. Watanabe, S. Dabdoub, et al., Site-specific characteristics of bone and progenitor cells in control and ovariectomized rats, *Bone* (2022), <https://doi.org/10.1016/j.bone.2022.116501>

This is a PDF file of an article that has undergone enhancements after acceptance, such as the addition of a cover page and metadata, and formatting for readability, but it is not yet the definitive version of record. This version will undergo additional copyediting, typesetting and review before it is published in its final form, but we are providing this version to give early visibility of the article. Please note that, during the production process, errors may be discovered which could affect the content, and all legal disclaimers that apply to the journal pertain.

© 2022 Published by Elsevier Inc.

Original Articles

## Site-specific characteristics of bone and progenitor cells in control and ovariectomized rats

Jie Liu <sup>a\*</sup>, Keiichiro Watanabe <sup>a\*</sup>, Shareef Dabdoub <sup>b</sup>, Beth S. Lee <sup>c\*\*</sup>, Do-Gyoon Kim <sup>a\*\*</sup>

<sup>a</sup> Division of Orthodontics, College of Dentistry, The Ohio State University, Columbus, OH 43210, USA

<sup>b</sup> Division of Biostatistics and Computational Biology, Department of Periodontics, College of Dentistry and Dental Clinics, The University of Iowa, Iowa City, IA 52242, USA

<sup>c</sup> Department of Physiology and Cell Biology, College of Medicine, The Ohio State University, Columbus, OH 43210, USA

\* Equal contribution

\*\* Equal contribution

For correspondence:

Do-Gyoon Kim, Ph.D.  
Professor, Division of Orthodontics,  
College of Dentistry  
The Ohio State University  
4088 Postle Hall  
305 W. 12<sup>th</sup> Ave  
Columbus, OH 43210, USA  
Email: kim.2508@osu.edu  
Tel: (614) 247-8089  
Fax: (614) 688-3077

Resubmitted to Bone (July 8, 2022)

**Abstract**

One-third of postmenopausal women experience at least one osteoporotic bone fracture in their lifetime that occurs spontaneously or from low-impact events. However, osteoporosis-associated jaw bone fractures are extremely rare. It was also observed that jaw bone marrow stem cells (BMSCs) have a higher capacity to form mineralized tissues than limb BMSCs. At present, the underlying causes and mechanisms of variations between jaw bone and limb bone during postmenopause are largely unknown. Thus, the objective of the current study was to examine the site-specific effects of estrogen deficiency using comprehensive analysis of bone quantity and quality, and its association with characterization of cellular components of bone. Nine rats (female, 6 months old) for each bilateral sham and ovariectomy (OVX) surgery were obtained and maintained for 2 months after surgery. A hemi-mandible and a femur from each rat were characterized for parameters of volume, mineral density, cortical and trabecular morphology, and static and dynamic mechanical analysis. Another set of 5 rats (female, 9 months old) was obtained for assays of BMSCs. Following cytometry to identify BMSCs, bioassays for proliferation, and osteogenic, adipogenic, chondrogenic differentiation, and cell mitochondrial stress tests were performed. In addition, mRNA expression of BMSCs was analyzed. OVX decreased bone quantity and quality (mineral content, morphology, and energy dissipation) of femur while those of mandible were not influenced. Cellular assays demonstrated that mandible BMSCs showed greater differentiation than femur BMSCs. Gene ontology pathway analysis indicated that the mandibular BMSCs showed most significant differential expression of genes in the regulatory pathways of osteoblast differentiation, SMAD signaling, cartilage development, and glucose transmembrane

transporter activity. These findings suggested that active mandibular BMSCs maintain bone formation and mineralization by balancing the rapid bone resorption caused by estrogen deficiency. These characteristics likely help reduce the risk of osteoporotic fracture in postmenopausal jawbone.

**Keywords:** Site-specific characteristics, OVX, Tissue mineral density, Dynamic mechanical analysis, Nanoindentation, Bone marrow stem cells

Journal Pre-proof

## 1. Introduction

Osteoporosis is a common and severe metabolic bone disease, afflicting more than 10 million individuals in the U.S, leading to about 1.5 million osteoporotic fractures per year<sup>1-3</sup>. The postmenopausal female population is at a particularly higher risk for fracture than other age groups and the male population<sup>2,4,5</sup>. Although bone mineral density (BMD) has been used to diagnose osteoporosis following World Health Organization (WHO) criteria<sup>6,7</sup>, a direct evidence of osteoporosis is fracture without significant trauma<sup>3,8</sup>. Postmenopausal women from 50 years of age onward have twice the lifetime risk of osteoporotic fracture in vertebrae and limbs compared with men at the same age<sup>3,9</sup>. In contrast, atraumatic fracture of the jaw bone is extremely rare (about 2% of all mandibular fractures), and the majority of these can be attributed to underlying pathological conditions such as inflammation, cysts, benign tumors, or malignancies<sup>10</sup>. These clinical observations indicate that postmenopausal osteoporosis may be a site-specific bone disease affecting vertebral and limb bones more severely than jaw bone.

Ovariectomized (OVX) animal models have been widely used to investigate the etiology of postmenopausal osteoporosis resulting from estrogen deficiency, and the OVX rat model in particular is approved by the Food and Drug Administration (FDA) for investigation of new therapeutic agents for osteoporosis<sup>8,11-13</sup>. While a great volume of studies has shown the substantial effects of estrogen deficiency on vertebral and limb bones of the OVX rat model, its effects on jaw bone have not been fully clarified. There exist a few studies that compared the estrogen deficient effects on jaw bone with those on bones in other anatomical sites<sup>11,14-16</sup>. These studies from different research groups consistently showed that BMD and trabecular morphology of jaw are significantly less

affected than those of vertebra and limb. In fact, all of the previous studies that investigated jaw BMD of OVX rat models showed no decrease or less than 10% decrease of mandibular BMD relative to the control sham group<sup>17</sup>. However, at present, the underlying causes and mechanisms of variations between jaw bone and limb bone during postmenopause are largely unknown.

The postmenopausal bone loss due to estrogen deficiency arising from menopause results in increased bone turnover in which bone resorption by osteoclasts outpaces bone formation by osteoblasts<sup>3,4</sup>. While osteoclasts develop from the systemic hematopoietic lineage<sup>3,18</sup>, osteoblasts arise from site-specific local bone marrow mesenchymal stem cells (BMSCs). *In vitro*, human and animal jaw BMSCs show significantly higher osteogenic potential than limb BMSCs, including amplified osteoblast gene expression, enhanced cell activities, and higher mineralization<sup>19-22</sup>. Thus, we hypothesize that greater osteogenic differentiation of BMSCs in the jaw bone is responsible for its lower risk of fracture due to aging and estrogen deficiency-induced osteoporosis than in the limb bone. The objective of the current study was to examine the site-specific effects of estrogen deficiency using comprehensive analysis of bone quantity and quality, and its association with characterization of cellular components of bone.

## **2. Materials and Methods**

### **2.1 Specimen preparation**

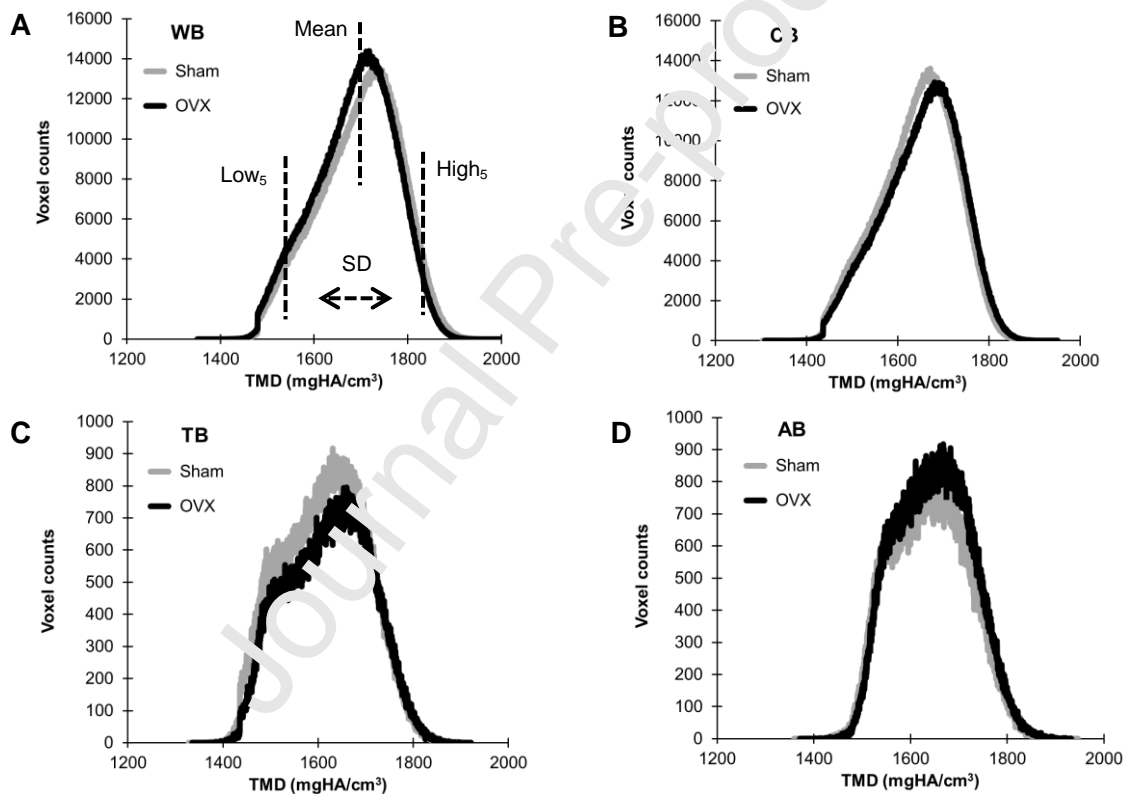
Eighteen Sprague-Dawley rats (female, 6 months old) were obtained following the protocol approved by the Institutional Animal Care and Use Committee (IACUC) of The Ohio State University. Nine rats were purchased for each bilateral sham and ovariectomy

(OVX) surgery, which were operated at Harlan Laboratories (Harlan Laboratories Inc, Indianapolis, IN, USA). The rats were transferred to OSU 5 days post-surgery, then were maintained with normal experimental animal care (12 hours dark-light cycles and standard rat chow) in ULAR (University Laboratory Animal Resources) for 2 months after surgery. The animals were euthanized by intraperitoneal injection of an overdose of pentobarbital sodium (100 mg/kg). A hemi-mandible and a femur were randomly dissected from each rat. After removal of soft tissues, the mandibles and femurs were wrapped in normal saline-soaked gauze and stored at -20°C until use. Another set of 5 Sprague-Dawley rats (female, 9 months old) was obtained from Charles River Laboratory (Wilmington, MA). After 7 days of acclimation under normal animal care, these rats were used for assays of BMSCs as described below.

## 2.2 Micro-computed tomography (micro-CT)

The specimens of mandible and femur (n=9 for each site) were thawed at a room temperature and scanned by micro-CT (Skyscan 1172-D, Kontich, Belgium) with 20×20×20  $\mu\text{m}^3$  voxel size (70 kVp, 142  $\mu\text{A}$ , 0.4° rotation per projection, 8 frames averaged per projection, and 40 ms exposure time) and with 27×27×27  $\mu\text{m}^3$  voxel size (70 kVp, 142  $\mu\text{A}$ , 0.4° rotation per projection, 6 frames averaged per projection, and 210 ms exposure time), respectively. The region of interest in the images of mandible were isolated by digitally cutting the mandible in the bucco-lingual direction using Image J software (NIH) (Supplementary Figs. 1-4). The teeth and periodontal ligament (PDL) were digitally extracted. Whole bone (WB) voxels in the images of mandible and femur were segmented from non-bone voxels using a heuristic algorithm as used in previous

studies (Supplementary Figs. 1 and 2) <sup>23-25</sup>. A bone volume (BV) of WB region was computed by multiplying the total count of segmented bone voxels by the voxel volume. A total volume (TV) was the sum of voxels inside bone surface including bone and marrow cavity after removing all non-bone voxels outside. A bone fraction (BV/TV) was also computed. Cortical bone (CB) regions were separated by subtracting masked regions of the trabeculae and marrow cavity from TV (Supplementary Figs. 1 and 2) using a compartmentalizing method <sup>23,24,26</sup>. Trabecular bone (TB) regions were obtained by



excluding the CB from the WB.

**Fig. 1** Mandibular tissue mineral density (TMD) parameters were determined in individual histograms of typical (A) whole bone (WB), (B) cortical bone (CB), (C) trabecular bone (TB), and (D) alveolar bone (AB) for sham and OVX groups.

A gray level of each bone voxel was converted to a value of tissue mineral density (TMD) using a calibration curve between the gray levels and known densities of commercial hydroxyapatite (HA) phantoms (1220 and 1540 mgHA/cm<sup>3</sup> with the same dimension of  $\varnothing 4 \times 5.5$  mm) that were provided by the micro-CT company. A total sum of TMDs in the WB was total mineral content (TMC). Then, bone mineral density (BMD) was obtained by dividing the TMC by the TV. A mean and a standard deviation (SD) of TMD histogram were computed for each region (Figs. 1 and 2A-D). Low and high TMD (Low<sub>5</sub> and High<sub>5</sub>) values were determined using lower and upper 5th percentile values of TMD histogram, respectively (Fig. 1A).

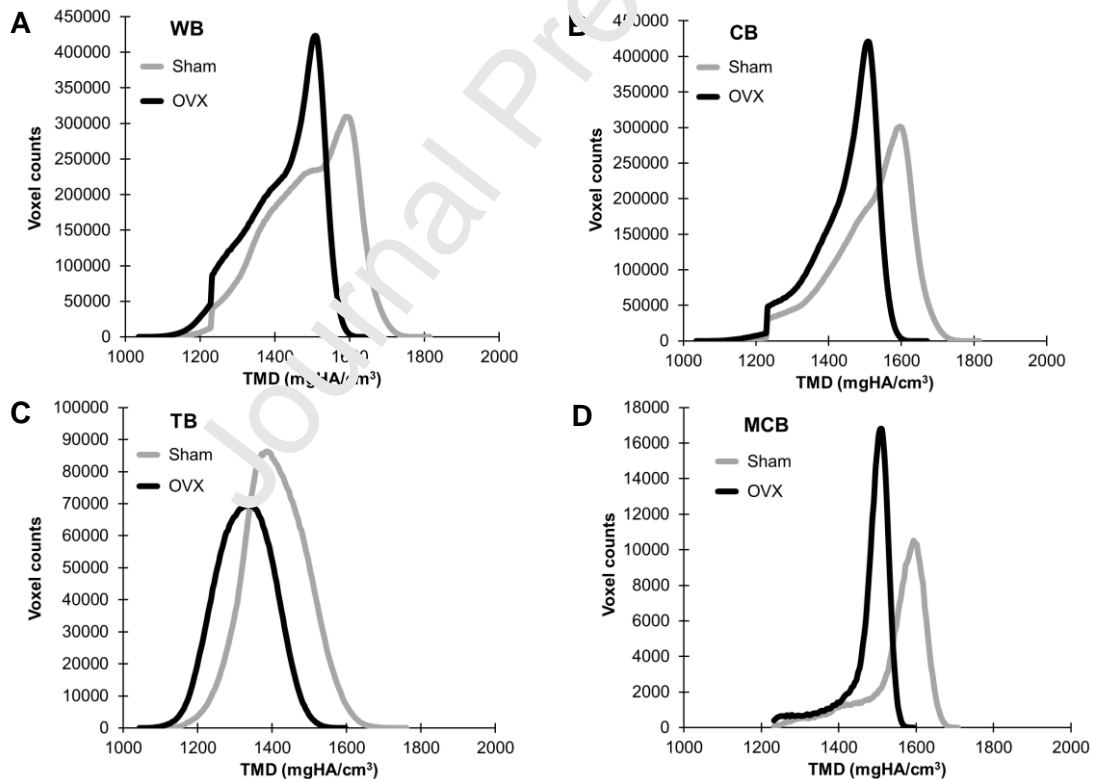


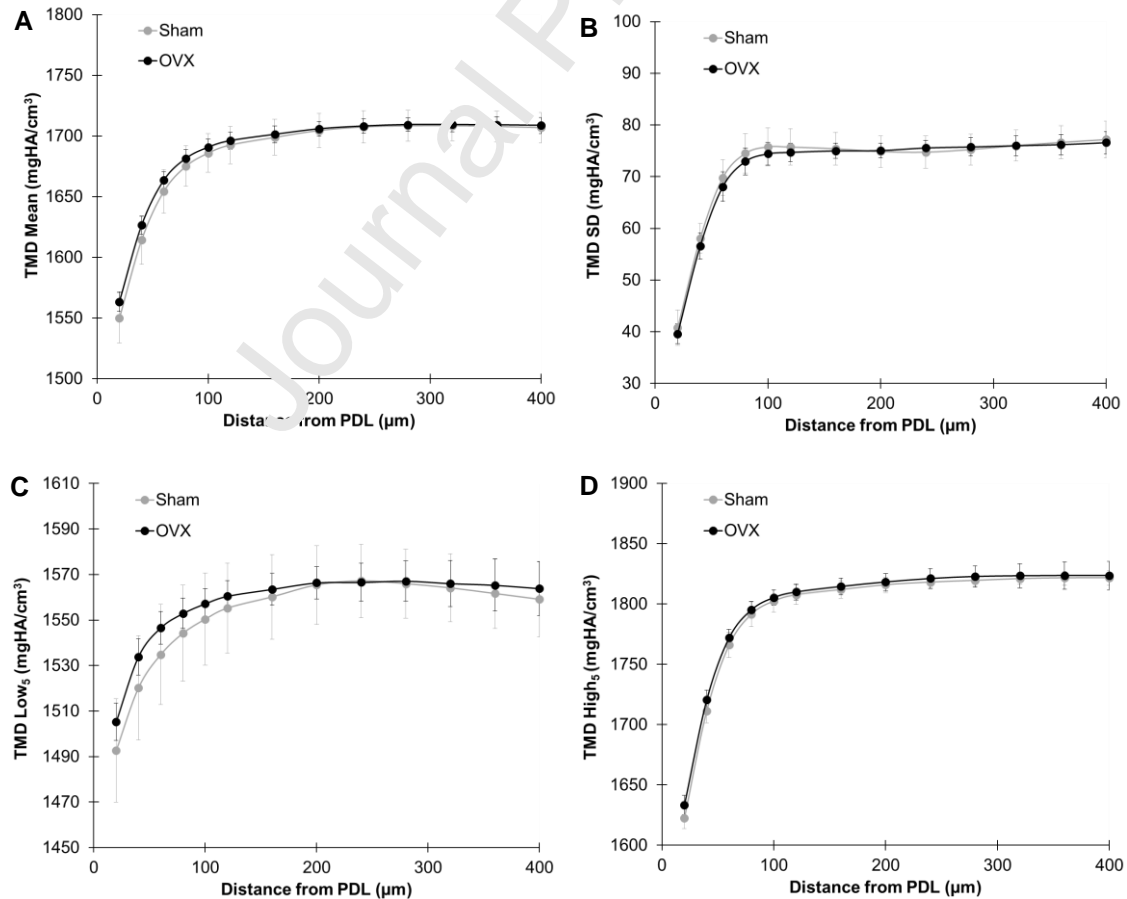
**Fig. 2** Femoral TMD parameters were determined in individual histograms of (A) typical whole bone (WB), (B) cortical bone (CB), (C) trabecular bone (TB), and (D) Marginal cortical bone (MCB) for sham and OVX groups.

The femur image was rotated in the axial direction without disturbing gray levels of voxels using DataViewer software (Bruker, Kontich, Belgium). Then, a femoral length (Length) was measured by counting axial slices from femoral head to distal end. A region centered at 55% (CB<sub>55</sub>) of the femoral length from the head was digitally cut with 50 voxels (1 mm) thickness. This region was the corresponding location at which 3-point bending load was applied in the previous and current studies<sup>24,27</sup>. Thus, morphological parameters of CB, which are associated with bending, were assessed at CB<sub>55</sub> (Supplementary Table 1). The parameters of CB<sub>55</sub> included cortex bone volume (BV<sub>55</sub>), total volume (TV<sub>55</sub>), fraction (BV<sub>55</sub>/TV<sub>55</sub>), thickness (Ct.Th), periosteal perimeter (Perimeter55), outer and inner diameters of anterior-posterior axis and medial-lateral axis (D<sub>AP\_outer</sub>, D<sub>AP\_inner</sub>, D<sub>ML\_outer</sub>, and D<sub>ML\_inner</sub>), outer diameter ratio (AP/ML), and minimum inertia (I<sub>min</sub>).

Architectural parameters of TB were determined at the region between molar roots and incisor of mandible and above growth plates at the distal condyle of femur. The dimension of the TB region of interest for mandible (0.64×0.64×0.64 mm<sup>3</sup>) and femur (0.97×0.97×2.03 mm<sup>3</sup>) were identical between rats. The traditional morphological parameters of TB were measured including trabecular bone fraction (BV/TV<sub>TB</sub>), surface-to-volume ratio (BS/BV), number (Tb.N), thickness (Tb.Th), and separation (Tb.Sp) using a morphological code (CTAn, Bruker, Kontich, Belgium). In addition, the PDL

between teeth and alveolar bone (AB) was isolated to measure the mean, standard deviation (SD), maximum (Max), and minimum (Min) of PDL thickness using the local thickness function of Image J software (NIH).

As parts of the CB in the mandible and femur, the AB was identified up to 100  $\mu\text{m}$  from the PDL and marginal cortical bone (MCB) was isolated within 162  $\mu\text{m}$  (6 voxels) from both endosteal and periosteal surfaces at CB<sub>55</sub> (Supplementary Figs. 1 and 2). For the AB region, bone voxel layers were determined with one-voxel thickness at 0-120  $\mu\text{m}$  from the PDL or with two-voxel thickness at 120-400  $\mu\text{m}$  from the PDL (Supplementary Fig. 3) and for the MCB region, one-voxel thickness from periosteum to endosteum (Supplementary Fig. 4). The TMD parameters were obtained for the AB, MCB and each



layer (Figs. 3 and 4A-D).

**Fig. 3** (A) Mean, (B) SD, (C) Low<sub>5</sub>, and (D) High<sub>5</sub> of issue mineral density (TMD) were measured at each layer from the periodontal ligament (PDL). The TMD values rapidly increased up to 60  $\mu\text{m}$  from the PDL. The mean values of all TMD parameters were not significantly different between sham and OVX groups ( $p > 0.08$ ).

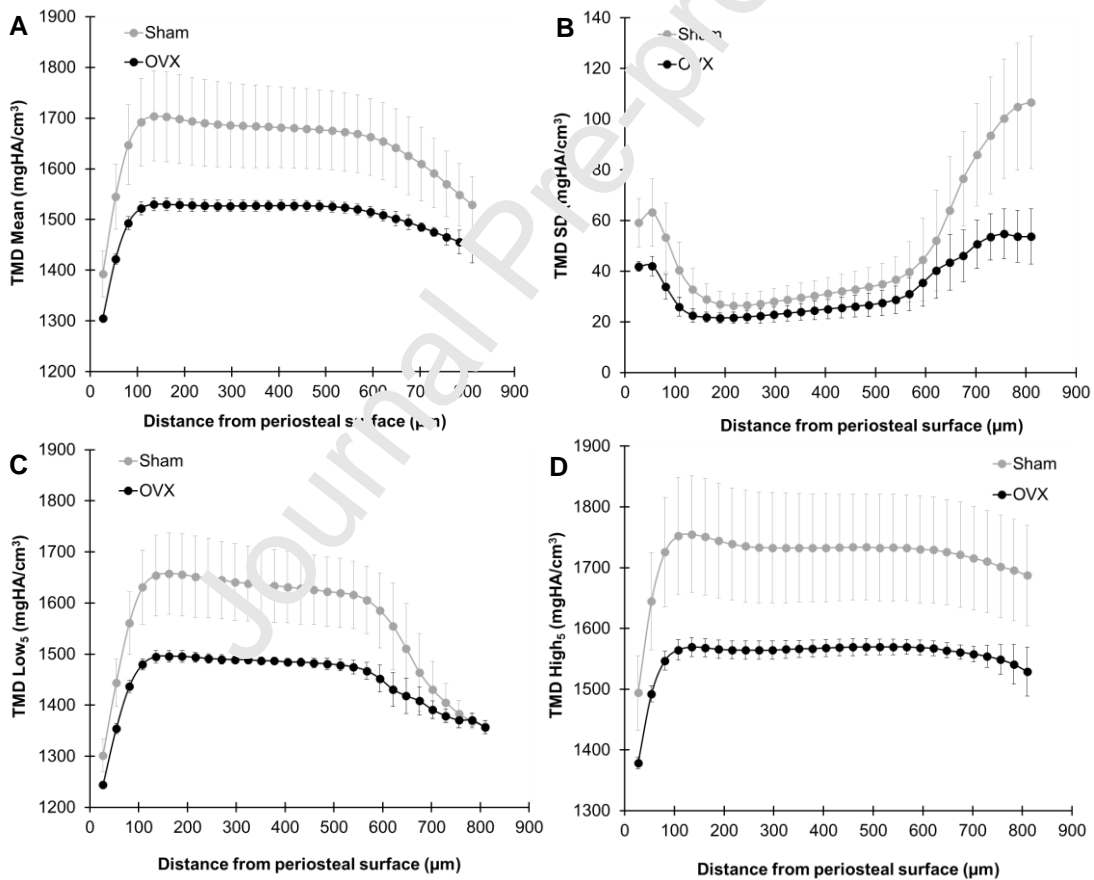
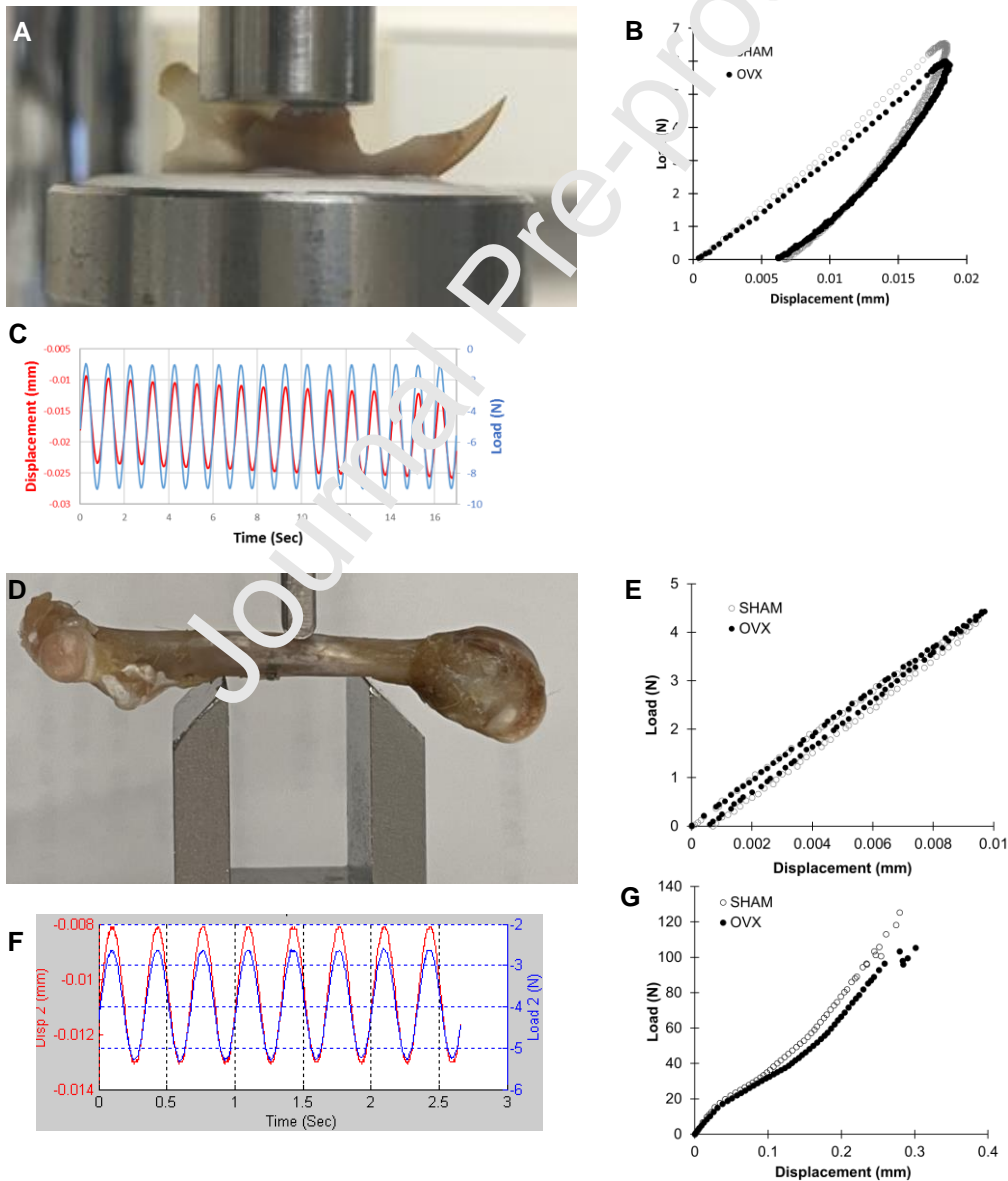


**Fig. 4** (A) Mean, (B) SD, (C) Low<sub>5</sub>, and (D) High<sub>5</sub> of tissue mineral density (TMD) were measured at each layer from periosteal surface. The TMD values rapidly increased up to

81  $\mu\text{m}$  from periosteal surface. Most of the TMD parameters had significantly lower values for the OVX group than the sham group ( $p < 0.041$ ).

### 2.3 Dynamic mechanical analysis (DMA)

After scanning using the non-destructive micro-CT, all specimens were prepared for mechanical testing. The hemi-mandibles ( $n=7$  for each group) were mounted in a loading jig by potting up to incisor height in the vertical direction with low expansion fast setting



mounting plaster in 5 min setting time (Whip Mix, Louisville, KY) (Fig. 5A).

**Fig. 5** (A) A hemi-mandibular specimen on compressive static mechanical and dynamic mechanical analysis (DMA) and (D) a femur specimen on 3-point bending at 55% of length from the femoral head, (B) higher hysteresis (W) due to larger energy loss of the periodontal ligament (PDL) in mandible (E) than that in femur under non-destructive static loading, and an example of DMA signals (C) under cyclic compressive loading ( $-5 \pm 4$  N) for mandible and (F) bending displacement ( $-0.01 \pm 0.005$  mm) for femur, and (G) typical static fracture curves for femurs of sham and OVX groups.

The top surface of molars was positioned parallel to the upper loading jig. Then, the hemi-mandible was loaded using an electromagnetic loading machine (Bose Corporation, Framingham, MA, USA) equipped with the load cells at the ranges of capacity between  $\pm 45$ N and  $\pm 450$ N, and a high resolution (15 nm) displacement transducer. Contacts between the regular surface of molar crown and the flat upper loading jig were achieved by filling with dental composite (Ultra Band-lok, Reliance Orthodontic Products) to confirm a uniform loading distribution on the entire molars. The femurs (n=9 for each group) were compressed in the anterior-posterior direction using a 3-point bending jig with 15 mm span length (Fig. 5D). The loading point was determined at 55% length of the femur from the femoral head. The specimens were moisturized with phosphate buffered saline (PBS)-soaked paper towels for the entire period of preparation and mechanical testing.

Static and dynamic mechanical testing were conducted following the protocols established in previous studies<sup>24,28,29</sup>. The preloads of 2 N and 10 N were applied to confirm contact between the specimen and loading jig for the hemi-mandible and femur, respectively. Non-destructive displacements up to 0.02 mm for the hemi-mandible and 0.01 mm for the femur were loaded and unloaded to the original position (Fig. 5B,E). A static stiffness was measured using a slope of the static load-displacement curve and a hysteresis (W) was computed by subtracting unloading energy from loading energy accounting for amount of energy loss during loading. Dynamic mechanical analysis (DMA) for the hemi-mandible utilized non-destructive compressive oscillatory force ( $-5\pm 4\text{N}$ ) at 1, 2 and 3 Hz (Fig. 5C) to simulate the frequency of chewing from 0.94 to 2.17 Hz<sup>30</sup>. DMA for the femur used non-destructive bending oscillatory displacements ( $0.01\pm 0.005\text{ mm}$ ) at 0.5, 1, 2, and 3 Hz (Fig. 5F). Dynamic complex ( $K^*$ ), elastic (storage) ( $K'$ ), and viscous (loss) ( $K''$ ) stiffness could be assessed by an equation of  $K^* = K' + iK''$ . Tangent delta ( $\tan \delta$ ) accounted for energy dissipation ability was computed using a relationship of  $K''/K'$ . The phase shift ( $\delta$ ) between cyclic load and displacement was obtained as a function of time. The averaged values of DMA parameters at each frequency were compared. Following the non-destructive DMA testing, the same femur was loaded at a bending displacement rate of 0.5 mm/second up to fracture. Maximum force ( $F_{\max}$ ) and displacement ( $d_{\max}$ ) were assessed and toughness (U) was computed as the area under the load-displacement curve up to the maximum point.

#### 2.4 Cell isolation and culture

Unless otherwise specified, chemicals for biological assays were obtained from Sigma-Aldrich or ThermoFisher. For culture of BMSCs, 5 female Sprague-Dawley rats (9-month age) were purchased from the Charles River Laboratory following the IACUC protocol. They were maintained in a temperature-controlled room with a 12-hour alternating light-dark cycle and were fed a standard laboratory diet. Immediately after euthanasia, a hemi-mandible and femur from one side of each rat were harvested for cell isolation. Briefly, BMSCs from limb bones were obtained by removing all soft tissues of femurs and cutting the ends, then performing repeated flushing of the bones with culture medium. BMSCs from mandibles were obtained by dissecting mandibles, removing all soft tissues and incisor to exposure the bone marrow, then the bone contained marrow was cut into small pieces and digested in a solution of 3 mg/ml collagenase type I (Worthington-Biochemical) and 4 mg/ml dispase II (Worthington-Biochemical) for 30-60 min at 37°C to release cells. Following collection, both mandibular and limb bone cells were filtered through a 70 µm mesh and cultured in 6-well plates in  $\alpha$ -minimum essential medium ( $\alpha$ -MEM; Life Technologies/GIBCO BRL) supplemented with 10% fetal bovine serum (FBS; Atlanta Biologicals), 2 mM L-glutamine, 100 mM L-ascorbic acid-2-phosphate, and antibiotic agents; and maintained under 5% CO<sub>2</sub> at 37°C. After 3 days, non-adherent cells were removed, and medium was changed every 3-4 days until near-confluence. These heterogeneous population of BMSCs isolated from each rat were grown separately without mixing cells from different rats. Cells used for experimentation were at passage 1-3<sup>31,32</sup>.

## 2.5 Flow Cytometry

Sub-confluent passage 1 BMSCs from femur and mandible were harvested for analysis and assessed for expression of CD105, CD90 and CD45 (BD Biosciences). Mandible/femur BMSCs were washed three times with 0.5% BSA in phosphate-buffered saline (PBS). Then, the cells were aliquoted into 12 × 75 mm pre-labeled sample tubes, with  $5 \times 10^5$  cells/100  $\mu$ L per antigen followed by incubation for 30 min at room temperature in the dark with CD105, CD90 and CD45 conjugated antibodies according to the manufacturer's recommendations. Cells were then washed twice and resuspended in 1% BSA/PBS for analysis on a flow cytometer (LSRII flow cytometer, BD Biosciences) using FlowJo X software (BD Biosciences).

## 2.6 Cell proliferation assays

For the MTT (3-[4,5-dimethylthiazol-2-yl]-2,5 diphenyl tetrazolium bromide) assay, mandible and femur BMSCs were seeded into 96-well plates at a density of  $1.25 \times 10^4$  cells/cm<sup>2</sup> and incubated for 4, 7 and 10 days with the medium changed every 3 days. At each time point, cell proliferation was visualized. Briefly, medium was removed and cells were washed twice with PBS, then tetrazolium salt MTT (Sigma-Aldrich) at 5 mg/ml was added to each well and incubated at 37°C for 4 hours. Formazan crystals generated by mitochondrial enzyme activity were dissolved by dimethyl sulfoxide (DMSO, Sigma-Aldrich) and the intensity of the reaction product was quantified by measuring absorbance at 570 nm. For the BrdU assay, cells were cultured as above for 4, 7, or 10 days and assayed using the BrdU Cell Proliferation Assay (Sigma-Aldrich), following the manufacturer's instruction. Absorbance of the reaction product was measured at dual wavelengths of 450 and 540 nm.

### 2.7 Osteogenic differentiation

Cells were seeded into 24-well plates, grown to 70–80% confluence and incubated in osteogenic differentiation medium containing 10 nM dexamethasone, 10 mM beta-glycerophosphate, 50 mg/mL ascorbate phosphate, and 10% FBS for 3 and 4 weeks and then processed for analyses. The medium was changed every 3 days. Cultures were fixed in 10% formalin for 15 minutes, washed with dH<sub>2</sub>O two to three times (each 2 minutes) and mineralization of extracellular matrix was stained with 1% Alizarin Red S (ARS) for 10 min. The red stain was then washed two to three times in dH<sub>2</sub>O and the images were taken under the microscope. For quantification, Alizarin Red S was extracted from the monolayer by incubation in 10% acetic acid for 30 min at room temperature. The dye was removed, 100 µL aliquots were transferred to a 96-well plate, and the absorbance was read at 405 nm.

### 2.8 Adipogenic differentiation

Cells were seeded in 24-well plates, grown to sub-confluence, and incubated in adipogenic medium (R&D Systems) for 3 weeks. The medium was changed every 3 days. Cells were then fixed in 10% formalin for 30 minutes, washed with water and incubated in 60% isopropanol for 5 minutes, and lipid droplets were stained with Oil Red O solution (Sigma-Aldrich) for 15 min and washed with water. Following microscopic imaging, Oil Red O staining was quantified by incubation in 100% isopropanol for 10 minutes at room temperature. Aliquots of 100 µL were transferred to a 96-well plate and the absorbances were read at 510 nm.

### 2.9 Chondrogenic differentiation

Cells were seeded in 48-well plates, grown to subconfluence and incubated in chondrogenic medium (R&D Systems) for 3–4 weeks. The medium was changed every 3 days. Cells were then fixed in 10% formalin for 20 min, washed with water and stained with alcian blue reagent (Sigma-Aldrich) for 45 min in dark at room temperature then washed with water. After images were taken under a microscope, dye was extracted by incubation in 6 M guanidine hydrochloride overnight at 4 °C. Then 100 µL aliquots were transferred to a 96-well plate and the absorbances were read at 595 nm.

### 2.10 Cell mitochondrial stress test by Seahorse assay

To investigate mitochondrial function, oxygen consumption rates (OCR) of both BMSCs and osteogenic differentiated BMSCs were directly measured by the Agilent Seahorse XFe24 extracellular flux analyzer (Seahorse Bioscience, North Billerica, MA) as previously described<sup>33</sup>. Briefly, non-differentiated BMSCs were seeded in XFe24 cell culture plates at 30,000 cells/well in growth medium and placed in a 37 °C incubator with 5% CO<sub>2</sub> overnight. The cells were washed twice with Seahorse assay medium (XF base medium supplemented with 25 mM glucose, 2 mM glutamine and 1 mM sodium pyruvate; pH 7.4) and incubated in the 37 °C incubator without CO<sub>2</sub> for 1 hour. Ten µM oligomycin, 2.7 µM FCCP, and 10 µM rotenone/antimycin A were injected into the cartridge, which was then calibrated by the Seahorse XFe24 analyzer and the assay continued using the Mito Stress Test assay protocol. For osteogenic differentiated BMSCs, cells were seeded in XFe24 cell culture plates at 4,000 cells/well and induced in

osteogenic medium for 2 weeks. The differentiated BMSCs were assayed by the Mito Stress Test as described above. After the assay, cells were collected in EBT buffer with protease inhibitor (ThermoFisher) and the protein content in each well was measured following the Bradford protocol. Seahorse assay data of the osteogenic differentiated BMSCs was calibrated by protein content. Each OCR value was an average of five independent replicates per experiment. Results represent an average of four to five animals.

### 2.11 RNA-Seq preparation

Total RNA was isolated using the RNeasy® Plus Mini Kit (Qiagen) according to the manufacturer's instructions. The purity and concentration were measured using a NanoDrop ND-1000 spectrophotometer (NanoDrop Technologies LLC). RNA integrity was assessed by a BioAnalyzer (Agilent Technologies). The mRNA libraries were generated using NEBNext® Ultra™ II Directional (stranded) RNA Library Prep Kit for Illumina (NEB #E7760L) and sequencing was performed on the Novaseq 6000 system with the SP flowcell and 150bp PE reads. In total, 8 samples were collected: 4 replicates for each group (Femur and Mandible). FASTQ files were lightly quality trimmed using Sickle v1.33 specifying a minimum average of Q10 over a 20bp window<sup>34</sup>. Trimmed reads were mapped to the *Rattus norvegicus* (Rnor\_6.0 [acc: GCF\_000001895.5]) genome using STAR v2.7.6a<sup>35</sup> with default parameters. Read counts of genomic features were determined using the feature counts program of the Subread package v2.0.1<sup>36</sup> with the -B parameter enabled (count reads with both ends aligned to the genomic feature).

The raw sequence data has been deposited in the NCBI Sequence Read Archive (SRA) under BioProject accession PRJNA828546.

### 2.12 Statistical analysis

Analysis of covariance (ANCOVA) was used to investigate whether there are interactions between sites (Mandible and Femur) and groups (Sham and OVX) for all bone quality parameters. ANCOVA was tested to determine whether differences between groups are dependent on sites. If the results of ANCOVA are significant, the data should be compared between groups for each site. A Student's t-test was performed to compare each parameter between sham and OVX groups of each site. A paired t-test was utilized to compare between mandible and femur sites of each group. The paired t-test was also performed to compare TMD parameters between layers of AB and CB<sub>55</sub>. Bioassay data were compared using a Student's t-test between mandible and femur cells.

Analysis of genomic count data was performed using the Bioconductor (v3.11) package edgeR (v3.32) with R (v4.0). The edgeR function glmQLFit was used to fit a quasi-likelihood negative binomial generalized log-linear model to the count data. The function glmTreat was used to perform gene-level differential expression analysis relative to a log<sub>2</sub>-fold-change threshold of 1.5. Significance was determined by conducting a quasi-likelihood (QL) F-test against the threshold. FDR-adjusted p-values were calculated using the Benjamini-Hochberg procedure<sup>37</sup> with significance set at q<0.05. GO pathway over-representation analysis was conducted using the goana function in the Bioconductor package limma (v3.44.0)<sup>38</sup>. Genes belonging to the over-represented pathways were determined by modification of code posted to the Bioconductor support

list (<https://support.bioconductor.org/p/69808/>) and the `org.Rn.eg.db` package (v3.14.0) for Bioconductor<sup>39</sup>.

### 3. Results

Regions of mandible and femur were successfully isolated using the compartmentation process for the 3D micro-CT images to obtain TMD histograms (Figs. 1 and 2). Interactions between sites (Mandible and Femur) and groups (Sham and OVX) were significant for all parameters ( $p < 0.003$ ) (Supplementary Table 1) suggesting that the values varied dependent on sites and groups.

The mean values of most volumetric, mineral density, TB morphology parameters in mandible were not significantly different between sham and OVX groups ( $p > 0.06$ ) while  $Low_5$  and  $High_5$  significantly increased and  $SD_{TB}$  decreased following OVX ( $p < 0.05$ ) (Supplementary Table 1). In contrast, OVX in femur significantly decreased the mean values of most volumetric, mineral density, TB morphology parameters, and some of CB morphology parameters including  $BV_{55}$  and  $Ct.Th$  ( $p < 0.03$ ) while significantly increasing  $AP/ML$ ,  $BS/BV$  and  $Th.Sp$  ( $p < 0.04$ ) (Supplementary Table 1).

OVX had no effects on the mean values of mechanical parameters in mandible ( $p > 0.25$ ) while OVX significantly decreased that of  $\tan \delta$  in femur ( $p = 0.03$ ) (Supplementary Table 1). The mean values of mineral density parameters of AB in mandible were not significantly changed by OVX ( $p > 0.06$ ) while those of MCB in femur significantly decreased as the same trend of CB ( $p < 0.04$ ) (Table 1).

**Table 1.** Comparison of measured parameters between sham and OVX groups for alveolar bone (AB) in mandibles and marginal cortical bone (MCB) in femurs

(mean±standard deviation). Significantly different parameters are highlighted in **bold** (p<0.05).

Parameters		Mandibular AB			Femoral MCB		
		Sham	OVX	P value	Sham	OVX	P value
Mineral Density	TMC (mgHA)	8.429 ±0.427	8.430 ±0.497	1.00	<b>9.63</b> <b>±0.90</b>	<b>7.96</b> <b>±0.49</b>	<b>0.001</b>
	Mean (mgHA/cm <sup>3</sup> )	1638.60 ±17.74	1647.79 ±7.05	0.17	<b>1618.55</b> <b>±69.98</b>	<b>1489.82</b> <b>±9.84</b>	<b>0.001</b>
	SD (mgHA/cm <sup>3</sup> )	81.55 ±3.78	78.52 ±2.23	0.06	<b>112.44</b> <b>±11.35</b>	<b>68.81</b> <b>±4.06</b>	<b>0.001</b>
	Low <sub>5</sub> (mgHA/cm <sup>3</sup> )	1511.82 ±22.77	1525.78 ±7.86	0.10	<b>1359.32</b> <b>±22.01</b>	<b>1330.77</b> <b>±5.80</b>	<b>0.001</b>
	High <sub>5</sub> (mgHA/cm <sup>3</sup> )	1774.61 ±12.25	1778.46 ±9.43	0.47	<b>1754.65</b> <b>±97.04</b>	<b>1562.34</b> <b>±14.81</b>	<b>0.001</b>

The mean values of TMD parameters at each layer rapidly increased up to 60 µm away from the PDL in mandible and up to 81 µm from the periosteal surface in femur (p<0.001) (Fig. 3A and 4A). While the mean values of all TMD parameters for AB were not significantly different between sham and OVX groups (p>0.084) (Fig. 3A-D), those of most TMD parameters for C<sub>55</sub> showed significantly lower values for the OVX group than the sham group (p<0.041) (Fig. 4A-D). These results demonstrate that while OVX significantly diminished femur bone quality, mandible quality was not affected. Therefore, BMSCs from each site were examined for possible differences in osteogenic potential.

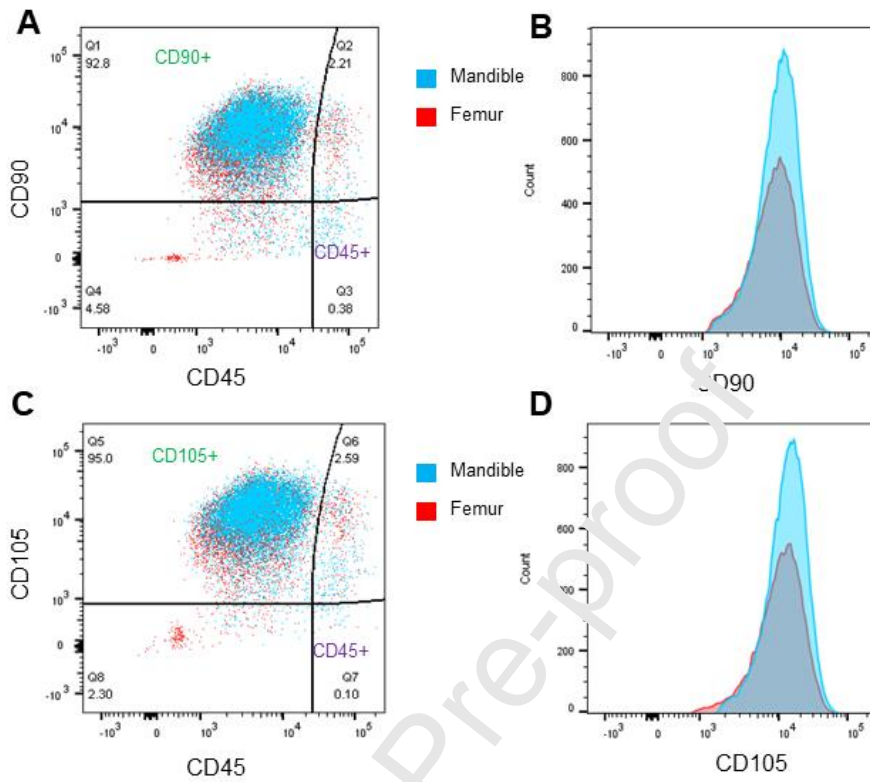
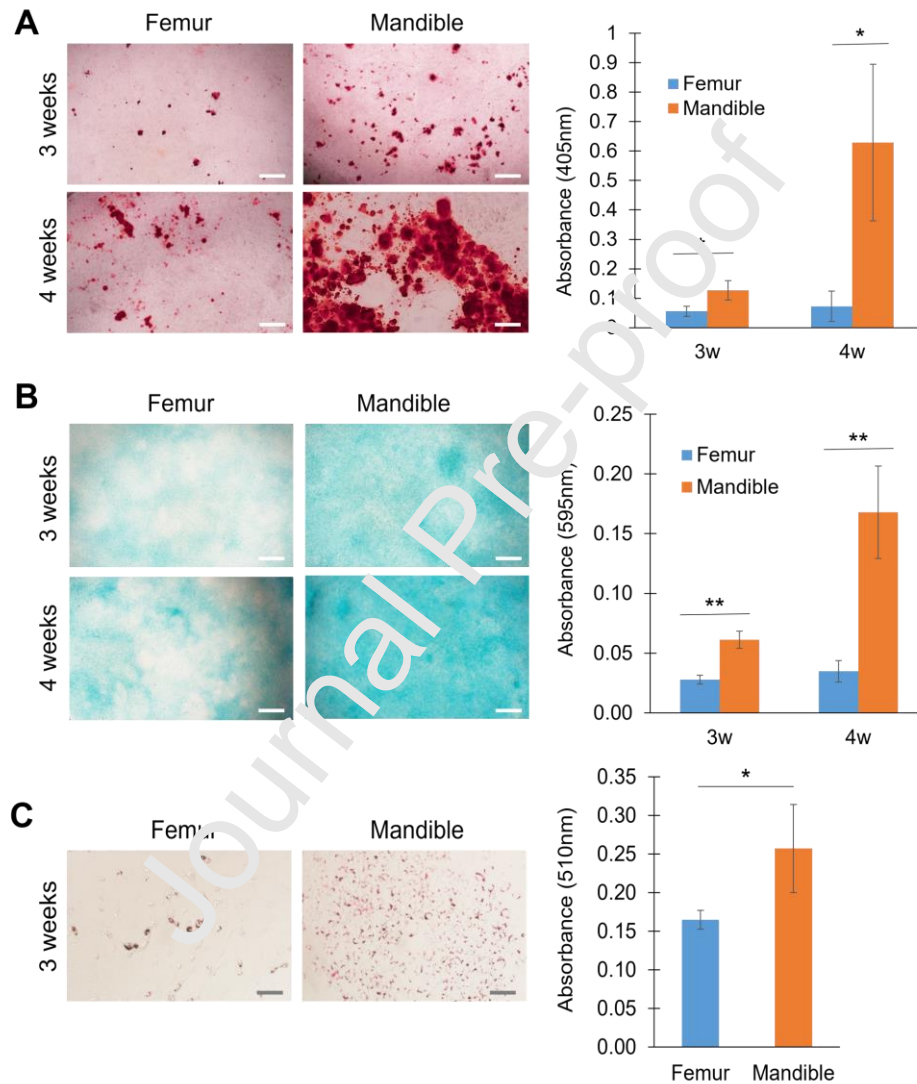


**Fig. 6** Flow cytometry of BMSCs isolated from femur and mandible. (A) and (C) demonstrate expression of mesenchymal markers (A) CD90 or (C) CD105 relative to hematopoietic marker CD45. As described in the text, the vast majority of cells from both



mandible and femur demonstrated positivity only for mesenchymal markers. (B) and (D) demonstrate the almost complete overlap of mesenchymal marker expression in cells from mandible and femur.

**Fig. 7** Differentiation of early passage BMSCs from femur and mandible. Cells were differentiated along (A) osteogenic, (B) chondrogenic, or (C) adipogenic lineages as described in the text. Photos indicate representative fields. For (A) and (B), scale bar = 200  $\mu\text{m}$ . For (C), scale bar = 100  $\mu\text{m}$ . For adipogenic differentiation, cells were assayed only at 3 weeks, since cells were poorly adherent to substrate at 4 weeks. \*:  $p < 0.05$ ; \*\*:  $p < 0.01$

Journal Pre-proof

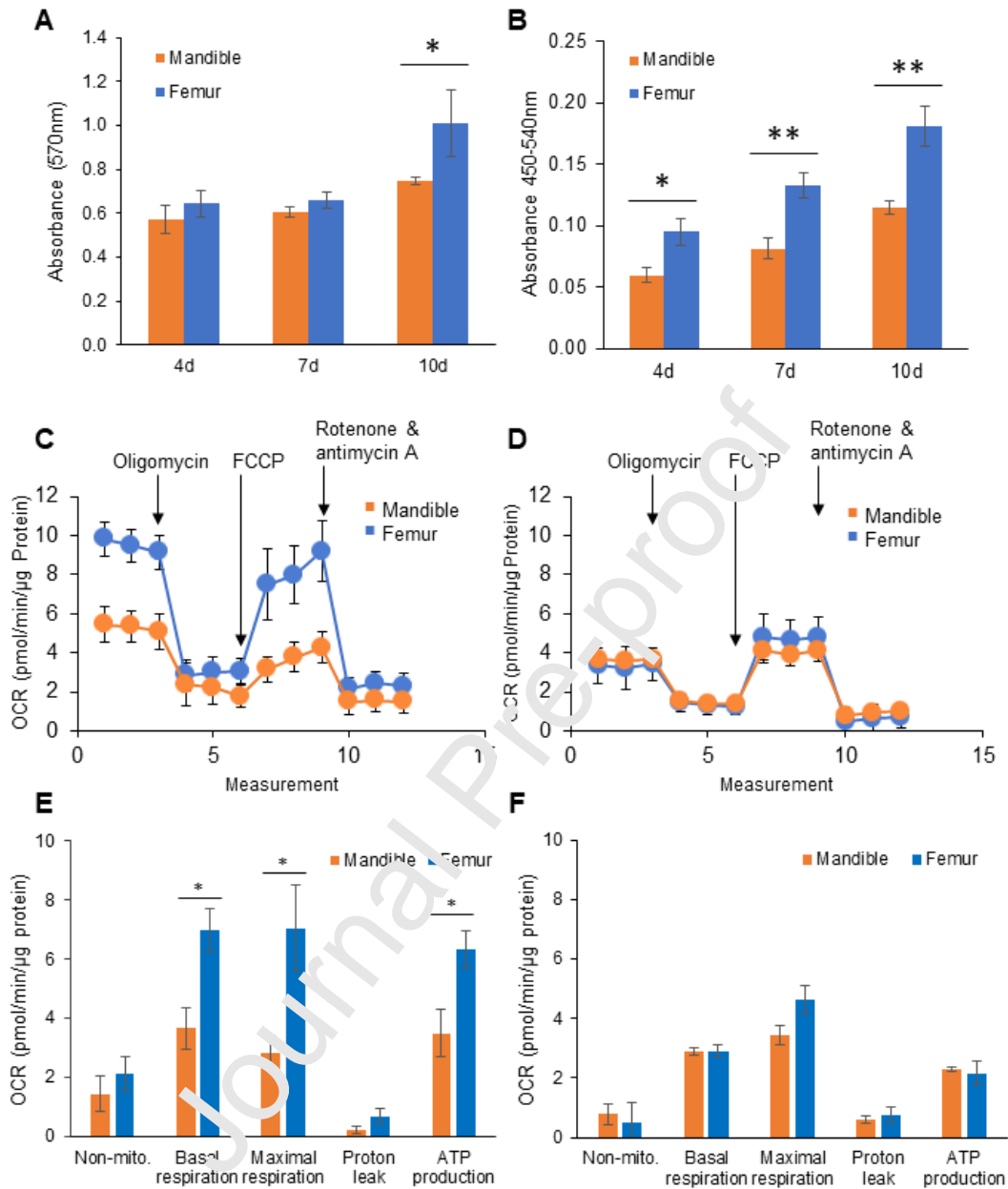


**Fig. 8** Proliferation and metabolic activity of early passage BMSCs from femur and mandible. Results represent averages from cells of 4 to 5 animals. Cellular proliferation was measured by (A) MTT ( $n = 4$ ) and (B) BrdU ( $n = 5$ ) assays. Oxygen consumption rates (OCR) were measured by Seahorse assay for (C) and (E) undifferentiated cells ( $n = 5$ ), and (D) and (F) cells differentiated along the osteogenic pathway ( $n = 4$ ). (D) and (F) Data were derived from the curves in (C) and (E), respectively. \*:  $p < 0.05$ ; \*\*:  $p < 0.01$

To validate BMSC isolation procedures according to established criteria for MSC identification<sup>40</sup>, cells were obtained from femur and mandible and subjected to flow cytometry for expression of CD90, CD105 (mesenchymal stem cell markers) and CD45 (a hematopoietic stem cell marker). When cells were dually labeled for CD45 and either CD90 or CD105, greater than 92% of cells from both femur and mandible demonstrated positivity for the mesenchymal marker, but fewer than 0.5% showed positivity for the hematopoietic marker (Fig. 6). Greater than 94% of cells demonstrated positivity for both mesenchymal markers (data not shown). To further characterize the isolates as MSCs, cells were subjected to culture conditions that induced osteogenic, chondrogenic, or adipogenic differentiation. All cells were capable of differentiating along these lineages, although in all cases, mandible cells demonstrated a significantly greater differentiation potential than femur cells ( $p < 0.05$ ) (Fig. 7A-C).

To determine whether the differences in responses to OVX between femur and mandible might originate from innate differences between osteogenic cells in these sites, several assays of isolated BMSC activity were undertaken. To examine the relative metabolic activities of these cells, mandible and femur BMSCs were assayed for proliferation and energy consumption. MTT assays, which are measurements of cellular mitochondrial activity and thus reflect cell number, showed significantly higher activity in femur cells than mandible cells after 10 days in culture ( $p < 0.05$ ), and higher but non-significant trends in activity at days 4 and 7 (Fig. 8A). More sensitive BrdU assays, which measure rates of DNA synthesis, revealed higher activity of femur cells at all time points (Fig. 8B).

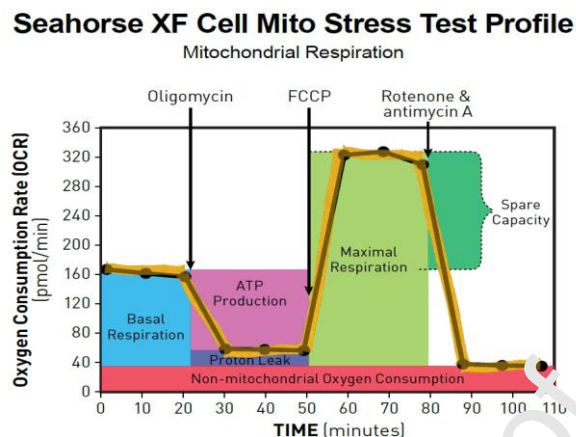


**Fig. 9** Key for interpretation of Seahorse OCR measurements

Because cells from mandible and femur differed in their abilities to both proliferate and differentiate, metabolic assays were undertaken to identify any potential variation in energy usage. Cells were subjected to analysis using Seahorse methodologies. Fig. 9 illustrates the key by which Seahorse measurements of oxygen consumption can be interpreted. Oxygen consumption rates (OCR) were measured in both undifferentiated femur and mandible cells (Fig. 8C,E) and cells subjected to 3 weeks of osteogenic differentiation (Fig. 8D,F). Both mandible and femur BMSCs showed high levels of respiratory activity. Each consumed oxygen at or near their maximal rate under basal conditions (Fig. 8E,F). However, consistent with their higher levels of proliferation, undifferentiated femur cells demonstrated significantly higher rates of basal mitochondrial respiration, maximal mitochondrial respiration, and ATP production than undifferentiated mandible cells (Fig. 8E). This higher respiratory activity dissipated after osteogenic differentiation (Fig. 8F). Although mitochondrial respiration is the predominant energy production method in the BMSCs assayed here, measurements of

glycolysis via the extracellular acidification rate (ECAR) also demonstrated differences between femur and mandible cells.

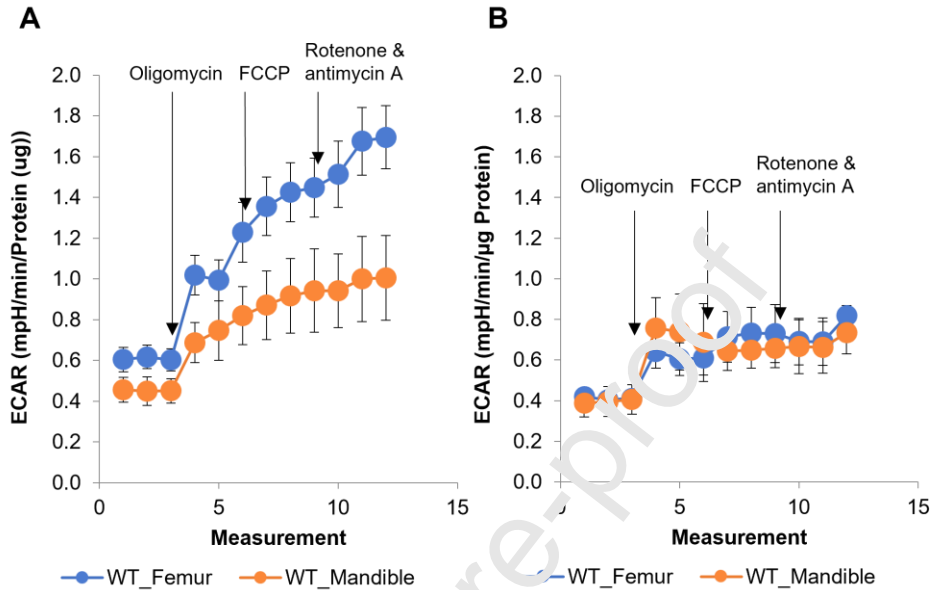


**Fig. 10** Extracellular acidification rates (ECAR) in undifferentiated BMSCs (panel A) and cells differentiated along the osteogenic pathway (panel B). ECAR is largely a product of lactate acid production and therefore measures cellular glycolysis.

Undifferentiated femur cells showed higher rates of glycolysis than mandible cells under basal conditions and could especially increase glycolysis under stressed conditions where mitochondrial respiration is inhibited by oligomycin or rotenone and antimycin A (Figure 10A). However, the differences in glycolysis between femur and mandible cells were eliminated following osteogenic differentiation (Figure 10B). In summary, these results indicate that undifferentiated femur-derived BMSCs have higher proliferative, mitochondrial, and glycolytic activity than BMSCs derived from mandible while the metabolic differences disappear following osteogenic differentiation.

To determine how differences in gene expression between mandible and femur BMSCs might account for the variations in phenotype, RNA-Seq was performed on early passage cells. Eight independent samples were sequenced (4 femur samples and 4 mandible samples) for a total of 114,680,221 reads. Three hundred eighteen genes were upregulated in mandible relative to femur, while 222 genes were downregulated, as shown in Figure 11 ( $p < 0.05$ ). Table 2 shows the top ten differentially expressed genes (DEGs; mandible – femur) as sorted by statistical significance. Figure 11 demonstrates a more comprehensive view of all DEGs as illustrated by volcano plot. With the exception of one long non-coding RNA, all top ten DEGs encoded either homeobox transcription factors or cytoskeletal proteins. Gene Ontology analysis revealed regulation of osteoblast and cartilage development, SMAD signaling, and glucose transporter activity to be the top upregulated pathways in mandible cells compared to femur cells (Fig. 12). This pathway analysis is consistent with the phenotypic differences we discovered between mandible and femur BMSCs.

**Table 2.** Top differentially expressed genes relative to a fold-change threshold. Genes are sorted by their FDR-adjusted p-value. Genes that are more highly expressed in mandible have positive logFC values; genes that are more highly expressed in femur have negative logFC values.

Gene ID	Entrez ID	logFC	FDR-adjusted p-value	Gene description
Barx1	364680	11.51	$5.80 \times 10^{-6}$	Homeobox transcription factor
LOC103694111	103694111	5.30	$1.06 \times 10^{-5}$	Long non-coding RNA
Thbs4	29220	13.41	$1.06 \times 10^{-5}$	Thrombospondin 4
Hoxc6	252885	-7.23	$1.06 \times 10^{-5}$	Homeobox transcription factor
Lhx8	365963	10.10	$1.88 \times 10^{-5}$	Homeobox transcription factor
Mkx	291228	5.60	$1.88 \times 10^{-5}$	Homeobox transcription factor
Fblim1	362650	-2.15	$3.66 \times 10^{-5}$	Filamin binding LIM protein 1

Nefm	24588	8.16	$3.66 \times 10^{-5}$	Neurofilament medium polypeptide
Hoxc10	315338	-12.54	$4.69 \times 10^{-5}$	Homeobox transcription factor
Baiap211	304282	-2.89	$4.69 \times 10^{-5}$	Actin bundling protein

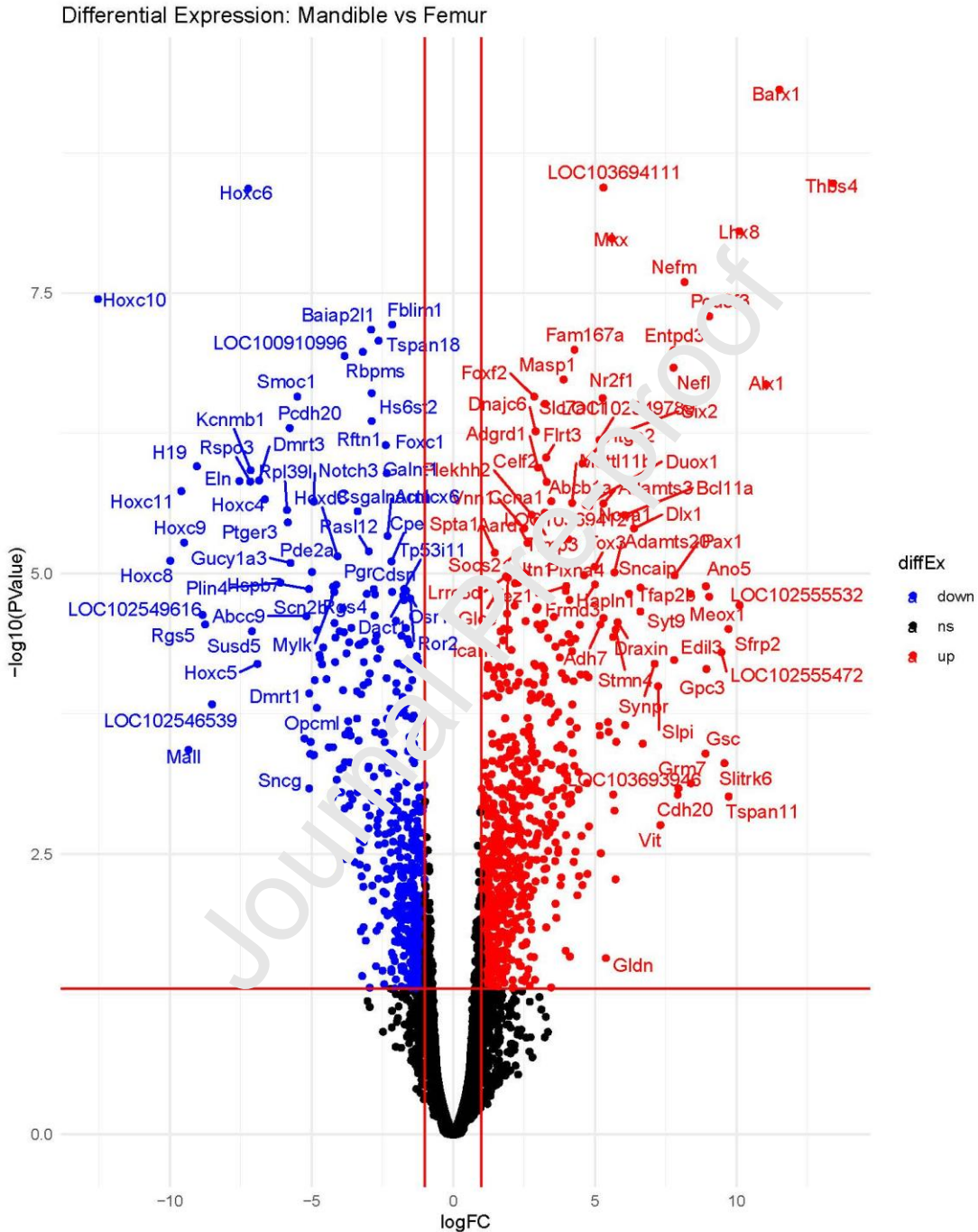


**Fig. 11** Volcano plot showing the dataset of differentially expressed genes (mandible-femur). DEGs that demonstrated greater than 2-fold difference between mandible and

femur are outside the vertical lines, while those comparisons with a p-value cutoff below 0.05 are above the horizontal line.

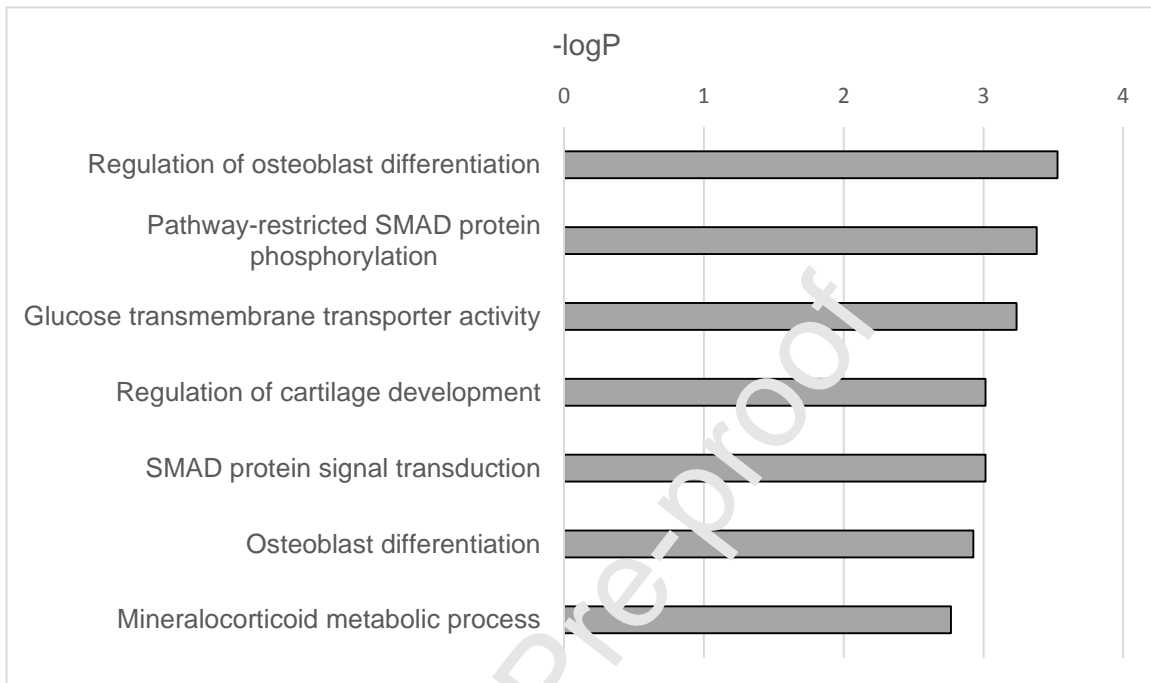


**Fig. 12** Top differentially regulated pathways in mandible BMSCs as assessed by Gene Ontology (GO) analysis. Numerical values indicate  $-\log_{10}$  of the p-value.

#### 4. Discussion

It is generally accepted that postmenopausal estrogen deficiency reduces bone mass and deteriorates TB morphology<sup>3,4</sup>. Estrogen deficiency stimulates osteoclasts' activities to remove more mineralized pre-existing bone tissues followed by osteoblasts' activities to form less mineralized new bone tissues<sup>3,41-43</sup>. As the activities of osteoclasts and osteoblasts are coupled, both cells can be activated by estrogen deficiency. However, estrogen deficiency-induced bone resorption by osteoclasts outpaces bone formation by osteoblasts, resulting in bone loss and alteration of TMD distribution<sup>27,50,51</sup>. In the

current study, the Low<sub>5</sub> value describes TMD changes at newly formed bone regions, while High<sub>5</sub> describes TMD changes at pre-existing bone regions<sup>23,44,45</sup>. In femur, OVX significantly reduced the values of Low<sub>5</sub> and High<sub>5</sub>, which can be explained by adding less mineralized new bone tissues and removing more mineralized pre-existing bone tissues, respectively. As more bone resorption occurs in the OVX femur, the values of High<sub>5</sub> was reduced more than those of Low<sub>5</sub>, producing a lower SD that reflects more homogeneous TMD distribution<sup>23,46,47</sup>. The femoral bone loss due to OVX is also assessed by decrease in bone volume (BV) and morphology (Ct.Th, Tb.N, and Tb.Th). More homogeneous TMD distribution in the OVX femur likely gives rise to more brittle mechanical behavior having slightly increased static and dynamic stiffness, with decreased static fracture strength and displacement, and significantly decreased viscoelastic energy dissipation. However, most of those parameters measured for the mandibles were not significantly different with OVX; indeed both Low<sub>5</sub> and High<sub>5</sub> increased after OVX in mandible. These results indicate that jaw bone is less sensitive to estrogen deficiency than limb bone, consistent with the findings by previous studies<sup>11,14-16</sup>.

Because bone is altered in response to mechanical loading<sup>48,49</sup>, masticatory functional demands in jaw were suggested to protect bone loss in postmenopause<sup>14,50</sup>. As the alveolar bone (AB) surrounds teeth, where dynamic masticatory impact force is directly transmitted through teeth and periodontal ligament (PDL), many observations indicated that force-induced active bone remodeling is localized to occur at the AB<sup>15,51-53</sup> and a histological study also identified the distance of active AB turnover up to 51  $\mu\text{m}$  from PDL<sup>51</sup>. The current findings are consistent with local active remodeling at the AB within

this region up to 60  $\mu\text{m}$  from PDL. However, the characteristics of AB were not different between sham and OVX groups. On the other hand, the femoral MCBs, which are actively remodeled endosteal and periosteal surfaces, had significantly lower TMD values in OVX group than sham group. The same patterns were also found for TMD values in TB where more bone remodeling is observed because the porous TB network provides more surface to support bone cell activity. It has been suggested that muscular and condylar reaction forces caused by mastication can stimulate bone remodeling in the entire jaw<sup>54</sup>. However, the jaw muscular forces resulting from the impact mastication produce strains at a similar level to those from vertebral muscles<sup>54,55</sup>, which are required to maintain normal bone integrity. In addition, chewing takes much shorter time than daily activities that need limb and vertebral muscles. Hence, the masticatory muscular force has no superior effects on stimulating active bone remodeling and mineralization than the locomotive or postural muscular force. In addition, previous studies indicated that anabolic response to mechanical loading is limited by estrogen deficiency<sup>56,57</sup>. As such, the masticatory force cannot fully explain the reduced effects of estrogen deficiency on jaw relative to other bones.

It is speculated that site-specific BMSC properties may arise because the BMSCs in jaw are derived from neural crest, while BMSCs from vertebral and limb bones are derived from mesoderm<sup>14,20,58,59</sup>. Thus, the two BMSC populations may possess subtle but significant differences in gene expression, leading to different osteogenic potentials. We were able to isolate nearly pure populations of BMSCs from rat femur and mandible, based on their cell surface marker characterization and ability to undergo multilineage differentiation. Initial characterization revealed consistent differences in proliferation,

differentiation, and metabolic properties between cells from different sites. Femur cells demonstrated higher rates of proliferation, while mandible cells showed greater ability to differentiate along osteogenic, chondrogenic, and adipogenic pathways. Femur cells also showed greater capacity for glycolysis and metabolic ATP production than mandible cells, consistent with their greater proliferation rate. Comparison of these findings to similar studies in the literature suggests that functional differences between BMSCs of different sites may be age-related. It is well established that BMSCs of humans and rodents undergo functional decline with age<sup>60</sup>. However, previous studies, which primarily used BMSCs from the appendicular skeleton, did not take into account the sites from which BMSCs were isolated. Although we saw differences in proliferation and differentiation of BMSCs from 9-month-old rats, a recent comparison of femur and mandible BMSCs from 3-month-old rats showed their proliferation and differentiation rates to be comparable<sup>61</sup>. These results suggest that orofacial BMSCs may be less prone to age-related decline than BMSCs from limb bones. These results also concur with previous studies from both human and animal models showing greater osteogenic differentiation of mandibular BMSCs than limb BMSCs, though age was not taken into account in these studies<sup>19,22,61-65</sup>.

Site-specific differences in stem cell activities may result from innate differences or from influences of their local environment or niche. To examine genetic differences that might account for site-specific variations in our model, RNA-Seq was performed. Analysis of the top differentially expressed genes revealed a marked difference in homeobox gene expression between rat mandible- and femur-derived BMSCs. Homeobox-containing transcription factors, particularly the HOX superfamily, are well-

established as controllers of skeletal patterning during embryonic development<sup>66</sup>. More recently, Hox genes have been shown to maintain critical functions in the adult skeleton. Hox gene expression profiles are generally maintained in adult tissues and organs, particularly in cells that maintain progenitor behavior such as periosteal stem cells<sup>67</sup>. Some homeobox-containing transcription factors have been shown to be reactivated during repair of bone fracture and are necessary for this repair. For example, Hox11 paralogs, which are expressed during development in the zeugopod skeleton (radius/ulna and tibia/fibula), are necessary for limb development, and their expression remains regionally restricted in these areas through adulthood<sup>68</sup>. Conditional deletion of the Hoxd11 allele in adults leads to abnormal remodeling. Although BMSC numbers and their expression of Runx2 (an early osteoblast differentiation marker) are not diminished by the lack of Hoxd11, cells are unable to proceed further to terminal osteoblast differentiation and osteocyte formation<sup>69</sup>. Additionally, through RNA sequencing, a recent study of human BMSCs from ilium, maxilla, and mandible, found clear differences in homeobox-containing gene expression among these populations. The authors found that BMSCs from the maxillofacial region were negative for the HOX superfamily, while BMSCs from other skeletal tissues were positive<sup>70</sup>. Hoxc6 and Hoxc10 were two of the most highly downregulated DEGs in facial MSCs relative to MSCs of non-facial origin. Additionally, the previous study found that genes for homeobox-containing proteins Lhx8 and Barx1 were strongly upregulated in maxillofacial-derived MSCs. Our results in rat cells concur with their human studies, with Hoxc6 and Hoxc10 as two of the ten most downregulated genes in mandible, and Lhx8 and Barx1 being two of the ten most upregulated genes. Both Lhx8 and Barx1 have

already been identified as playing key roles in craniofacial development and odontogenesis<sup>71,72</sup>. These results not only demonstrate the proper identities of our isolated MSCs, but also indicate rat as a suitable model for mimicking human homeobox-containing gene expression in maxillofacial bone. How the differential expression of homeobox-containing transcription factors might contribute to the phenotypes of BMSCs from different sites is unclear and is almost certain to produce a highly complex network of gene regulation.

In addition to homeobox-containing transcription factors, the other major class of top DEGs in our study was cytoskeletal proteins. One of these, *Fblim1* (filamin-binding LIM protein 1/FBLP-1/migfilin), already has been shown to play a crucial role in bone remodeling. Knockout of *Fblim1* in mice resulted in severe osteopenia, decreased the growth and survival of BMSCs *in vitro*, and decreased osteoblast progenitors and differentiation *in vivo*. Further, *Fblim1*-deficient BMSCs expressed markedly higher levels of RANKL than wild-type cells, resulting in increased osteoclast differentiation *in vivo*<sup>73</sup>. However, it is unclear how *Fblim1* activity correlates to the findings presented here. Although the previous study indicated that this protein was necessary for osteoblastogenesis, our results show decreased expression of the mRNA in mandible BMSCs relative to femur cells, even though the mandible BMSCs showed higher osteogenic capacity. The discrepancy may be due to a dose effect (i.e. decreased expression vs. full knockout), external factors from the relevant stem cells niches, or it may be that mandible cells express a different but functionally similar filamin binding protein. More research is required to elucidate how *Fblim1* might differentially affect femur- and mandible-derived BMSCs.

By Gene Ontology pathway analysis, we found that the top differentially regulated pathways between mandible and femur BMSCs are involved in osteoblast differentiation, SMAD signaling, cartilage development, and glucose transmembrane transporter activity. Differentially expressed genes from this study involved in osteoblastogenesis pathways include regulators of Wnt signaling such as *Wnt4* and *Sfrp2*<sup>74</sup>. DEGs involved in cartilage development include *Six2*, a homeobox gene that regulates cartilage formation in the cranial base<sup>75</sup>. Finally, DEGs that may play a role in glucose transmembrane transport include *Slc2a4* and *Slc2a5*, also known as GLUT4 and GLUT5<sup>76</sup>. Differential regulation of these pathways is consistent with our cellular assays demonstrating diverse cellular functions such as proliferation, metabolic activity, and differentiation potential. Examination of how these genes are expressed under varying conditions such as differentiation and aging will help illuminate the mechanisms behind the differing activities of BMSCs from diverse sites in the skeleton.

While this study clearly defined differences between femur and mandible BMSCs, a limitation is that cellular and RNA-Seq studies were performed only on cells from non-OVX animals. A previous study showed that jaw BMSCs obtained from OVX mice have comparable osteogenic capacity with BMSCs from sham surgery mice, while limb BMSCs from the OVX mice had significantly lower activities for mineralization<sup>20</sup>. The influences of BMSC site, estrogen status, and age on cellular activity and gene expression require further study, so experiments using OVX and sham rats of different ages are underway. However, we have compared our DEGs to the response to estrogen GO pathway (GO 0043627) and found little overlap. No significantly down-regulated genes of mandible were present in this pathway, and only one up-regulated gene was found (the

transcriptional activator *gata6*, upregulated 3.32-fold). This result is suggestive of estrogen-independent mechanisms for the differential bone metabolism in jaw bone and is consistent with our other findings.

In summary, we found that in femurs, estrogen deficiency did decrease bone quantity (mass and BMD) and quality (TMD, morphology, and energy dissipation). Thus, these findings are consistent with other models of postmenopausal osteoporosis in limb bones. However, the BMD, morphologies, and mechanical properties of mandible were not influenced by OVX. Further, the mandibular TMD values observed were higher for the OVX group than the sham group. In addition, we found that the active local remodeling at the AB due to masticatory force continues up to a 60  $\mu\text{m}$  distance from the PDL, producing the steep gradient of TMD parameters. Thus, the effects of masticatory force are likely to be limited to alveolar bone without controlling the whole jawbone. We also found that mandibular BMSCs showed greater osteogenic differentiation than limb BMSCs, consistent with previous studies from both human and animal models<sup>19,22,61-65</sup>. Further, genes of *Lhx8* and *Parx1* were most upregulated in mandible, which are related to craniofacial development and odontogenesis<sup>21,22</sup>. Gene ontology pathway analysis indicated that the mandibular BMSCs showed heightened gene expression in the regulatory pathways of osteoblast differentiation, SMAD signaling, cartilage development, and glucose transmembrane transporter activity. These findings suggested that active mandibular BMSCs maintain bone formation and mineralization by balancing the rapid bone resorption caused by estrogen deficiency. These characteristics likely help reduce the risk of osteoporotic fracture in postmenopausal jawbone.

**Acknowledgements**

The project described here was supported by Grant Number AG033714 from the National Institute on Aging (Kim, D-G), Biomedical Research Award from an American Association of Orthodontists Foundation (Kim, D-G), and research seed grant from the College of Dentistry, The Ohio State University (Kim, D-G). Its contents are solely the responsibility of the authors and do not necessarily represent the official views of the National Institute on Aging. The authors would also like to thank Drs. Kristin Stanford and Lisa Baer (Department of Physiology and Cell Biology, The Ohio State University) for their advice in performing Seahorse metabolic analysis of BMSCs. They also thank Dr. Jim Cray (Department of Biomedical Education and Anatomy, The Ohio State University) for use of his microscope.

**Conflict of interests**

There are no conflicts of interest for any author.

## References

1. Kaye, E.K., *Bone health and oral health*. J Am Dent Assoc. 2007. **138**(5): p. 616-19.
2. NIH Consensus Development Panel on Osteoporosis Prevention D, Therapy. *Osteoporosis Prevention, Diagnosis, and Therapy*. JAMA. 2001. **285**(6): p. 785-95.
3. Eastell, R., O'Neill, T.W., Hofbauer, L.C., et al. *Postmenopausal osteoporosis*. Nat Rev Dis Primers. 2016. **2**: p. 16069.
4. Seeman, E., *Pathogenesis of osteoporosis*. J Appl Physiol. 2003. **95**: p. 2142-2151.
5. Seeman, E., *Reduced bone formation and increased bone resorption: rational targets for the treatment of osteoporosis*. Osteoporos Int. 2003. **14**: p. S2-8.
6. *Assessment of fracture risk and its application to screening for postmenopausal osteoporosis*. Report of a WHO Study Group. World Health Organization technical report series. 1994. **843**: p. 1-129.
7. Kanis, J.A., Melton, L.J., Christiansen, C., Johnston, C.C., Khaltaev, N., *The diagnosis of osteoporosis*. J Bone Miner Res. 1994. **9**(8): p. 1137-41.
8. Lelovas, P.P., Xanthos, T.T., Thoma, S.E., Lyritis, G.P., Dontas, I.A., *The laboratory rat as an animal model for osteoporosis research*. Comp Med. 2008. **58**(5): p. 424-30.
9. van Staa, T.P., Dennison, E.M., Jefferson, H.G., Cooper, C., *Epidemiology of fractures in England and Wales*. Bone. 2001. **29**(6): p. 517-22.
10. Gerhards, F., Kuffner, H.D., Wagner, W., *Pathological fractures of the mandible. A review of the etiology and treatment*. Int J Oral Maxillofac Surg. 1998. **27**(3): p. 186-90.
11. Liu, X.L., Li, C.L., Lu, W.W., Cai, W.X., Zheng, L.W., *Skeletal site-specific response to ovariectomy in a rat model: change in bone density and microarchitecture*. Clin Oral Implants Res. 2015. **26**(4): p. 392-98.
12. Turner, R.T., Maran, A., Lotinun, S., et al. *Animal models for osteoporosis*. Rev Endocr Metab Disord. 2001. **2**(1): p. 117-27.
13. Thompson, D.D., Simmons, H.A., Pirie, C.M., Ke, H.Z., *FDA guidelines and animal models for osteoporosis*. Bone. 1995. **17**(4): p. S125-33.
14. Mavropoulos, A., Rizzoli, R., Ammann, P., *Different responsiveness of alveolar and tibial bone to bone loss stimuli*. J Bone Miner Res. 2007. **22**(3): p. 403-10.
15. Gallina, S., Barranco-Piedra, S., Torres-Lagares, D., et al. *Estrogen withdrawal transiently increased bone turnover without affecting the bone balance along the tooth socket in rats*. J Periodontol. 2009. **80**(12): p. 2035-44.
16. Chen, C.H., Wang, L., Serdar, T.U., et al. *An osteopenic/osteoporotic phenotype delays alveolar bone repair*. Bone. 2018. **112**: p. 212-19.
17. Johnston, B.D., Ward, W.E., *The Ovariectomized Rat as a Model for Studying Alveolar Bone Loss in Postmenopausal Women*. Biomed Res Int. 2015.
18. Arnett, T.R., Orriss, I.R., *Metabolic properties of the osteoclast*. Bone. 2018. **115**: p. 25-30.

19. Aghaloo, T.L., Chaichanasakul, T., Bezouglaia, O., et al. *Osteogenic potential of mandibular vs. long-bone marrow stromal cells*. J Dent Res. 2010. **89**(11): p. 1293-98.
20. Yamaza, T., Ren, G., Akiyama, K., Chen, C., Shi, Y., Shi, S., *Mouse mandible contains distinctive mesenchymal stem cells*. J Dent Res. 2011. **90**(3): p. 317-24.
21. Gong, X., Yu, W., Zhao, H., Su, J., Sheng, Q., *Skeletal Site-specific Effects of Zoledronate on in vivo Bone Remodeling and in vitro BMSCs Osteogenic Activity*. Sci Rep. 2017. **7**: p. 36129.
22. Akintoye, S.O., Lam, T., Shi, S., Brahim, J., Collins, M.T., Robey, P.G., *Skeletal site-specific characterization of orofacial and iliac crest human bone marrow stromal cells in same individuals*. Bone. 2006. **38**(6): p. 758-68.
23. Kim, D.G., Navalgund, A.R., Tee, B.C., Noble, G J., Hart, R.T., Lee, H.R., *Increased variability of bone tissue mineral density resulting from estrogen deficiency influences creep behavior in a rat vertebral body*. Bone. 2012. **51**(5): p. 868-75.
24. Kim, D.G., Jeong, Y.H., McMichael, B.K., et al. *Relationships of bone characteristics in MYO9B deficient femurs*. J Mech Behav Biomed Mater. 2018. **84**: p. 99-107.
25. Zauel, R., Yeni, Y.N., Christopherson, C.T., Cody, D.D., Fyhrie, D.P., *Segmentation algorithm for accurate 3D representation of microcomputed tomographic images of human vertebra bodies*. Trans of Orthopaedic Res Society, 2004. **29**: p. 1018.
26. Buie, H.R., Campbell, G.M., Link, R.J., MacNeil, J.A., Boyd, S.K., *Automatic segmentation of cortical and trabecular compartments based on a dual threshold technique for in vivo micro-CT bone analysis*. Bone. 2007. **41**(4): p. 505-15.
27. Voide, R., van Lenthe, C.F., Muller, R., *Bone morphometry strongly predicts cortical bone stiffness and strength, but not toughness, in inbred mouse models of high and low bone mass*. J Bone Miner Res. 2008. **23**(8): p. 1194-1203.
28. Kim, D.G., Haghighi, A., Kwon, H.J., et al. *Sex dependent mechanical properties of the human mandibular condyle*. J Mech Behav Biomed Mater. 2017. **71**: p. 184-91.
29. Kim, D.G., Kwon, H.J., Jeong, Y.H., et al. *Associations of Resonance Frequency Analysis with Dynamic Mechanical Analysis of Dental Implant Systems*. Clin Implant Dent Relat Res. 2016. **18**(2): p. 332-41.
30. Po, J.M.C., Kieser, J.A., Gallo, L.M., Tésenyi, A.J., Herbison, P., Farella, M., *Time-Frequency Analysis of Chewing Activity in the Natural Environment*. J Dent Res. 2011. **90**(10): p. 1206-10.
31. Cordeiro, M.M., Dong, Z., Kaneko, T., et al. *Dental pulp tissue engineering with stem cells from exfoliated deciduous teeth*. J Endodon. 2008. **34**(8): p. 962-69.
32. Huang, G.T.J., Yamaza, T., Shea, L.D., et al. *Stem/progenitor cell-mediated de novo regeneration of dental pulp with newly deposited continuous layer of dentin in an in vivo model*. Tissue Eng Part A. 2010. **16**(2): p. 605-15.
33. Stanford, K.I., Lynes, M.D., Takahashi, H., et al. *12,13-diHOME: An Exercise-Induced Lipokine that Increases Skeletal Muscle Fatty Acid Uptake*. Cell Metab. 2018. **27**(5): p. 1111-20.

34. Joshi, N.A., Fass, J.N., Sickel: *A sliding-window, adaptive, quality-based trimming tool for FastQ files* (Version 1.33) [Software]. Available at <https://github.com/najoshi/sickle>. 2011.
35. Dobin, A., Davis, C.A., Schlesinger, F., et al. *STAR: ultrafast universal RNA-seq aligner*. *Bioinform.* 2012. **29**(1): p. 15-21.
36. Liao, Y., Smyth, G.K., Shi, W., *featureCounts: an efficient general purpose program for assigning sequence reads to genomic features*. *Bioinform.* 2013. **30**(7): p. 923-30.
37. Benjamini, Y., Hochberg, Y., *Controlling the False Discovery Rate: A Practical and Powerful Approach to Multiple Testing*. *J R Stat Soc Series B.* 1995. **57**(1): p. 289-300.
38. Ritchie, M.E., Phipson, B., Wu, D., et al. *limma povers differential expression analyses for RNA-sequencing and microarray studies*. *Nucleic Acids Res.* 2015. **43**(7): p. e47-e47.
39. Carlson, M., Carlson, M., *org.Rn.eg.db: Genome wide annotation for Rat*. R package version 3.8.2. . 2019.
40. Dominici, M., Le Blanc, K., Mueller, I., et al. *Minimal criteria for defining multipotent mesenchymal stromal cells*. *Cytotherapy.* 2006. **8**(4): p. 315-17.
41. Seeman, E., *Age- and menopause-related bone loss compromise cortical and trabecular microstructure*. *J Gerontol A Biol Sci Med Sci.* 2013. **68**(10): p. 1218-25.
42. Garnero, P., Sornay-Rendu, E., Chapuy, M.C., Delmas, P.D., *Increased bone turnover in late postmenopausal women is a major determinant of osteoporosis*. *J Bone Miner Res.* 1996. **11**(3): p. 377-49.
43. Sims, N.A., Civitelli, R., *Cell-Cell Signaling: Broadening Our View of the Basic Multicellular Unit*. *Calcif Tissue Int.* 2014. **94**(1): p. 2-3.
44. Watanabe, K., Lewis, S., Cuo, X., et al. *Regional variations of jaw bone characteristics in an ovariectomized rat model*. *J Mech Behav Biomed Mater.* 2020. **110**: p. 103952.
45. Liu, J., Kim, E.K., Ni, A., et al. *Multiscale characterization of ovariectomized rat femur*. *J Biomech.* 2021. **122**: p. 110462.
46. Roschger, P., Paschalis, E.P., Fratzl, P., Klaushofer, K., *Bone mineralization density distribution in health and disease*. *Bone.* 2008. **42**(3): p. 456-66.
47. Busse, B., Pahn, M., Soltan, M., et al. *Increased calcium content and inhomogeneity of mineralization render bone toughness in osteoporosis: mineralization, morphology and biomechanics of human single trabeculae*. *Bone.* 2009. **45**(6): p. 1034-43.
48. Frost, H.M., *Vital biomechanics. Proposed general concepts for skeletal adaptations to mechanical usage*. *Calc Tiss Int.* 1986. **42**: p. 145-55.
49. Huiskes, R., Ruimerman, R., van Lenthe, GH., Janssen, J.D., *Effects of mechanical forces on maintenance and adaptation of form in trabecular bone*. *Nature.* 2000. **405**(8): p. 704-06.
50. Mavropoulos, A., Kiliaridis, S., Bresin, A., Ammann, P., *Effect of different masticatory functional and mechanical demands on the structural adaptation of the mandibular alveolar bone in young growing rats*. *Bone.* 2004. **35**(1): p. 191-97.

51. Sebaoun, J.D., Kantarci, A., Turner, J.W., Carvalho, R.S., Van Dyke, T.E., Ferguson, D.J., *Modeling of trabecular bone and lamina dura following selective alveolar decortication in rats*. J Periodontol. 2008. **79**(9): p. 1679-88.
52. Ejiri, S., Toyooka, E., Tanaka, M., Anwar, R.B., Kohno, S., *Histological and histomorphometrical changes in rat alveolar bone following antagonistic tooth extraction and/or ovariectomy*. Arch Oral Biol. 2006. **51**(11): p. 941-50.
53. Naveh, G.R., Lev-Tov Chattah, N., Zaslansky, P., Shahar, R., Weiner, S., *Tooth-PDL-bone complex: response to compressive loads encountered during mastication - a review*. Arch Oral Biol. 2012. **57**(12): p. 1575-84.
54. Daegling, D.J., Hylander, W.L., *Occlusal forces and mandibular bone strain: is the primate jaw "overdesigned"?* J Hum Evol. 1997. **33**(6): p. 705-17.
55. Rubin, C.T., Lanyon, L.E., *Dynamic strain similarity in vertebrates; an alternative to allometric limb bone scaling*. J Theor Biol. 1984. **107**(2): p. 321-27.
56. Lee, K., Jessop, H., Suswillo, R., Zaman, G., Lanyon, L., *Bone adaptation requires oestrogen receptor- $\alpha$* . Nature. 2003. **424**(6947): p. 389.
57. Riggs, B.L., Khosla, S., Melton, L.J., *Sex steroids and the construction and conservation of the adult skeleton*. Endocr Rev. 2002. **23**(3): p. 279-302.
58. Helms, J.A., Schneider, R.A., *Cranial skeletal biology*. Nature. 2003. **423**(6937): p. 326-31.
59. Chai, Y., Jiang, X., Ito, Y., et al. *Fate of the mammalian cranial neural crest during tooth and mandibular morphogenesis*. Development. 2000. **127**(8): p. 1671-79.
60. Lin, H., Sohn, J., Shen, H., Janghans, M.T., Tuan, R.S., *Bone marrow mesenchymal stem cells: Aging and tissue engineering applications to enhance bone healing*. Biomaterials. 2019. **203**: p. 96-110.
61. Lee, D.J., Kwon, J., Current, J., et al. *Osteogenic potential of mesenchymal stem cells from rat mandible to regenerate critical sized calvarial defect*. J Tissue Eng. 2019. 10:2041731419830427.
62. Yamaza, T., Ren, G., Akiyama, K., Chen, C., Shi, Y., Shi, S., *Mouse mandible contains distinctive mesenchymal stem cells*. J Dent Res. 2011. **90**(3): p. 317-24.
63. Gong, X., Yu, W., Zhao, H., Su, J., Sheng, Q., *Skeletal Site-specific Effects of Zoledronate on *in vivo* Bone Remodeling and *in vitro* BMSCs Osteogenic Activity*. Sci Rep. 2017. 7: p. 36129-29.
64. Watanabe, K., Lewis, S., Deguchi, T., Lee, B.S., Kim, D-G., *Effects of estrogen deficiency on jaw bone*. Trans of Orthopaedic Res Society. 2019.
65. Liu, J., Kim, E.K., Zheng, F., Shin, H.S., Kim, Y.R., Kim, D-G., *Multiscale Characterization Of Bone In Estrogen Deficiency*. Trans of Orthopaedic Res Society. 2019.
66. Rux, D.R., Wellik, D.M., *Hox genes in the adult skeleton: Novel functions beyond embryonic development*. Dev Dyn. 2017. **246**(4): p. 310-17.
67. Bradaschia-Correa, V., Leclerc, K., Josephson, A.M., et al. *Hox gene expression determines cell fate of adult periosteal stem/progenitor cells*. Sci Rep. 2019. **9**(1): p. 5043.
68. Rux, D.R., Song, J.Y., Swinehart, I.T., et al. *Regionally Restricted Hox Function in Adult Bone Marrow Multipotent Mesenchymal Stem/Stromal Cells*. Dev Cell. 2016. **39**(6): p. 653-66.

69. Song, J.Y., Pineault, K.M., Dones, J.M., Raines, R.T., Wellik, D.M., *Hox genes maintain critical roles in the adult skeleton*. Proc Natl Acad Sci U S A. 2020. **117**(13): p. 7296-304.
70. Onizuka, S., Yamazaki, Y., Park, S.J., et al. *RNA-sequencing reveals positional memory of multipotent mesenchymal stromal cells from oral and maxillofacial tissue transcriptomes*. BMC Genomics. 2020. **21**(1): p. 417.
71. Nichols, J.T., Pan, L., Moens, C.B., Kimmel, C.B., *barx1 represses joints and promotes cartilage in the craniofacial skeleton*. Development. 2013. **140**(13): p. 2765-75.
72. Zhao, Y., Guo, Y.J., Tomac, A.C., et al. *Isolated cleft palate in mice with a targeted mutation of the LIM homeobox gene *lhx8**. Proc Natl Acad Sci U S A. 1999. **96**(26): p. 15002-06.
73. Xiao, G., Cheng, H., Cao, H., et al. *Critical role of filamin-binding LIM protein 1 (FBLP-1)/migfilin in regulation of bone remodeling*. J Biol Chem. 2012. **287**(25): p. 21450-60.
74. Baron, R., Kneissel, M., *WNT signaling in bone homeostasis and disease: from human mutations to treatments*. Nat Med. 2013. **19**(2): p. 179-92.
75. He, G., Tavella, S., Hanley, K.P., et al. *Inactivation of Six2 in mouse identifies a novel genetic mechanism controlling development and growth of the cranial base*. Dev Biol. 2010. **344**(2): p. 720-30.
76. Mobasheri, A., *Glucose: an energy currency and structural precursor in articular cartilage and bone with emerging roles as an extracellular signaling molecule and metabolic regulator*. Front Endocrinol (Lausanne). 2012. **3**: p. 153.

**Author Contributions:**

**Jie Liu, Keiichiro Watanabe:** Data curation; Investigation; Methodology; Software; Validation; Visualization; Roles/Writing - original draft; Writing - review & editing.

**Shareef Dabdoub:** Data curation; Formal analysis; Investigation; Methodology; Software; Validation; Visualization; Roles/Writing - original draft; Writing - review & editing.

**Beth S. Lee, Do-Gyoon Kim:** Conceptualization; Data curation; Formal analysis; Funding acquisition; Investigation; Methodology; Project administration; Resources; Software; Supervision; Validation; Visualization; Roles/Writing - original draft; Writing - review & editing.

**Highlights**

- Ovariectomy decreased bone quantity and quality of femur while those attributes of mandible were not affected.
- Bone marrow stem cells (BMSCs) from mandible showed greater multi-lineage differentiation than BMSCs from femur.
- Mandibular BMSCs showed higher expression of genes related to osteogenesis than BMSCs from femur.
- Active mandibular BMSCs appear superior to femoral BMSCs in balancing increased bone resorption caused by estrogen deficiency.



Contents lists available at ScienceDirect

## Journal of Biomechanics

journal homepage: [www.elsevier.com/locate/jbiomech](http://www.elsevier.com/locate/jbiomech)  
[www.JBiomech.com](http://www.JBiomech.com)

## Multiscale characterization of ovariectomized rat femur

Jie Liu<sup>a,b</sup>, Eun Kyoung Kim<sup>a</sup>, Ai Ni<sup>c</sup>, Yong-Rak Kim<sup>d</sup>, Fengyuan Zheng<sup>b</sup>, Beth S. Lee<sup>e</sup>,  
Do-kyoon Kim<sup>a,\*</sup><sup>a</sup> Division of Orthodontics, College of Dentistry, The Ohio State University, Columbus, OH 43210, USA<sup>b</sup> Division of Restorative Science and Prosthodontics, College of Dentistry, The Ohio State University, Columbus, OH, USA<sup>c</sup> Division of Biostatistics, College of Public Health, The Ohio State University, Columbus, OH, USA<sup>d</sup> Zachry Department of Civil & Environmental Engineering, Texas A&M University, College Station, TX, USA<sup>e</sup> Department of Physiology and Cell Biology, College of Medicine, The Ohio State University, Columbus, OH 43210, USA

## ARTICLE INFO

## Article history:

Accepted 12 April 2021

## Keywords:

Osteoporosis  
Estrogen  
Matrix mineralization  
Bone micro-CT  
Nanoindentation

## ABSTRACT

Estrogen deficiency activates bone resorbing cells (osteoclasts) and to a lesser extent bone forming cells (osteoblasts), resulting in a gap between resorption and formation that leads to a net loss of bone. These cell activities alter bone architecture and tissue composition. Thus, the objective of this study is to examine whether multiscale ( $10^{-2}$  to  $10^{-7}$  m) characterization can provide more integrated information to understand the effects of estrogen deficiency on the fracture risk of bone. This is the first study to examine the effects of estrogen deficiency on multiscale characteristics of the same bone specimen. Sprague-Dawley female rats (6 months old) were obtained for a bilateral ovariectomy (OVX) or a sham operation (sham). Micro-computed tomography of rat femurs provided bone volumetric, mineral density, and morphological parameters. Dynamic mechanical analysis, static elastic and fracture mechanical testing, and nanoindentation were also performed using the same femur. As expected, the current findings indicate that OVX reduces bone quantity (mass and bone mineral density) and quality (morphology, and fracture displacement). Additionally, they demonstrated reductions in amount and heterogeneity of tissue mineral density (TMD) and viscoelastic properties. The current results validate that multiscale characterization for the same bone specimen can provide more comprehensive insights to understand how the bone components contributed to mechanical behavior at different scales.

© 2021 Elsevier Ltd. All rights reserved.

## 1. Introduction

About 50% of the postmenopausal female population older than 50 years of age shows symptoms of osteoporosis and has a particularly higher risk for fracture than the male population and other age groups (Eastell et al. 2016; Seeman 2003a; 2003b; van Staa et al. 2001). Bone mineral density (BMD) has been widely used to diagnose osteoporosis and estimate the fracture risk of bone (Kanis et al. 1994). However, BMD, which measures mineral in a given bone volume that includes empty spaces, cannot fully explain bone fragility, as both bone architecture and composition play key roles in determining bone strength (Heaney 2003; McCreadie and Goldstein 2000). In contrast, tissue mineral density (TMD) is the mineral content in a unit volume of bone matrix only (Tassani et al. 2011; Yao et al. 2007). Bone cells involved in the high

bone turnover due to estrogen deficiency produce heterogeneous bone matrix at different points in time during postmenopause and inevitably change the TMD distribution (Ames et al. 2010; Marcus 1996; Yao et al. 2007). As the mineral contents are associated with mechanical responses of bone matrix (Mulder et al. 2008; Mulder et al. 2007), it is likely that the abnormal osteoporotic bone matrix has different elastic, plastic, and time-dependent viscoelastic properties from normal healthy bone matrix. These characteristics of bone matrix are critical in maintaining its mechanical stability to resist static and dynamic loading at the organ level of bone (Bart et al. 2014; Donnelly et al. 2010; Kim et al. 2017; Kim et al. 2015; Kim et al. 2018; Shah et al. 2018).

Traditional methodologies directly characterize the irregular shape and heterogeneous composition of bone by measuring elastic stiffness, fracture force, elastic modulus and plastic hardness at the different levels of bone (Donnelly 2011). Recently, we have developed additional novel technologies to analyze TMD distribution and characteristics including static and dynamic elastic, viscoelastic, and plastic mechanical properties at the multiscale of bone in the same individual (Kim et al. 2015; Kim et al. 2018).

\* Corresponding author at: Division of Orthodontics, College of Dentistry, The Ohio State University, 4088 Postle Hall, 305 W. 12th Ave, Columbus, OH 43210, USA.

E-mail address: [kim.2508@osu.edu](mailto:kim.2508@osu.edu) (D.-G. Kim).

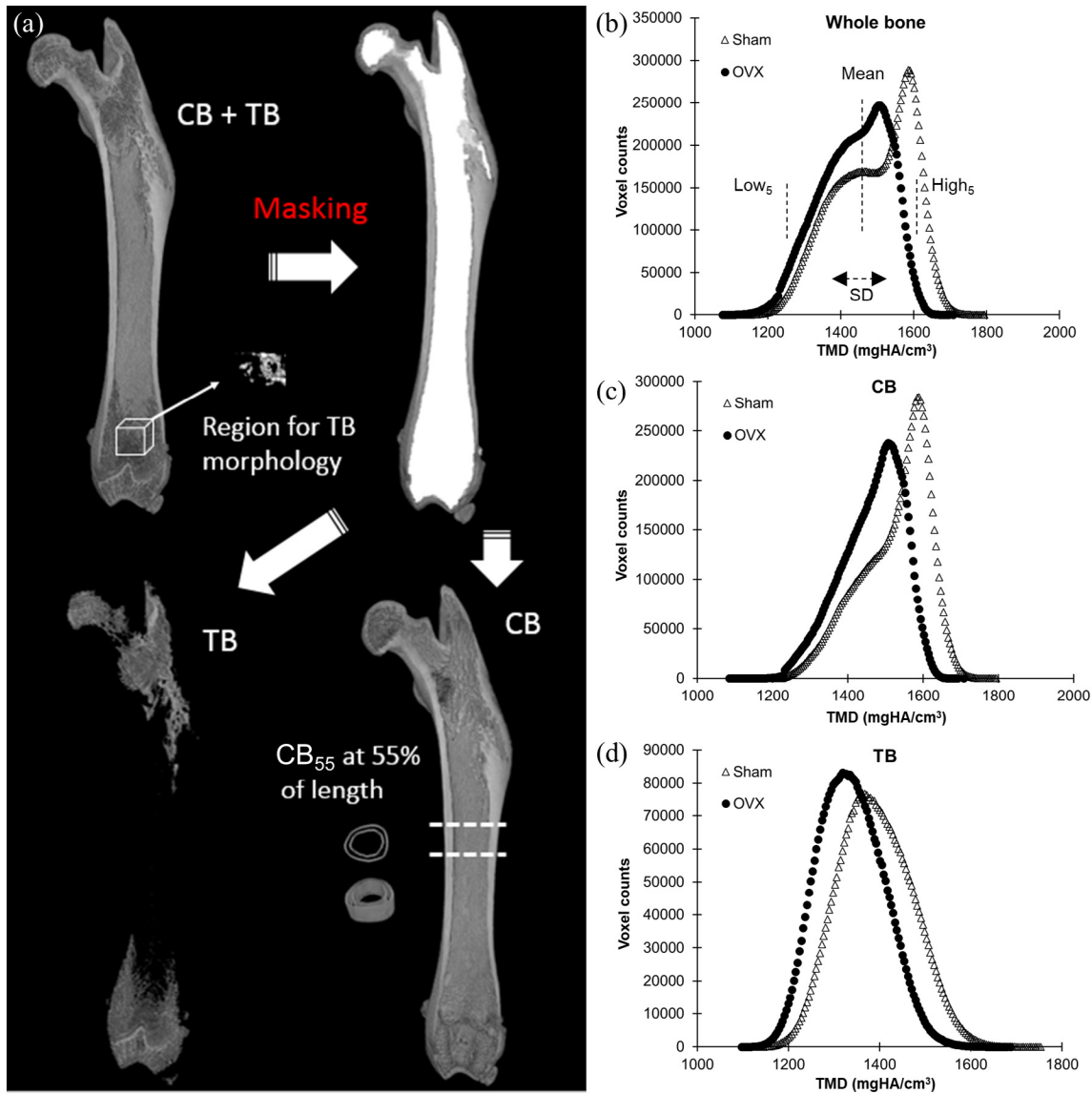


**Fig. 1.** (a) Steps of compartmentation for the 3D micro-CT image of a femoral bone. Masking was performed to identify the bone marrow cavity including trabecular bone (TB). CB<sub>55</sub> (55% of length) was digitally isolated. The total volume was determined, including CB, TB, and masked voxels. The TMD parameters were determined in individual TMD histograms of typical (b) whole bone, (c) CB, and (d) TB for sham and OVX groups.

Thus, the objective of this study is to examine whether the multi-scale ( $10^{-2}$  to  $10^{-7}$  m) characterization can provide more integrated information to understand the effects of estrogen deficiency on the fracture risk of bone. We used a rat model because ovariectomized (OVX) rats have been widely accepted to investigate the etiology of osteoporosis resulting from estrogen deficiency (Chen et al. 2015; Comelekoglu et al. 2007; Fox et al. 2006; Liu et al. 2015).

## 2. Materials and methods

### 2.1. Specimen preparation

Following the protocol approved by Institutional Animal Care and the Use Committee of The Ohio State University, 40 Sprague-Dawley female rats were obtained after a bilateral OVX or a sham operation (sham) at 6 months of age ( $n = 20$  for each group) by Harlan Laboratories (Harlan Laboratories Inc., Indianapolis, IN, USA). After 2 months post-OVX, the rats were euthanized and a femur was randomly obtained from each rat.

### 2.2. Micro-computed tomography (micro-CT)

These femurs were scanned using micro-computed tomography (SkyScan1172-D, Kontich, Belgium) with  $27 \times 27 \times 27 \mu\text{m}^3$  voxel size under an identical scanning condition of 70 kV, 141  $\mu\text{A}$ ,  $0.4^\circ$  rotation per projection, 6 frames averaged per projection, and 210 ms exposure time (Fig. 1). Gray value of each voxel was calibrated to tissue mineral density (TMD) using known density hydroxyapatite (HA) phantoms (1220 and 1540 mg HA/cm<sup>3</sup> with the same dimension of  $\text{Ø}4 \times 5.5$  mm). Bone voxels were segmented from non-bone voxels using a heuristic algorithm (Kim et al. 2012). Bone volume (BV) was obtained by counting the whole bone (WB) voxels. The BMD was assessed by dividing a total sum of TMD in each bone voxel by the total volume (TV) including bone, pores and marrow cavity. Cortical bone (CB) was digitally separated from trabecular bone (TB) by subtracting the masked regions from the whole femur (Buie et al. 2007; Kim et al. 2018; Kim et al. 2012) (Fig. 1a). Mean, standard deviation (SD), coefficient of variation (COV = SD/Mean), Low and High (Low<sub>5</sub> and High<sub>5</sub> for the lower and upper 5th percentile values, respectively) were determined

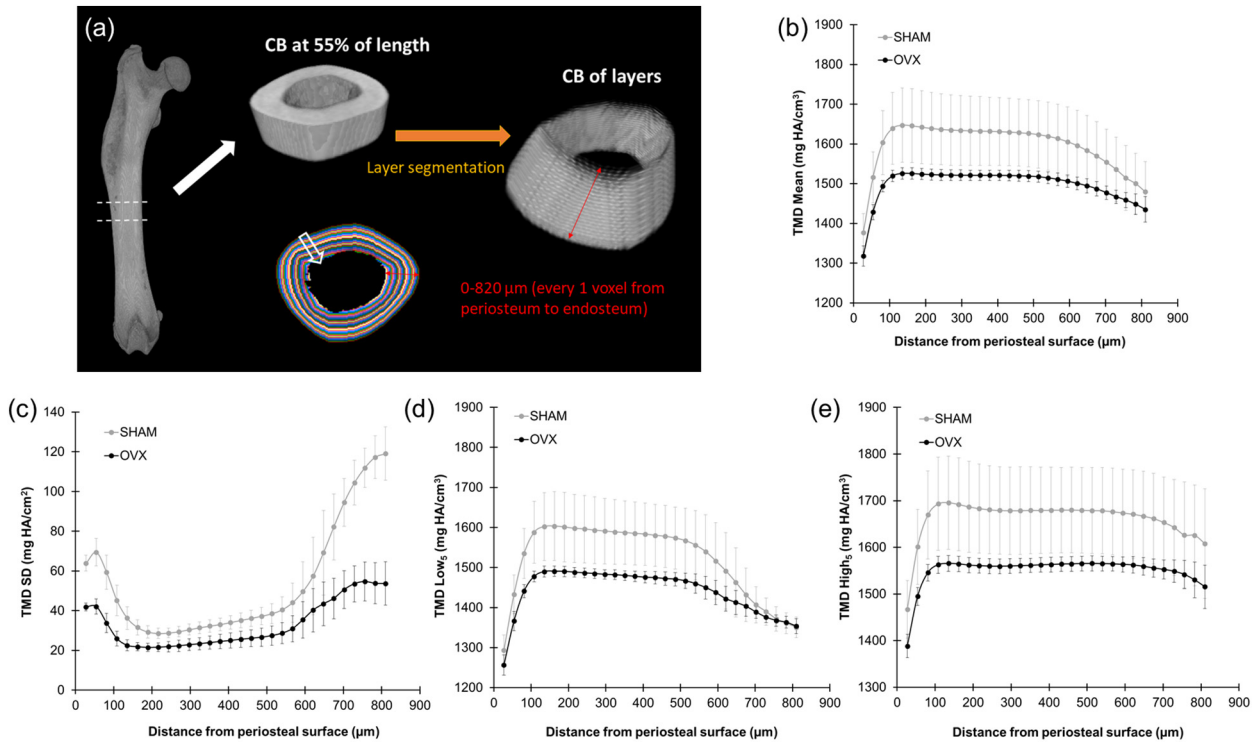


**Fig. 2.** Steps of segmentation for (a) cortical bone (CB<sub>55</sub>, 55% of length) layers from periosteum to endosteum to obtain TMD (b) mean, (c) SD, (d) Low<sub>5</sub>, and (e) High<sub>5</sub>. The OVX group had significantly lower values of all TMD parameters at each distance compared to the sham group ( $p < 0.046$ ), except SD between 350  $\mu\text{m}$  and 540  $\mu\text{m}$ , and Low<sub>5</sub> between 675  $\mu\text{m}$  and 810  $\mu\text{m}$  ( $p > 0.051$ ).

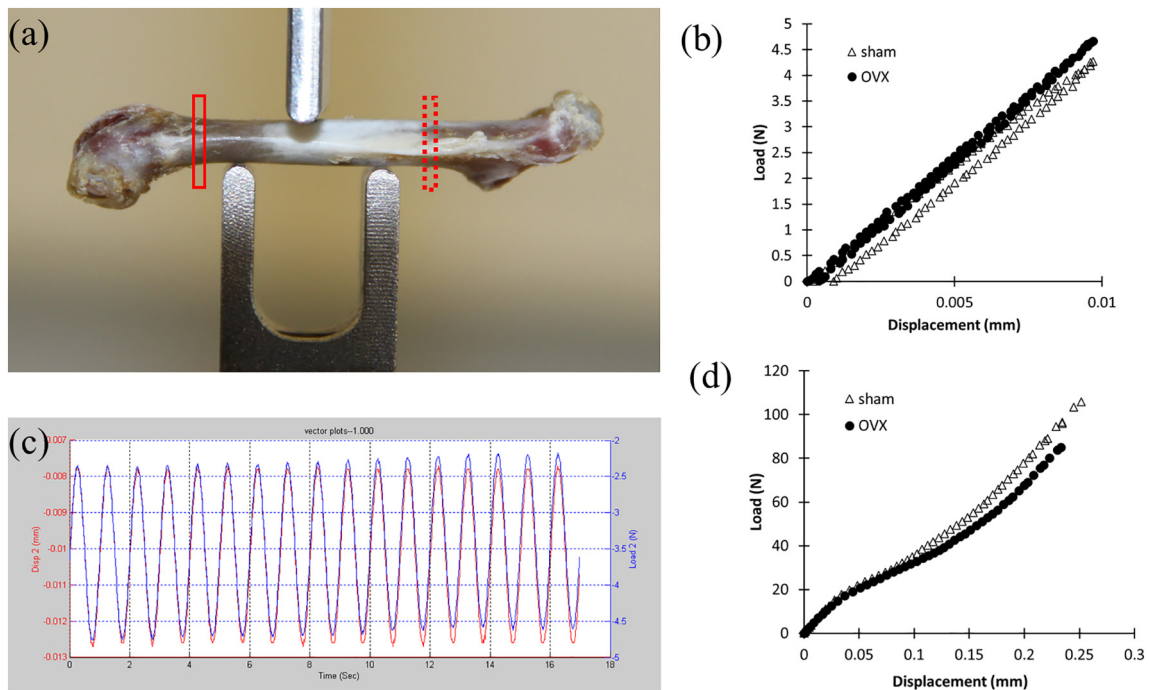


**Fig. 3.** (a) 3-point bending at 55% of femur length from the femoral head, (b) hysteresis (W) computed using a non-destructive load–displacement up to 0.01 mm, (c) non-destructive oscillatory bending displacement using a mean level of 0.01 mm and amplitude of 0.005 mm at the range of 0.5 to 3 Hz of DMA, and (d) static fracture tests for typical femurs of sham and OVX groups. Red dashed lines: nanoindentation locations. (For interpretation of the references to colour in this figure legend, the reader is referred to the web version of this article.)

using TMD histograms for each region (Fig. 1b,c,d). The femur length (Length) from femoral head to distal end was measured by counting axial slices in the micro-CT image. A cross-sectioned

cortical region at 55% (CB<sub>55</sub>) of the femoral length from the head was digitally cut with 50 voxels (1 mm) thickness (Fig. 1a). The parameters of CB<sub>55</sub> were assessed for TMD distribution, cortex

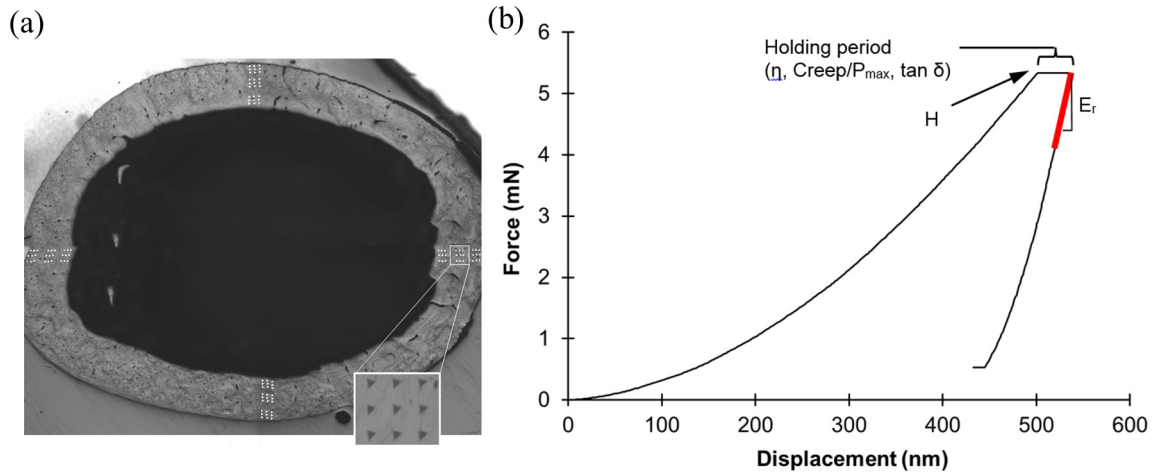


**Fig. 4.** (a) Nanoindentation sites in a femur. Although this figure shows a bigger size with 1000 nm depth of indentation to clearly illustrate the locations, the real size of indentation is smaller (5 to 6  $\mu\text{m}$  width) with 500 nm depth for  $3 \times 3$  array sites for periosteal, core, and endosteal regions of the cortical bone. (b) Elastic modulus ( $E_b$ ), plastic hardness ( $H$ ), static viscoelastic normalized creep ( $\text{Creep}/P_{\text{max}}$ ) and viscosity ( $\eta$ ), and dynamic viscoelastic tangent delta ( $\tan \delta$ ) are provided using a cycle of nanoindentation at the same site of bone matrix.

bone volume ( $BV_{55}$ ), total volume ( $TV_{55}$ ), fraction ( $BV_{55}/TV_{55}$ ), thickness ( $Ct.Th$ ), periosteal perimeter (Periosteal Perimeter55), endosteal perimeter (Endosteal Perimeter55), outer and inner diameters of anterior-posterior axis and medial-lateral axis ( $D_{AP\_outer}$ ,  $D_{AP\_inner}$ ,  $D_{ML\_outer}$ , and  $D_{ML\_inner}$ ), outer diameter ratio (AP/ML), maximum inertia ( $I_{\text{max}}$ ), and minimum inertia ( $I_{\text{min}}$ ). In particular, the axis of minimum inertia is the direction of least bending resistance, which is the AP direction of bending used in the current study. Further, layers of  $CB_{55}$  were segmented by one voxel thickness to obtain TMD parameters from periosteum to endosteum (Fig. 2). A trabecular bone (TB) region ( $0.97 \times 0.97 \times 2.03 \text{ mm}^3$ ) above the growth plate at the distal femoral condyle was digitally isolated to compute TB morphology. Trabecular morphologies including trabecular bone fraction ( $BV/TV_{\text{TB}}$ ), surface-to-volume ratio ( $BS/BV$ ), number (Tb.N), thickness (Tb.Th), and separation (Tb.Sp) were computed.

### 2.3. Dynamic mechanical analysis (DMA) and static fracture testing

After the non-destructive scanning, a series of mechanical testing was performed as described in previous studies (Amorosa et al. 2013; Kim et al. 2017; Kim et al. 2018; Kim et al. 2016). The specimen was kept wet during the whole mounting process on an electromagnetic loading machine (Bose Corporation, Framingham, MA, USA) with a displacement transducer with 15 nm resolution (Fig. 3a). The anterior-posterior loading location was determined at 55% of the femur length from the femoral head. A preload of 10 N was applied to confirm contact between the specimen and loading jig. The  $K$  and  $W$  were assessed by applying a static displacement up to 0.01 mm (Fig. 3b). The DMA used non-destructive oscillatory bending displacement with a mean level of 0.01 mm and amplitude of 0.005 mm at the range of 0.5 to 3 Hz (Fig. 3c). A dynamic complex stiffness ( $K^*$ ) was computed from elastic (storage) ( $K'$ ) and viscous (loss) ( $K''$ ) stiffness with an equation of  $K^* = K' + iK''$ . Tangent delta ( $\tan \delta$ ), which accounts for ability of loading energy dissipation, was computed by  $K''/K'$ . The phase shift ( $\delta$ ) was detected in cyclic load and displacement curve. Following the non-destructive DMA testing, static fracture testing was conducted with a displacement rate of 0.5 mm/second up to fracture. Maximum force and displacement at the fracture point were used to determine strength ( $F_{\text{max}}$ ) and displacement ( $d_{\text{max}}$ ), respectively (Fig. 3d). Toughness ( $U$ ) was obtained by computing area under the load-displacement curve up to the fracture point.

### 2.4. Nanoindentation

After fracture testing, the non-damaged regions of femur outside the jig were dissected and the surface of specimens was polished for nanoindentation (Fig. 4a,b). A pyramidal Berkovich tip for the nanoindenter was used to probe the specimen up to 500 nm deep with a displacement rate of 10 nm/sec (Fig. 4c). The plastic hardness ( $H$ ) was measured at a peak indenting load ( $P_{\text{max}}$ ). The viscosity ( $\eta$ ) and normalized creep ( $\text{Creep}/P_{\text{max}}$ ) were assessed during a 30-second hold period under peak load.  $\tan \delta$  was also assessed by continuous stiffness measurement (CSM) using a phase shift under 45 Hz oscillatory force corresponding to 2 nm of displacement during the 30-second holding period (Kim et al. 2015).  $\tan \delta$  is computed by

$$\delta = \tan^{-1} \left( \frac{\omega C}{K - m\omega^2} \right)$$

where  $\delta$  is a phase angle between the force and displacement signals,  $\omega$  is the oscillation frequency,  $C$  is the damping coefficient of indentation contact,  $K$  is the spring constant of the contact, and  $m$  is the indenter mass. Finally, the elastic modulus ( $E_b$ ) was measured during the unloading period of nanoindentation. As results, the five parameters ( $E_b$ ,  $H$ ,  $\eta$ ,  $\text{Creep}/P_{\text{max}}$  and  $\tan \delta$ ) of elastic, plastic, and viscoelastic mechanical properties could be assessed at the same site of bone matrix using a cycle of nanoindentation.

### 2.5. Statistical analysis

One specimen of the OVX group was lost, one specimen of the sham group had experimental errors during mechanical testing, and distal condyles obtained from 3 specimens of OVX group had been broken at the process of dissecting. As a result, femurs of 19 sham and 16 OVX rats were analyzed. However, 20 sham surgery and 19 OVX rats were included for obtaining  $CB_{55}$  parameters. For assessing DMA and static mechanical parameters, 19 femurs of each group were analyzed.

The current study measured 54 parameters as listed in Table 1. A Student's  $t$ -test was utilized to compare between sham and OVX groups for each parameter except nanoindentation parameters that were analyzed using a linear mixed effect model with individual animal-specific random intercept to account for the intra-specimen correlation. A total of 1396 nanoindentation sites (734 for sham group and 662 for OVX group) was analyzed for each parameter. To test if the within-specimen variance of the nanoin-

**Table 1**

Comparison of measured parameters (mean ± standard deviation) between sham and OVX groups. Significantly different parameters between sham and OVX groups are highlighted in **bold** (p < 0.05). Var: within-specimen variance, heterogeneity.

Parameters	sham	OVX	p value		
Volumetric	BV (mm <sup>3</sup> )	<b>354.470 ± 38.271</b>	<b>325.143 ± 23.213</b>	<b>0.012</b>	
	TV (mm <sup>3</sup> )	508.259 ± 32.689	501.825 ± 29.235	0.547	
	BV/TV	<b>0.698 ± 0.064</b>	<b>0.648 ± 0.020</b>	<b>0.005</b>	
Mineral Density	BV <sub>CB</sub> (mm <sup>3</sup> )	273.720 ± 34.937	257.477 ± 19.623	0.108	
	BV <sub>TB</sub> (mm <sup>3</sup> )	<b>80.750 ± 7.327</b>	<b>67.666 ± 6.831</b>	<b>0.001</b>	
	TMC (mg HA)	<b>533.580 ± 70.226</b>	<b>464.748 ± 32.114</b>	<b>0.001</b>	
	BMD (mg HA/cm <sup>3</sup> )	<b>1050.334 ± 126.482</b>	<b>925.918 ± 28.058</b>	<b>0.001</b>	
	Mean (mg HA/cm <sup>3</sup> )	<b>1502.244 ± 52.102</b>	<b>1429.209 ± 9.998</b>	<b>0.001</b>	
	SD (mg HA/cm <sup>3</sup> )	<b>119.738 ± 22.575</b>	<b>98.821 ± 4.446</b>	<b>0.001</b>	
	COV	<b>0.079 ± 0.012</b>	<b>0.069 ± 0.003</b>	<b>0.003</b>	
	Low <sub>5</sub> (mg HA/cm <sup>3</sup> )	<b>1296.442 ± 23.095</b>	<b>1254.363 ± 11.298</b>	<b>0.001</b>	
	High <sub>5</sub> (mg HA/cm <sup>3</sup> )	<b>1672.154 ± 86.215</b>	<b>1564.623 ± 14.133</b>	<b>0.001</b>	
	Mean <sub>CB</sub> (mg HA/cm <sup>3</sup> )	<b>1531.334 ± 55.486</b>	<b>1454.175 ± 9.931</b>	<b>0.001</b>	
	SD <sub>CB</sub> (mg HA/cm <sup>3</sup> )	<b>112.378 ± 24.170</b>	<b>88.630 ± 4.381</b>	<b>0.001</b>	
	COV <sub>CB</sub> (mg HA/cm <sup>3</sup> )	<b>0.073 ± 0.013</b>	<b>0.061 ± 0.003</b>	<b>0.001</b>	
	Low <sub>5CB</sub> (mg HA/cm <sup>3</sup> )	<b>1315.444 ± 24.533</b>	<b>1281.287 ± 13.521</b>	<b>0.001</b>	
	High <sub>5CB</sub> (mg HA/cm <sup>3</sup> )	<b>1678.632 ± 86.971</b>	<b>1569.751 ± 14.251</b>	<b>0.001</b>	
	Mean <sub>TB</sub> (mg HA/cm <sup>3</sup> )	<b>1403.102 ± 33.124</b>	<b>1336.105 ± 12.643</b>	<b>0.001</b>	
	SD <sub>TB</sub> (mg HA/cm <sup>3</sup> )	<b>83.502 ± 6.864</b>	<b>76.974 ± 3.790</b>	<b>0.002</b>	
	COV <sub>TB</sub> (mg HA/cm <sup>3</sup> )	0.059 ± 0.004	0.058 ± 0.003	0.141	
	Low <sub>5TB</sub> (mg HA/cm <sup>3</sup> )	<b>1272.258 ± 30.482</b>	<b>1214.363 ± 14.668</b>	<b>0.001</b>	
	High <sub>5TB</sub> (mg HA/cm <sup>3</sup> )	<b>1545.189 ± 45.187</b>	<b>1465.647 ± 12.876</b>	<b>0.001</b>	
	Morphology	Length (mm)	36.383 ± 0.674	36.676 ± 1.224	0.377
BV <sub>55</sub> (mm <sup>3</sup> )		8.574 ± 0.789	8.394 ± 0.474	0.432	
TV <sub>55</sub> (mm <sup>3</sup> )		13.594 ± 1.006	13.476 ± 0.757	0.701	
Ct.Th (mm)		0.710 ± 0.072	0.705 ± 0.037	0.836	
D <sub>AP_outer</sub> (mm)		3.171 ± 0.129	3.179 ± 0.092	0.831	
D <sub>ML_outer</sub> (mm)		3.993 ± 0.179	3.974 ± 0.125	0.730	
AP/ML		0.795 ± 0.023	0.800 ± 0.014	0.411	
D <sub>AP_inner</sub> (mm)		1.837 ± 0.245	1.855 ± 0.144	0.801	
D <sub>ML_inner</sub> (mm)		2.495 ± 0.284	2.487 ± 0.161	0.924	
I <sub>max</sub> (mm <sup>4</sup> )		8.541 ± 1.245	8.229 ± 0.786	0.353	
I <sub>min</sub> (mm <sup>4</sup> )		5.687 ± 0.741	5.644 ± 0.616	0.853	
Periosteal Perimeter <sub>55</sub> (mm)		12.080 ± 0.449	12.011 ± 0.331	0.618	
Endosteal Perimeter <sub>55</sub> (mm)		8.789 ± 0.601	8.861 ± 0.361	0.654	
BV/TV <sub>TB</sub>		<b>0.299 ± 0.17</b>	<b>0.069 ± 0.051</b>	<b>0.001</b>	
BS/BV (mm <sup>-1</sup> )		<b>31.872 ± 4.965</b>	<b>43.336 ± 5.191</b>	<b>0.001</b>	
Tb.N (mm <sup>-1</sup> )		<b>2.453 ± 1.278</b>	<b>0.670 ± 0.478</b>	<b>0.001</b>	
Tb.Th (mm)		<b>0.118 ± 0.011</b>	<b>0.096 ± 0.008</b>	<b>0.001</b>	
Tb.Sp (mm)		<b>0.303 ± 0.178</b>	<b>0.552 ± 0.157</b>	<b>0.001</b>	
DMA		K* (N/mm)	517.644 ± 38.899	538.723 ± 28.82	0.068
		K' (N/mm)	517.499 ± 38.905	538.602 ± 29.599	0.068
	K'' (N/mm)	11.839 ± 2.378	11.098 ± 1.789	0.285	
	tan δ	0.023 ± 0.005	0.021 ± 0.003	0.073	
Static Mechanical	W (Nmm)	0.002 ± 0.001	0.001 ± 0.001	0.093	
	K (N/mm)	529.114 ± 75.33	555.026 ± 52.427	0.226	
	F <sub>max</sub> (N)	144.804 ± 24.857	131.814 ± 21.511	0.094	
	d <sub>max</sub> (mm)	<b>0.374 ± 0.072</b>	<b>0.316 ± 0.072</b>	<b>0.019</b>	
Nano-indentation	U (Nmm)	43.341 ± 40.72	26.915 ± 14.984	0.108	
	E <sub>b</sub> (GPa)	Mean	20.693 ± 4.586	19.949 ± 3.953	0.524
		Var	11.228	10.009	0.135
	H (GPa)	Mean	0.735 ± 0.158	0.722 ± 0.136	0.632
		Var	0.018	0.016	0.166
	η (GPa.S)	Mean	46475.28 ± 14095.79	45003.7 ± 11100.94	0.579
		Var	<b>1.37E + 08</b>	<b>1.03E + 08</b>	<b>0.001</b>
	Creep/P <sub>max</sub> (nm/mN)	Mean	8.723 ± 3.412	8.597 ± 2.606	0.725
		Var	<b>7.470</b>	<b>5.996</b>	<b>0.004</b>
	tan δ	Mean	0.048 ± 0.028	0.046 ± 0.021	0.557
Var		<b>0.000539</b>	<b>0.000409</b>	<b>0.001</b>	

dentation parameters is different between sham and OVX groups, a likelihood ratio test was performed based on a mixed effect model assuming heterogeneous residual variance between the two groups, and a mixed effect model assuming homogeneous residual variance. A paired *t*-test was used to compare between CB<sub>55</sub> layers of sham and OVX groups. Since the number of tests is fairly large, false discovery rate (FDR) was examined. FDR is the proportion of significant tests that are false positive. We used the Benjamini-Hochberg procedure (Benjamini and Hochberg 1995) to calculate the *q*-value for each test. The *q* value of a given test can be interpreted as that, if one rejects all null hypotheses with *p* values less than that of the given test, on average 100\**q*% of those null hypotheses will be falsely rejected. Significance was set at *p* < 0.05.

### 3. Results

The OVX group had significantly lower values of BV, BV/TV, BMD, whole and regional TMD, BV/TV<sub>TB</sub>, Tb.N, and Tb.Th than the sham group (*p* < 0.005) while it had significantly higher BS/BV and Tb.Sp (*p* < 0.001). For mechanical testing, the OVX femur group had significantly less fracture displacement and heterogeneity (within-specimen variance) of viscoelastic nanoindentation parameters ( $\eta$ , Creep/*P*<sub>max</sub>, and tan  $\delta$ ) than the sham femur group (*p* < 0.03). All other parameters were not significantly different between sham and OVX groups (*p* > 0.063) (Table 1). The values of CB<sub>55</sub> TMD were significantly lower for the OVX group than the sham group at most of the layers (*p* < 0.042) (Fig. 2b). The *q* values of all significant tests based on the original *p* values were below 0.05. Therefore, we expect <5% of the significant tests to be false positive.

### 4. Discussion

Previous studies using OVX rat models showed that BMD, trabecular morphology, static elastic stiffness and strength, and nanoindentation modulus of femoral bone were altered due to estrogen deficiency (Chen et al. 2015; Comelekoglu et al. 2007; Fox et al. 2006; Liu et al. 2015). However, these properties were partly determined for different rats from several independent studies. As such, it was hard to correlate those previous results obtained under different experimental conditions and draw conclusions to elucidate the effects of estrogen deficiency on bone properties. The multiscale characterization of bone used in the current study was able to determine parameters of TMD distribution and viscoelastic characteristics responsible for controlling mechanical behavior of bone at the multiscale (10<sup>-2</sup> to 10<sup>-7</sup> m) of the same femur as well as those traditional parameters.

Consistent with previous studies (Chen et al. 2015; Comelekoglu et al. 2007; Fox et al. 2006; Liu et al. 2015), the current study found that OVX deteriorates bone quantity and quality of femur, resulting in reduction of its load bearing capacity. The bone quantity is represented by bone mass (TMC and BMD) and bone quality includes regional variations of volume and mineral density distribution, morphology, dynamic and static mechanical responses, and elastic and viscoelastic properties of femur. Previous studies also observed multiscale characterization of bone, indicating that the microscale material behavior plays a critical role in determining skeletal load-bearing ability (Bart et al. 2014; Donnelly et al. 2010; Shah et al. 2018). For example, a previous study (Shah et al. 2018) investigated properties of bone matrix at the nano- and micro-level using the OVX rat model and found that the OVX group diminished BMD but increased bone mass through periosteal apposition compared with the wild-type control rats. However, the authors did not find differences in nanomechanical behavior and mineralized collagen fibrils, indicating that rats

ovariectomized at 3 months undergo simultaneous bone loss and growth, resulting in the effects of OVX being less obvious. In contrast, the study presented here used rats at 6 months of age that are fully matured and have reached social maturity (Adams and Boice 1983; Johnston and Ward 2015), showing the best osteoporotic response by OVX (Francisco et al. 2011). In addition, the effects of estrogen deficiency on bone were observed starting at 2 months following OVX (Lelovas et al. 2008; Wronski et al. 1988). As a result, we also found that the nanoindentation properties were not different between sham and OVX groups, but we show that the distribution of TMD and viscoelastic properties at the tissue level of bone can affect mechanical behaviors at the organ level.

Estrogen deficiency caused by menopause or OVX results in high bone turnover with increased activity of both osteoclasts and osteoblasts. However, bone resorption outpaces formation, leading to net bone loss (Eastell et al., 2016; Seeman 2003a; Wronski et al., 1988). This results in smaller bone volume (BV) and fraction (BV/TV) of OVX animals than those of the sham control group, as observed in the current study. The BMD, which was computed by multiplying the mean value of TMD by BV/TV, also decreased because both TMD and BV/TV were reduced in the OVX group. The lower mean TMD of the OVX group resulted in part from decreases in both Low<sub>5</sub> and High<sub>5</sub> values that shifted the TMD histograms of OVX leftward (Table 1 and Fig. 1). TMD Low<sub>5</sub> values measure mineralization of the 5% least mineralized bone and therefore reflect new bone matrix that is not yet fully mineralized. In contrast, High<sub>5</sub> values measure mineralization of the 5% most mineralized bone and therefore reflect mature bone (Kim et al. 2012; Kim et al., 2015). As such, the decreased Low<sub>5</sub> value of the OVX group indicates an increase in less mineralized, newly formed bone, while the decreased High<sub>5</sub> value indicates greater active resorption of more fully mineralized pre-existing bone tissues. These results likely arose because estrogen deficiency induced rapid bone turnover and increased activity of both osteoblasts and osteoclasts (Eastell et al. 2016; Evans et al. 1994). These patterns of TMD alteration due to OVX were observed regardless of whether cortical or trabecular bone was observed. Therefore, the results demonstrate that analyses of TMD distribution can depict biological activities of bone cells.

A limitation of the current study should be mentioned. We did not aim to clarify the detailed mechanisms of how viscoelastic properties are interrelated with crack initiation and propagation at the bone matrix and development of bone fracture at the organ level. It is accepted that the mineral contents mainly control elastic and plastic responses, while collagen and water are more responsible for determining viscoelastic responses of bone. As such, the viscoelastic behavior of bone likely results from interactions between these components responding to loading. Nair et al. (Nair et al. 2013) simulated that the energy dissipation capacity of the mineral-collagen interactions enables a stick-slip deformation process activated at large deformation. The current study observed that the brittle characteristics of OVX bone could result from decreased heterogeneity of TMD and viscoelastic properties. We speculate that uniform properties of bone matrix could limit local viscoelastic energy dissipation more than heterogeneous properties, thus increasing brittleness. Further studies are certainly needed to integrate these components in understanding the multiscale bone fracture.

Our multiscale characterization included innovative analyses for TMD distribution and viscoelastic characteristics in addition to the traditional BMD, morphology, elastic, and fracture parameters. The current findings indicate that OVX reduces bone quantity (mass and BMD) and quality (TMD distribution, TB morphology, mechanical properties). As the cortical bone morphology at the bending point was not different between sham and OVX groups,

the more brittle property of OVX femur at the organ level likely resulted from its decreased ability to resist deformation at the tissue level compared to the sham control femur. These results are consistent with previous studies that speculated postmenopausal bone becomes brittle, resulting in micro-damage accumulation in the bone tissue and eventual reduction of bone integrity at the organ level (McNamara 2010; Schaffler 2003). The current study investigated direct connections between the multiscale characteristics at the tissue and organ levels using the same age and strain of OVX animals. Therefore, we demonstrate that the brittle characteristics of OVX bone could result from decreased heterogeneity of TMD and viscoelastic properties. Combinations of these characteristics likely increase the risk of micro-crack initiation and propagation at the tissue level under loading at the organ level. Therefore, these results validate that multiscale characterization of the same bone specimen can provide more comprehensive insights to understand how the bone components contributed to mechanical behavior at different levels. These results also allow speculation that if clinical CT analysis can assess BMD distribution in a manner similar to the methodology presented here, these data will suggest additional information on diagnosis of the fracture risk of postmenopausal patients.

### Declaration of Competing Interest

The authors declared that there is no conflict of interest.

### Acknowledgment

The project described here was supported by Grant Number AG033714 from the National Institute on Aging (Kim, D-G) and an American Association of Orthodontists Foundation Award (Kim, D-G). Its contents are solely the responsibility of the authors and do not necessarily represent the official views of the National Institute on Aging.

### References

- Adams, N., Boice, R., 1983. A longitudinal study of dominance in an outdoor colony of domestic rats. *J. Comp. Psychol.* 97 (1), 24–33.
- Ames, M.S., Hong, S., Lee, H.R., Fields, H.W., Johnston, W.M., Kim, D.G., 2010. Estrogen deficiency increases variability of tissue mineral density of alveolar bone surrounding teeth. *Archives Oral Biology*. 55 (8), 599–605.
- Amorosa, L.F., Lee, C.H., Aydemir, A.B., Nizami, S., Hsu, A., Patel, N.R., Gardner, T.R., Navalgund, A., Kim, D.G., Park, S.H., et al., 2013. Physiologic load-bearing characteristics of autografts, allografts, and polymer-based scaffolds in a critical sized segmental defect of long bone: An experimental study. *Int. J. Nanomed.* 8, 1637–1643.
- Bart, Z.R., Hammond, M.A., Wallace, J.M., 2014. Multi-scale analysis of bone chemistry, morphology and mechanics in the oim model of osteogenesis imperfecta. *Connect. Tissue Res.* 55 (Suppl 1), 4–8.
- Benjamini, Y., Hochberg, Y., 1995. Controlling the false discovery rate: A practical and powerful approach to multiple testing. *J. Roy. Stat. Soc.: Ser. B (Methodol.)* 57 (1), 289–300.
- Buie, H.R., Campbell, G.M., Klinck, R.J., MacNeil, J.A., Boyd, S.K., 2007. Automatic segmentation of cortical and trabecular compartments based on a dual threshold technique for in vivo micro-ct bone analysis. *Bone* 41 (4), 505–515.
- Chen, H.L., Tung, Y.T., Chuang, C.H., Tu, M.Y., Tsai, T.C., Chang, S.Y., Chen, C.M., 2015. Kefir improves bone mass and microarchitecture in an ovariectomized rat model of postmenopausal osteoporosis. *Osteoporos. Int.* 26 (2), 589–599.
- Comelekoglu, U., Bagis, S., Yalin, S., Ogenler, O., Yildiz, A., Sahin, N.O., Oguz, I., Hatungil, R., 2007. Biomechanical evaluation in osteoporosis: Ovariectomized rat model. *Clin. Rheumatol.* 26 (3), 380–384.
- Donnelly, E., 2011. Methods for assessing bone quality: A review. *Clin. Orthop. Relat. Res.* 469 (8), 2128–2138.
- Donnelly, E., Chen, D.X., Boskey, A.L., Baker, S.P., van der Meulen, M.C., 2010. Contribution of mineral to bone structural behavior and tissue mechanical properties. *Calcif. Tissue Int.* 87 (5), 450–460.
- Eastell, R., O'Neill, T.W., Hofbauer, L.C., Langdahl, B., Reid, I.R., Gold, D.T., Cummings, S.R., 2016. Postmenopausal osteoporosis. *Nature Reviews Disease Primers*. 2, 16069.
- Evans, G., Bryant, H.U., Magee, D., Sato, M., Turner, R.T., 1994. The effects of raloxifene on tibia histomorphometry in ovariectomized rats. *Endocrinology* 134 (5), 2283–2288.
- Fox, J., Miller, M.A., Newman, M.K., Metcalfe, A.F., Turner, C.H., Recker, R.R., Smith, S. Y., 2006. Daily treatment of aged ovariectomized rats with human parathyroid hormone (1–84) for 12 months reverses bone loss and enhances trabecular and cortical bone strength. *Calcif. Tissue Int.* 79 (4), 262–272.
- Francisco, J.L., Yu, Y., Oliver, R.A., Walsh, W.R., 2011. Relationship between age, skeletal site, and time post-ovariotomy on bone mineral and trabecular microarchitecture in rats. *J. Orthop. Res.* 29 (2), 189–196.
- Heaney, R.P., 2003. Is the paradigm shifting?. *Bone* 33, 457–465.
- Johnston, B.D., Ward, W.E., 2015. The ovariectomized rat as a model for studying alveolar bone loss in postmenopausal women. *Biomed. Res. Int.* 2015, 635023.
- Kanis, J.A., Melton 3rd, L.J., Christiansen, C., Johnston, C.C., Khaltaev, N., 1994. The diagnosis of osteoporosis. *J. Bone Miner. Res.* 9 (8), 1137–1141.
- Kim, D.G., Haghghi, A., Kwon, H.J., Coogan, J.S., Nicoletta, D.P., Johnson, T.B., Kim, H. D., Kim, N., Agnew, A.M., 2017. Sex dependent mechanical properties of the human mandibular condyle. *J. Mech. Behav. Biomed. Mater.* 71, 184–191.
- Kim, D.G., Jeong, Y.H., Kosel, E., Agnew, A.M., McComb, D.W., Bodnyk, K., Hart, R.T., Kim, M.K., Han, S.Y., Johnston, W.M., 2015. Regional variation of bone tissue properties at the human mandibular condyle. *Bone* 77, 98–106.
- Kim, D.G., Jeong, Y.H., McMichael, B.K., Bahler, M., Bodnyk, K., Sedlar, R., Lee, B.S., 2018. Relationships of bone characteristics in myo9b deficient femurs. *J. Mech. Behav. Biomed. Mater.* 84, 99–107.
- Kim, D.G., Kwon, H.J., Jeong, Y.H., Chien, H.H., Crance, S., Agnew, A.M., Battula, S., Lee, J.W., Wen, H.B., 2016. Associations of resonance frequency analysis with dynamic mechanical analysis of dental implant systems. *Clinical Implant Dentistry Related Res.* 18 (2), 332–341.
- Kim, D.G., Navalgund, A.R., Tee, B.C., Noble, G.J., Hart, R.T., Lee, H.R., 2012. Increased variability of bone tissue mineral density resulting from estrogen deficiency influences creep behavior in a rat vertebral body. *Bone* 51 (5), 868–875.
- Lelovas, P.P., Xanthos, T.T., Thoma, S.E., Lyritis, G.P., Dontas, I.A., 2008. The laboratory rat as an animal model for osteoporosis research. *Comp. Med.* 58 (5), 424–430.
- Liu, X.L., Li, C.L., Lu, W.W., Cai, W.X., Zheng, L.W., 2015. Skeletal site-specific response to ovariectomy in a rat model: Change in bone density and microarchitecture. *Clin. Oral Implant Res.* 26 (4), 392–398.
- Marcus, R., 1996. The nature of osteoporosis. *J. Clin. Endocrinol. Metab.* 81 (1), 1–5.
- McCreadie, B.R., Goldstein, S.A., 2000. Biomechanics of fracture: Is bone mineral density sufficient to assess risk?. *J. Bone Miner. Res.* 15 (12), 2305–2308.
- McNamara, L.M., 2010. Perspective on post-menopausal osteoporosis: Establishing an interdisciplinary understanding of the sequence of events from the molecular level to whole bone fractures. *J. R. Soc. Interface* 7 (44), 353–372.
- Mulder, L., Koolstra, J.H., den Toonder, J.M., van Eijden, T.M., 2008. Relationship between tissue stiffness and degree of mineralization of developing trabecular bone. *J. Biomed. Mater. Res. Part A* 84 (2), 508–515.
- Mulder, L., Koolstra, J.H., den Toonder, J.M.J., van Eijden, T.M.G.J., 2007. Intratrabecular distribution of tissues stiffness and mineralization in developing trabecular bone. *Bone* 41, 256–265.
- Nair, A.K., Gautieri, A., Chang, S.W., Buehler, M.J., 2013. Molecular mechanics of mineralized collagen fibrils in bone. *Nat. Commun.* 4, 1724.
- Schaffler MB. 2003. Role of bone turnover in microdamage. *Osteoporosis International*. 14 Suppl 5:S73-77; discussion S77-80.
- Seeman, E., 2003a. Pathogenesis of osteoporosis. *J. Appl. Physiol.* 95, 2142–2151.
- Seeman, E., 2003b. Reduced bone formation and increased bone resorption: Rational targets for the treatment of osteoporosis. *Osteoporos. Int.* 14 (Suppl 3), S2–S8.
- Shah, F.A., Stoica, A., Cardemil, C., Palmquist, A., 2018. Multiscale characterization of cortical bone composition, microstructure, and nanomechanical properties in experimentally induced osteoporosis. *J. Biomed. Mater. Res. Part A* 106 (4), 997–1007.
- Tassani, S., Ohman, C., Baruffaldi, F., Baleani, M., Viceconti, M., 2011. Volume to density relation in adult human bone tissue. *J. Biomech.* 44 (1), 103–108.
- van Staa, T.P., Dennison, E.M., Leufkens, H.G., Cooper, C., 2001. Epidemiology of fractures in England and Wales. *Bone* 29 (6), 517–522.
- Wronski, T.J., Cintron, M., Dann, L.M., 1988. Temporal relationship between bone loss and increased bone turnover in ovariectomized rats. *Calcif. Tissue Int.* 43 (3), 179–183.
- Yao, W., Cheng, Z., Koester, K.J., Ager, J.W., Balooch, M., Pham, A., Chefo, S., Busse, C., Ritchie, R.O., Lane, N.E., 2007. The degree of bone mineralization is maintained with single intravenous bisphosphonates in aged estrogen-deficient rats and is a strong predictor of bone strength. *Bone* 41, 804–812.

Contents lists available at [ScienceDirect](https://www.sciencedirect.com)

Journal of the Mechanical Behavior of Biomedical Materials

journal homepage: <http://www.elsevier.com/locate/jmbbm>

## Regional variations of jaw bone characteristics in an ovariectomized rat model

Keiichiro Watanabe<sup>a</sup>, Samantha Lewis<sup>a</sup>, Xiaohan Guo<sup>b</sup>, Ai Ni<sup>b</sup>, Beth S. Lee<sup>c</sup>, Toru Deguchi<sup>a</sup>, Do-Gyoon Kim<sup>a,\*</sup>

<sup>a</sup> Division of Orthodontics, College of Dentistry, The Ohio State University, Columbus, OH, 43210, USA

<sup>b</sup> Division of Biostatistics, College of Public Health, The Ohio State University, Columbus, OH, 43210, USA

<sup>c</sup> Department of Physiology and Cell Biology, College of Medicine, The Ohio State University, Columbus, OH, 43210, USA

### ARTICLE INFO

#### Keywords:

Jaw bone  
Rat  
Ovariectomy  
Tissue mineral density  
Nanoindentation

### ABSTRACT

Postmenopausal osteoporosis causes severe loss of bone quantity and quality in limb bone but has a lesser effect on jaw bone. Thus, the objective of this study was to examine whether ovariectomy (OVX) and mastication alter the regional variation of jaw bone characteristics. Sprague-Dawley female rats (6 months) were given a bilateral OVX or a sham operation (SHAM) ( $n = 10$  for each group). After 2 months post-OVX, the hemi-mandible from each rat was dissected. A micro-computed tomography based mean, standard deviation (SD), the lower and upper 5th percentile (Low<sub>5</sub> and High<sub>5</sub>) values of tissue mineral density (TMD) histograms were assessed for whole bone (WB), alveolar bone (AB), cortical bone (CB), and trabecular bone (TB) regions. Morphology of TB and periodontal ligament (PDL) was also obtained. Layers of AB were segmented up to 400  $\mu\text{m}$  from the PDL. Mechanical properties at the tissue level were measured by nanoindentation at the same site by a single loading-unloading cycle of indentation in hydration. The AB and TB regions had significantly lower TMD Mean, Low<sub>5</sub>, and High<sub>5</sub> but higher SD than the CB region for both sham and OVX groups ( $p < 0.01$ ). TMD parameters of the OVX group rapidly increased up to 60  $\mu\text{m}$  away from the PDL and were significantly higher than those of the sham group starting at 280  $\mu\text{m}$  and farther in the CB region ( $p < 0.05$ ). All values of morphological and nanoindentation parameters were not significantly different between sham and OVX groups ( $p > 0.06$ ). Estrogen deficiency induced by OVX did not deteriorate bone characteristics including mineral density, morphology, and nanoindentation parameters in rat mandibles. Masticatory loading had an effect on the TMD parameters at the limited region of AB. These results provide insight into why osteoporosis-associated jaw bone fractures are extremely rare.

### 1. Introduction

Postmenopausal bone loss is a severe disorder that places up to 50% of women at the risk of fracture after menopause (Eastell et al., 2016; Kaye, 2007; NIH Consensus Development Panel on Osteoporosis Prevention and Therapy, 2001). Approximately 30% of postmenopausal women have spontaneous or low-impact fractures of vertebra or hip in their lifetime. However, osteoporosis-associated atraumatic fractures of the jaw bone are extremely rare. It has been speculated that osteoporosis causes a higher risk of tooth loss for elderly women than men (Buen-camino et al., 2009; Kaye, 2007; Kribbs et al., 1990), but many more studies have shown no correlations between tooth loss and bone mineral density (BMD) of the jaws in postmenopausal patients (Earnshaw et al.,

1998; Elders et al., 1992; Famili et al., 2005; Klemetti et al., 1993; Mattson et al., 2002; Naitoh et al., 2007; Pilgram et al., 1999).

Postmenopausal osteoporosis develops due to loss of ovarian estrogen production with age (Eastell et al., 2016; Seeman, 2003). Estrogen deficiency increases differentiation and activities of bone resorptive cells (osteoclasts) and suppresses the function of bone forming cells (osteoblasts), resulting in bone loss (Eastell et al., 2016). Ovariectomized (OVX) animal models have been widely used to investigate the etiology of postmenopausal osteoporosis resulting from estrogen deficiency (Johnston and Ward, 2015; Lelovas et al., 2008; Turner et al., 2001). The OVX rat model in particular is approved by the Food and Drug Administration (FDA) for investigation of new therapeutic agents (Thompson et al., 1995). While a great volume of studies has shown the

\* Corresponding author. Division of Orthodontics, College of Dentistry, The Ohio State University, 4088 Postle Hall, 305 W. 12th Ave, Columbus, OH, 43210, USA.  
E-mail address: [kim.2508@osu.edu](mailto:kim.2508@osu.edu) (D.-G. Kim).

<https://doi.org/10.1016/j.jmbbm.2020.103952>

Received 18 March 2020; Received in revised form 21 June 2020; Accepted 22 June 2020

Available online 29 June 2020

1751-6161/© 2020 Elsevier Ltd. All rights reserved.

substantial effects of estrogen deficiency on vertebral and limb bones of the OVX rat model, its effects on jaw bone have not been fully clarified. In fact, a recent review indicated that all of the eight previous studies that investigated jaw BMD of OVX rat models showed no decrease or less than 10% decrease of mandibular BMD (Johnston and Ward, 2015). While the insensitivity of estrogen deficiency-dependent osteoporosis for jaw bone has not been fully elucidated, it was suggested that masticatory functional demands in jaw may protect against bone loss in postmenopause (Mavropoulos et al. 2004, 2007). However, these results were obtained from a limited region of alveolar bone surrounding teeth, where dynamic masticatory impact force is directly transmitted through teeth and periodontal ligament (PDL).

The previous studies focused on measuring traditional BMD using imaging devices that could not provide sufficient resolution to assess mineral density distribution at the tissue level of small OVX animal jaw bones (Johnston and Ward, 2015). The BMD includes not only mineralized bone tissues but also marrow and porosity between bone tissues. On the other hand, estrogen deficiency activates bone remodeling that produces rapid bone turnover by increasing removal of pre-existing (more mineralized) bone tissue while adding immature (less mineralized) bone tissue (Busse et al., 2009; Kim et al., 2012). As such, a regional variation of tissue mineral density (TMD) can provide more dynamic information to elucidate the process of mineralization than the overall value of BMD. It has been also observed that the TMD is responsible for determining mechanical characteristics of bone tissue (Ferguson et al., 2003; Mulder et al., 2007). Thus, the objective of this study was to examine whether OVX and mastication alter the regional variation of jaw bone characteristics. The bone characteristics include mineral density, morphology, and nanoindentation parameters in rat mandibles.

## 2. Materials and methods

### 2.1. Specimen preparation

All experiments were approved by the Institutional Animal Care and Use Committee of The Ohio State University. Twenty 6-month-old female Sprague-Dawley rats were used. Ten rats were bilaterally ovariectomized (OVX) and the other 10 rats received a sham surgery (SHAM) at Harlan Laboratories (Harlan Laboratories Inc, Indianapolis, IN, USA). Following 2 months after surgery, an intraperitoneal injection of calcein (25 mg/kg, Sigma-Aldrich Co., St. Louis, MO, USA) was conducted 3 days before euthanization. Animals were euthanized by intraperitoneal injection of an overdose of pentobarbital sodium (100 mg/kg). A hemi-mandible was randomly chosen from each rat and soft tissues were removed. A 5 mm section of molar region was dissected in the bucco-lingual direction of the mandible using two parallel diamond blades of a low speed saw under irrigation (Fig. 1a). These sections of teeth-bone constructs were wrapped in normal saline-soaked gauze and frozen at  $-20^{\circ}\text{C}$  until use.

### 2.2. Micro-computed tomography (micro-CT)

After the mandibles were thawed at a room temperature, the specimens were scanned and reconstructed by a micro-CT (Inveon, Siemens, Malvern, PA, USA) with  $20 \times 20 \times 20 \mu\text{m}^3$  voxel size under identical scanning conditions of 80 kV, 500  $\mu\text{A}$ , and 600 ms exposure time. All parameters obtained by the current study are described in Table 1. The region of interest was determined by digitally cutting the mandible in the bucco-lingual direction with 3.4 mm width starting from the center of first molar to the mesio-distal direction using Image J software (NIH) (Fig. 1a). A heuristic algorithm was used to segment bone voxels from non-bone voxels (Kim et al. 2012, 2018; Zael et al., 2004). The teeth, including incisor and periodontal ligament (PDL), were digitally extracted (Fig. 1a). All bone and non-bone voxels in the cortical and internal trabecular regions of the mandible were maintained to mask the

trabeculae and marrow cavity using a compartmentalizing method (Buie et al., 2007; Kim et al. 2012, 2018). Whole bone (WB) measurements were obtained by multiplying the total number of segmented bone voxels by the voxel size. Alveolar bone (AB) was identified as the region within 100  $\mu\text{m}$  from the PDL. Trabecular bone (TB) was isolated as the region between molar roots and incisor by masking. The cortical bone (CB) region was determined inside of the WB by 3-dimensional eroding 200  $\mu\text{m}$  (10 voxels) from internal and external surfaces of bone. Layers of bone were segmented by one voxel for 0–120  $\mu\text{m}$  from the PDL or two voxels for 120–400  $\mu\text{m}$  from the PDL (Fig. 2a).

Tissue mineral density (TMD) of each bone voxel was obtained using CT attenuation that was calibrated using known densities of commercial phantoms provided by the micro-CT company. A total sum of TMD in each bone voxel produces total mineral content (TMC). A total volume (TV) of WB was the sum of voxels, combining cortical and masked regions of the mandible (Fig. 1a). Then, bone mineral density (BMD) of the WB was assessed by dividing the TMC by the TV. Histograms of TMD were obtained (Fig. 1b-f). A mean of TMD (Mean) was an average of the TMC in the bone volume of each region. Standard deviation (SD) of the histogram accounted for heterogeneity of TMD distribution. Low and high TMD (Low<sub>5</sub> and High<sub>5</sub>) values were determined at lower and upper 5th percentile values of TMD histogram, respectively. Architectural parameters of TB were computed using the same dimension of the region of interest ( $0.64 \times 0.64 \times 0.64 \text{ mm}^3$ ). Trabecular bone fraction (BV/TV), surface-to-volume ratio (BS/BV), and trabecular number (Tb.N), thickness (Tb.Th), and separation (Tb.Sp) were calculated from the segmented micro-CT images using a commercial morphological code (CTAn, SkyScan, Kontich, Belgium). The mean, maximum (Max), and standard deviation (SD) of PDL thickness were measured using the local thickness function of Image J software (NIH) after isolating it between teeth and AB.

### 2.3. Nanoindentation

Following the non-destructive micro-CT scanning, a hemi-mandible was randomly chosen from each rat and tooth-bearing 5 mm mandibular bone sections were cut using a low speed saw (Buehler, Lake Bluff, IL) under water irrigation. The dissected surfaces of the mandible were polished using silicon carbide abrasive papers with decreasing grit sizes (800, 1200, and 1500 grits) and  $\text{Al}_2\text{O}_3$  pastes (1.0 and 0.3  $\mu\text{m}$ ) on soft polishing cloths in a wet condition using a normal saline solution. The specimens were subsequently sonicated in deionized water to remove debris.

The polished specimens were placed on a polycarbonate holder and mounted into a fluid drainage system on a nanoindenter (Nano-XP, MTS, Oakridge, TN) as described in previous studies (Huja et al., 2006; Kim et al. 2010, 2013, 2015). A high resolution x-y motorized stage with an accuracy level of 0.5  $\mu\text{m}$  was controlled by an operating software to move the specimen to the indent locations (Fig. 3a). A pyramidal Berkovich tip was used to indent sites at least 50  $\mu\text{m}$  apart to prevent any interruptions with the adjacent indents. All nanoindentations were performed in hydration using the fluid drainage system as introduced in previous studies (Kim et al. 2010, 2013). The indenter was probed under load control corresponding to a displacement rate of 50 nm/s, up to 500 nm depth (Fig. 3b). This indentation depth was determined to surpass the effect of surface roughness on measurements (Hoffler et al., 2005). Following holding for 30 s under a constant peak load, the indenter was unloaded at the same displacement rate. The 30-s holding period was set to reduce viscoelastic errors in assessing elastic modulus during unloading (Fan and Rho, 2003). The current study assessed viscoelastic energy that is released during this period to measure the viscoelastic properties of the specimens. As a result, elastic modulus ( $E_b$ ), plastic hardness (H), static viscoelastic normalized creep (Creep/ $P_{\text{max}}$ ) and viscosity ( $\eta$ ), and dynamic viscoelastic tangent delta ( $\tan \delta$ ) could be obtained by a cycle of nanoindentation at the same site of bone tissue.

The contact hardness (H) was computed by Eq. (1).

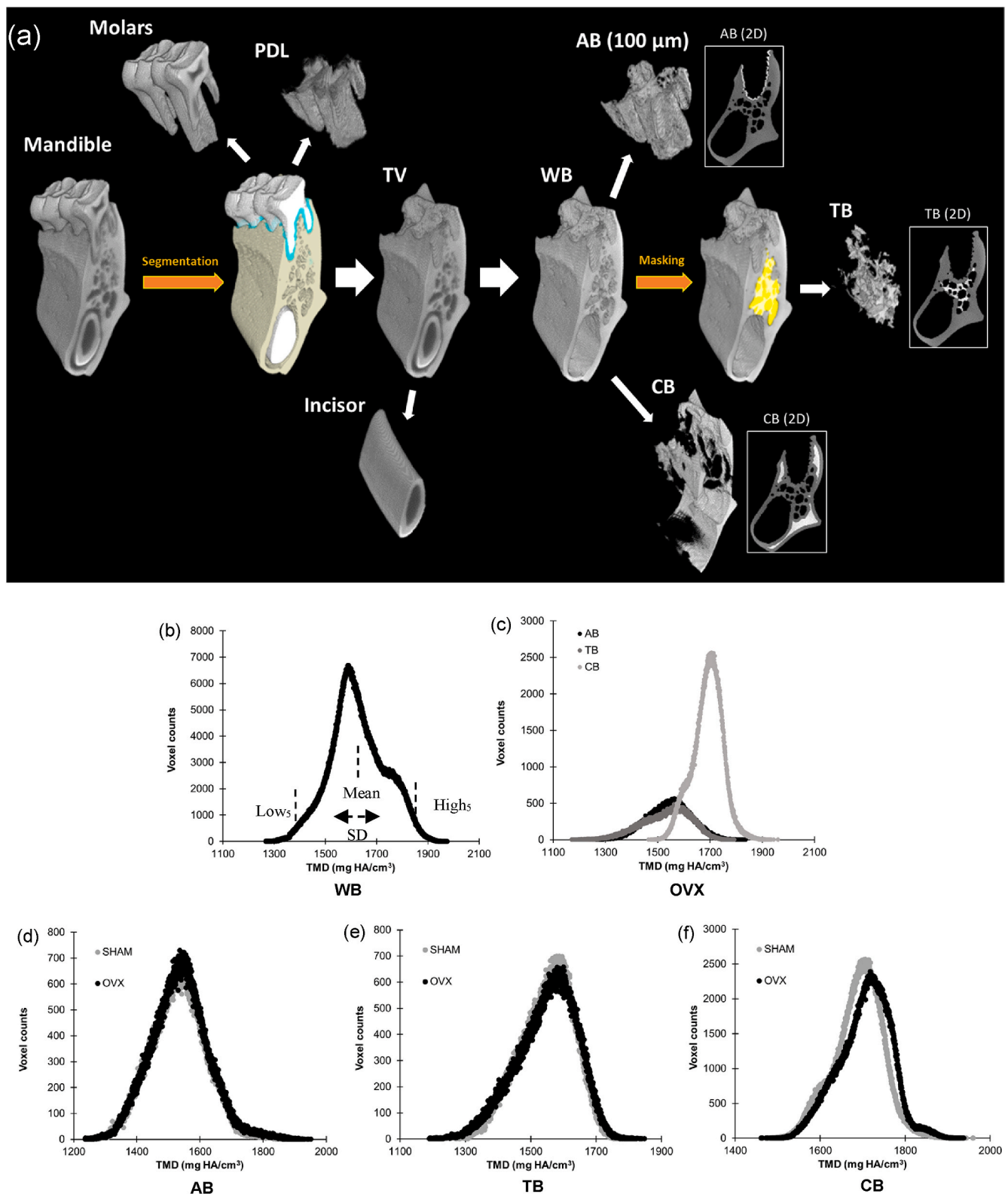


**Fig. 1.** (a) Steps of compartmentation for the 3D micro-CT image of a mandible. The whole bone (WB) was determined by removal of teeth and periodontal ligament (PDL). Alveolar bone (AB) was identified as the region up to 100  $\mu\text{m}$  from the PDL. Masking was used to isolate the bone marrow cavity, including trabecular bone (TB). The cortical bone (CB) region was located at 200  $\mu\text{m}$  from the bone surface. Tissue mineral density (TMD) parameters were determined in individual histograms of typical (b) whole bone. (c) Regional variation of TMD distribution in the mandibular bone. TMD distributions of (d) AB, (e) TB, and (f) CB for sham and OVX groups.

**Table 1**  
Nomenclature of each parameter.

Parameters	Description	
Mineral Density	BMD (mg HA/cm <sup>3</sup> )	WB mineral density
	Mean (mg HA/cm <sup>3</sup> )	mean values of tissue mineral density (TMD)
	SD (mg HA/cm <sup>3</sup> )	standard deviations of TMD histogram
	Low <sub>5</sub> (mg HA/cm <sup>3</sup> )	lower 5th percentile values of TMD histogram
	High <sub>5</sub> (mg HA/cm <sup>3</sup> )	higher 5th percentile values of TMD histogram
Morphology	BV/TV	trabecular bone fraction
	BS/BV (mm <sup>-1</sup> )	trabecular surface-to-volume ratio
	Tb.N (mm <sup>-1</sup> )	trabecular number
	Tb.Th (mm)	trabecular thickness
	Tb.Sp (mm)	trabecular separation
	PDL Thickness Mean (mm)	mean values of periodontal ligament (PDL) thickness
	PDL Thickness SD (mm)	standard deviations of PDL thickness
Nano-indentation	E <sub>b</sub> (GPa)	nanoindentation elastic modulus of bone
	H (GPa)	hardness
	η (GPa·S)	internal friction to resist a flow
	Creep/P <sub>max</sub> (nm/mN)	normalized viscoelastic creep at the peak load (P <sub>max</sub> )
	tan δ	ability of viscoelastic energy dissipation at the tissue

$$H = \frac{P_{max}}{A} \quad (\text{Eq. 1})$$

where  $P_{max}$  is the peak indenting load (mN) and  $A$  is the projected indenting contact area (mm<sup>2</sup>) that is computed using the indent depth during the unloading process at the indented site (Roy et al., 1999).

Creep was estimated using the displacement-time curve during the 30-s holding period, which was fit to the traditional viscoelastic Voigt model (Eq. (2)).

$$h^2(t) = \frac{\pi}{2} P_{max} \cot \alpha \left[ \frac{1}{E_2} (1 - e^{-tE_2/\eta}) \right] \quad (\text{Eq. 2})$$

where  $h(t)$  is creep (nm) as a function of time,  $\alpha$  is face angle (65.27°) of the Berkovich indenter (Fischer-Cripps, 2004),  $E_2$  (GPa) is an elastic component and  $\eta$  is an indentation viscosity (GPa·S) that account for a resistance to viscous deformation. As the peak load changes depending on the intrinsic properties of bone tissue, the amount of creep was normalized by the peak load (Creep/P<sub>max</sub>) to minimize the effects due to different loading levels between specimens.

The indenter can generate a harmonic oscillatory force corresponding to 2 nm of displacement at 45 Hz using a special function of continuous stiffness measurements (CSM). Thus, tangent delta (tan δ) during the 30-s holding period was able to be obtained using the CSM function with Eq. (3).

$$\delta = \tan^{-1} \left( \frac{\omega C}{K - m\omega^2} \right) \quad (\text{Eq. 3})$$

where  $\delta$  is a phase angle between the force and displacement signals,  $\omega$  is the angular frequency,  $C$  is the damping coefficient of indentation contact,  $K$  is the spring constant of the contact, and  $m$  is the indenter mass. Potential errors were corrected to accurately compute tan δ (Herbert et al., 2013).

Nanoindentation elastic modulus ( $E_b$ ) was measured by Eq. (4) (Oliver and Pharr, 1992).

$$\frac{1}{E_r} = \frac{(1 - \nu_b^2)}{E_b} + \frac{(1 - \nu_i^2)}{E_i} \quad (\text{Eq. 4})$$

where  $E_r$  (reduced modulus) is the slope of unloading force-displacement curve. For the diamond indenter, typical values used for

$E_i$  is 1141 GPa and Poisson's ratio ( $\nu_i$ ) is 0.07. The  $\nu_b$  of bone is assumed 0.3 (Huja et al., 2007).  $E_b$  is the elastic modulus of bone tissue to be determined. After nanoindentation, calcein labeled regions on the specimen surface were identified using a Leica fluorescent microscope (Buffalo Grove, IL, USA).

#### 2.4. Statistical analysis

Twenty hemi-mandibles (10 sham and 10 OVX) were randomly obtained. The current study measured 26 parameters as listed in Table 2. Linear mixed effect models were performed for the TMD parameters (Mean, SD, Low<sub>5</sub>, High<sub>5</sub>) with region, group, and their interaction as the covariates. A Student's t-test was utilized to compare between sham and OVX groups for each parameter, including BMD and morphology (BV/TV<sub>TB</sub>, BS/BV, Tb.N, Tb.Th, Tb.Sp, PDL Thickness). Paired t-tests were performed to compare TMD parameters between layers of AB.

Nanoindentation parameters ( $E_b$ , H, η, Creep/P<sub>max</sub>, and tan δ) were analyzed using a linear mixed effect model with individual animal-specific random intercept to account for the intra-specimen correlation. A total of 356 nanoindentation sites (174 for sham and 182 for OVX groups) was analyzed for each nanoindentation parameter. To test if the within-specimen standard deviation of the nanoindentation parameters is different between groups, a likelihood ratio test was performed based on a mixed effect model assuming heterogeneous residual variance between the groups and a mixed effect model assuming homogeneous residual variance. Significance was set at  $p < 0.05$ .

### 3. Results

The regions of mandibular bone were successfully isolated in the process of compartmentation for the 3D micro-CT images to obtain TMD histograms (Fig. 1). Interactions between groups (Sham and OVX) and regions (AB, TB, CB) were significant for TMD Low<sub>5</sub> ( $p = 0.003$ ) and marginally significant for TMD Mean and SD ( $p = 0.079$  and  $0.075$ , respectively) but not significant for TMD High<sub>5</sub> ( $p = 0.65$ ). The AB and TB regions had significantly lower TMD values of Mean, Low<sub>5</sub> and High<sub>5</sub> but higher SD than the CB region for both sham and OVX groups ( $p < 0.02$ ) (Fig. 4). The AB region had a significantly higher Low<sub>5</sub> value than the TB region in the OVX group ( $p = 0.04$ ) while all other TMD values were not significantly different between AB and TB regions ( $p > 0.1$ ).

The OVX group had significantly higher TMD Mean values for CB and WB regions, Low<sub>5</sub> value for CB region, and High<sub>5</sub> value for WB region ( $p < 0.02$ ), with marginally higher TMD SD value for WB region and High<sub>5</sub> value for CB region ( $p < 0.08$ ), compared to the sham group (Table 2). All other TMD parameters did not have significantly different values between sham and OVX groups ( $p > 0.09$ ). The values of TMD parameters rapidly increased up to 60 μm away from PDL (Fig. 2d), corresponding to the newly mineralized alveolar bone region as shown with calcein labels adjacent to the PDL (Fig. 2b,c). The TMD Mean, High<sub>5</sub>, and SD values of the OVX group were significantly higher than those of the sham group at 280 μm and farther distances away from the PDL ( $p < 0.05$ ) while Low<sub>5</sub> was not significantly different at any distance ( $p > 0.58$ ).

All values of morphological and nanoindentation parameters were not significantly different between sham and OVX groups ( $p > 0.06$ ).

### 4. Discussion

The mandibles used in the current study were obtained from the same rats examined in a previous study that showed significant decrease in BMD, BV/TV, and Tb.Th of vertebrae following OVX (Kim et al., 2012), demonstrating the validity of this animal model. Rats at 6 months of age show the best osteoporotic response by OVX (Francisco et al., 2011) and osteoporosis progressively develops in limb bone up to 3 months following OVX (Lelovas et al., 2008; Wronski et al., 1988). In contrast, the current study shows that OVX has no deleterious effect on

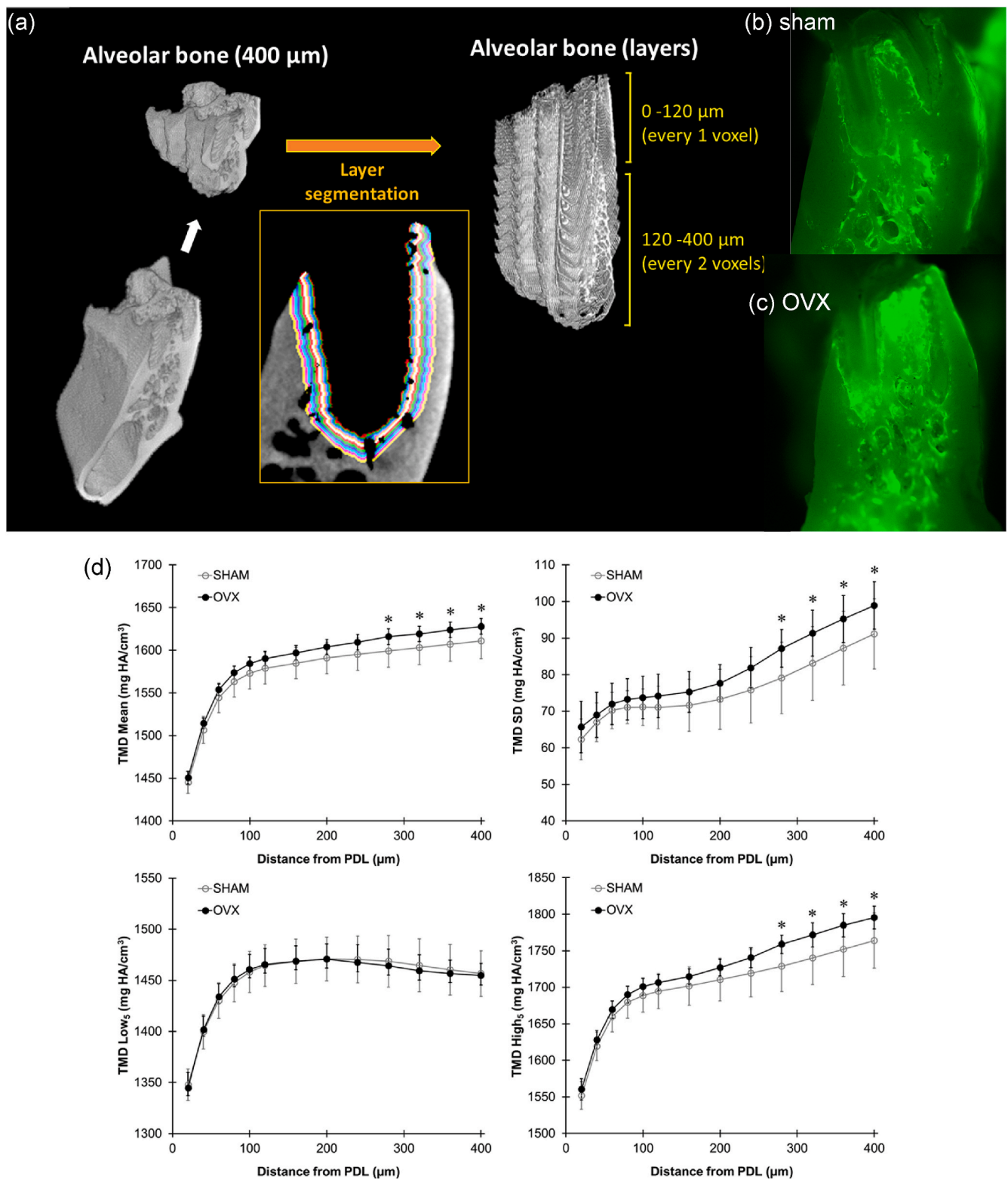


**Fig. 2.** (a) Steps of segmentation for alveolar bone layers up to 400 μm from the periodontal ligament (PDL). The first six layers, between 0 and 120 μm from the PDL, were segmented by one voxel layer (20 μm), and the next fourteen layers, between 120 and 400 μm from the PDL, were segmented by two voxel layers (40 μm). Fluorescent microscopic image for calcein labels (magnification × 10) of (b) sham group and (c) OVX group. Calcein labeled regions identified newly mineralized bone tissues. (d) Tissue mineral density (TMD) parameters measured at each layer. All parameters were significantly different between distances ( $p < 0.01$ ). TMD rapidly increased up to 60 μm from the PDL. The TMD Mean, High<sub>5</sub>, and SD of OVX group were significantly higher than those of sham group starting at 280 μm from the PDL ( $p < 0.05$ ).

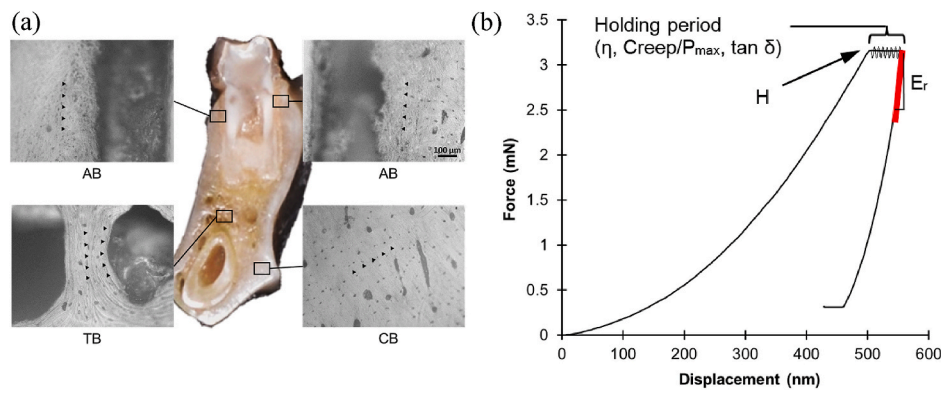


Fig. 3. (a) Nanoindentation sites in a mandible. (b) Elastic modulus ( $E_b$ ), plastic hardness (H), static viscoelastic normalized creep ( $Creep/P_{max}$ ) and viscosity ( $\eta$ ), and dynamic viscoelastic tangent delta ( $\tan \delta$ ) were provided using a cycle of nanoindentation at the same site of bone tissue.

Table 2

Comparison of measured parameters between sham and OVX groups ( $n = 10$  for each group, mean  $\pm$  standard deviation) of mandibular bone regions including alveolar (AB), cortical (CB), trabecular (TB), and whole (WB) bones. Marginally significant and significant differences are highlighted in **bold** and *italic bold*, respectively. Var: within-specimen variance, heterogeneity.

Parameters	Region	Sham	OVX	p value			
Mineral Density	BMD (mg HA/cm <sup>3</sup> )	WB	1003.56 $\pm$ 41.92	1015.12 $\pm$ 24.79	0.46		
		AB	1529.96 $\pm$ 16.35	1538.90 $\pm$ 7.15	0.13		
	TMD Mean (mg HA/cm <sup>3</sup> )	TB	1536.73 $\pm$ 18.72	1542.86 $\pm$ 10.49	0.38		
		<b>CB</b>	<b>1690.11 <math>\pm</math> 17.24</b>	<b>1707.84 <math>\pm</math> 12.55</b>	<b>0.02</b>		
		<b>WB</b>	<b>1623.29 <math>\pm</math> 15.1</b>	<b>1639.03 <math>\pm</math> 8.92</b>	<b>0.01</b>		
		AB	82.08 $\pm$ 4.55	85.15 $\pm$ 4.84	0.16		
	TMD SD (mg HA/cm <sup>3</sup> )	TB	83.42 $\pm$ 9.61	89.12 $\pm$ 9.07	0.19		
		CB	68.23 $\pm$ 6.07	66.05 $\pm$ 4.99	0.39		
		<b>WB</b>	<b>107.68 <math>\pm</math> 7.11</b>	<b>113.01 <math>\pm</math> 5.11</b>	<b>0.07</b>		
		AB	1393.10 $\pm$ 14.82	1394.27 $\pm$ 11.56	0.85		
	TMD Low <sub>5</sub> (mg HA/cm <sup>3</sup> )	TB	1387.37 $\pm$ 27.33	1382.07 $\pm$ 21.06	0.63		
		<b>CB</b>	<b>1573.42 <math>\pm</math> 10.37</b>	<b>1594.52 <math>\pm</math> 12.80</b>	<b>&lt;0.01</b>		
		WB	1444.70 $\pm$ 12.98	1450.03 $\pm$ 11.55	0.34		
		AB	1663.18 $\pm$ 20.95	1673.88 $\pm$ 10.99	0.17		
TMD High <sub>5</sub> (mg HA/cm <sup>3</sup> )	TB	1661.94 $\pm$ 20.00	1675.68 $\pm$ 13.88	0.09			
	<b>CB</b>	<b>1794.53 <math>\pm</math> 19.62</b>	<b>1808.70 <math>\pm</math> 14.04</b>	<b>0.08</b>			
	<b>WB</b>	<b>1804.26 <math>\pm</math> 26.48</b>	<b>1827.53 <math>\pm</math> 12.18</b>	<b>0.02</b>			
	TB	0.42 $\pm$ 0.07	0.42 $\pm$ 0.08	0.92			
	TB	19.67 $\pm$ 2.03	21.42 $\pm$ 2.42	0.10			
	TB	2.85 $\pm$ 0.43	2.80 $\pm$ 0.44	0.79			
Morphology	Tb.Th (mm)	TB	0.19 $\pm$ 0.03	0.18 $\pm$ 0.03	0.39		
	Tb.Sp (mm)	TB	0.22 $\pm$ 0.05	0.20 $\pm$ 0.03	0.31		
	PDL Thickness ( $\mu$ m)	PDL	Mean	138.04 $\pm$ 8.25	138.78 $\pm$ 6.09	0.82	
		PDL	Max	389.41 $\pm$ 40.17	424.16 $\pm$ 47.84	0.10	
		PDL	SD	34.24 $\pm$ 6.15	36.24 $\pm$ 6.12	0.48	
	Nano-indentation	$E_b$ (GPa)	WB	Mean	15.35 $\pm$ 5.57	16.29 $\pm$ 6.00	0.51
			Var	5.155	5.535	0.065	
		H (GPa)	WB	Mean	0.61 $\pm$ 0.25	0.69 $\pm$ 0.28	0.13
			Var	0.244	0.262	0.077	
		$\eta$ (GPa·S)	WB	Mean	14787.98 $\pm$ 8414.80	16915.84 $\pm$ 9003.67	0.39
Var			7623.655	7904.601	0.348		
Creep/ $P_{max}$ (nm/mN)		WB	Mean	16.94 $\pm$ 14.34	14.3 $\pm$ 15.15	0.32	
		Var	14.048	14.625	0.296		
$\tan \delta$	WB	Mean	0.068 $\pm$ 0.029	0.065 $\pm$ 0.031	0.75		
	Var	0.025	0.023	0.073			

jaw bone. Many previous studies of jaw bone of OVX rat models focused on assessing BMD and trabecular morphology using 2D images of dual-energy X-ray absorptiometry (DXA), radiology, and histomorphometry, or low resolution images of 3D quantitative computed tomography (QCT) (Ejiri et al., 2006; Jiang et al., 2008; Johnston and Ward, 2015). These limitations of the traditional imaging tools for human patients could result in the inconsistency of the OVX induced changes of the BMD and trabecular morphology among previous studies that used small rat models (Johnston and Ward, 2015). The current study utilized high resolution 3D micro-CT that allows for investigating the regional variation of TMD parameters in addition to the

conventional BMD and trabecular morphology. In addition, the elastic, viscoelastic, and plastic nanoindentation properties directly measured at the same site using a single cycle of indentation provided more complete mechanical characteristics of bone tissue than assessing only the traditional E and H. These methodologies to assess TMD and nanoindentation parameters have been well established from the previous studies (Kim et al. 2015, 2017).

Masticatory force stimulates active bone remodeling of the alveolar bone (AB) surrounding teeth (Daegling and Hylander, 1997; Ejiri et al., 2006; Gallina et al., 2009; Naveh et al., 2012; Sebaoun et al., 2008). The active bone remodeling removes more mineralized, pre-existing bone

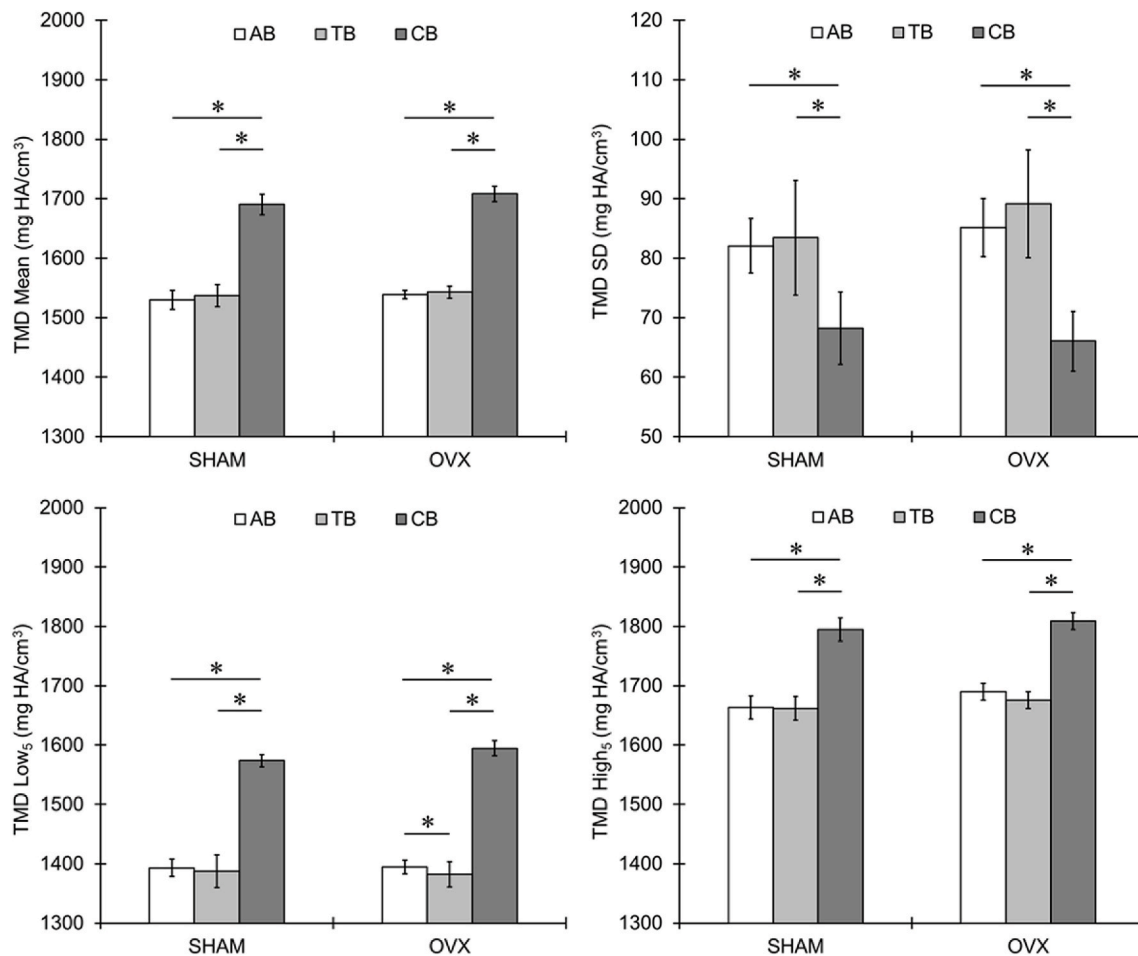


Fig. 4. Regional variations (AB, TB, CB) for tissue mineral density (TMD) (a) Mean, (b) SD, (c) Low<sub>5</sub>, and (d) High<sub>5</sub> of sham and OVX groups. \*: p < 0.04.

tissues and adds more newly formed, less mineralized bone tissues (Buie et al., 2007; Kim et al., 2012). As a result, the TMD Mean, Low<sub>5</sub>, and High<sub>5</sub> of the AB region were lower than those of the less active CB region, while SD (heterogeneity) was higher. Similarly, the trabecular bone (TB) region, which undergoes more rapid remodeling than cortical bone, had lower TMD Mean, Low<sub>5</sub> and High<sub>5</sub>, but higher SD than the CB region.

Estrogen deficiency systematically increases bone turnover by stimulating more proliferation and differentiation of osteoclasts, which results in imbalance with activities of osteoblasts in bone remodeling, leading to a net loss of bone (Eastell et al., 2016; Garnero et al., 1996; Seeman, 2013; Sims and Civitelli, 2014). However, the current results show that the mineral density, morphology and nanoindentation characteristics of jaw bone were not reduced by estrogen deficiency due to OVX. These findings suggest that, for alveolar bone, active bone turnover maintained by masticatory force can limit the deteriorating effects of estrogen deficiency. A lack of morphological changes in the periodontal ligament (PDL) by OVX also supports this suggestion. The active local remodeling at the AB continues up to a 60  $\mu$ m distance from the PDL, producing the steep gradient of TMD parameters (Fig. 2d). This result is consistent with observations of a histological study that also identified the distance of active alveolar bone turnover up to 51  $\mu$ m from the PDL (Sebaoun et al., 2008). As such, it is likely that the masticatory force triggers bone remodeling at the limited AB region. On the other hand, it remains to be investigated why trabecular bone properties were not altered by OVX. The mineral density and morphology of TB in the vertebra of the same rat were substantially reduced by OVX (Kim et al., 2012). It was suspected that masticatory loading might also influence the TB region under teeth. However, this TB region is located outside of

the limited AB region that is influenced by masticatory loading. Further studies, including assays of site-specific cell activities, are needed to elucidate these results.

The OVX group had somewhat higher values of the TMD Mean, Low<sub>5</sub>, and High<sub>5</sub> in CB than those of the sham control group. It was also found that the TMD parameters had higher values in the CB of OVX group at 280  $\mu$ m and farther distances from the PDL (Fig. 2b). As the CB region was isolated starting at 200  $\mu$ m and farther distance from the PDL, the increasing trend of TMD well describes how the CB is gradually mineralized to be higher in the OVX group than the sham group. However, the exact mechanism of how estrogen deficiency increases the TMD inside the thick cortical bone of jaw, which undergoes only limited bone remodeling, is unknown (Meta et al., 2008; Turner et al., 2001). It has been suggested that muscular and condylar reaction forces caused by mastication can stimulate bone remodeling in the entire jaw (Daegling and Hylander, 1997). However, the jaw muscular forces resulting from the impact of mastication produce levels of strain similar to those of vertebral muscles (Daegling and Hylander, 1997). As such, the muscular forces under normal daily mastication are likely required to maintain normal oral bone integrity but have no superior effects on stimulating active bone remodeling and mineralization. In addition, previous studies indicated that anabolic response to mechanical loading is limited by estrogen deficiency (Lee et al., 2003; Riggs et al., 2002). Thus, the jaw muscular forces associated with mastication cannot fully explain how estrogen deficiency increases TMD parameters in jaw while decreasing them in bone at other anatomical sites (Kim et al., 2012).

Regarding the increase in TMD of jawbone, we suggest two hypotheses based on the current and other previous studies. The first scenario may be that human and animal dental bone marrow stem cells

(BMSCs) have significantly higher osteogenic potential than orthopedic BMSCs (Aghaloo et al., 2010; Akintoye et al., 2006; Gong et al., 2017; Lee et al., 2019; Yamaza et al., 2011). The superior capability of bone mineralization by jaw BMSCs may be maintained under estrogen deficiency. The second scenario may be that osteocytes in jaw bone can produce more minerals than those in other anatomic sites. Different from human bone, rodent bone has very limited Haversian systems suggesting that a typical remodeling consisting of bone resorption and formation may not be a way to alter mineralization. Instead, osteocytes dominates in the rodent bone and can produce minerals (Dallas et al., 2013). The osteocyte is derived from bone forming cells (osteoblasts) that are differentiated from BMSCs (Cheung et al., 2016; Hadjiargyrou and O'Keefe, 2014; Lee et al., 2019). As such, osteocytes in jaw bone might also have a superior ability of mineralization. However, these hypotheses must be addressed by many further experiments that are beyond the scope of the current study.

Nanoindentation provides direct measurements of bone properties at the tissue level. It was indicated that  $E_b$  and  $H$  have strong positive correlations with TMD (Mulder et al., 2007). It was also shown that increase in mineralization likely helps viscoelastic resistance of deformation but reduces dissipating ability of loading energy (Kim et al., 2015). The current results follow the relationships between TMD and nanoindentation parameters showing trends of higher values of  $E_b$ ,  $H$ ,  $\eta$  but lower values of Creep/ $P_{max}$  and  $\tan \delta$  for the OVX group than the sham group. However, the mean values and heterogeneity of nanoindentation parameters were not significantly different between the two groups. These findings suggest that estrogen deficiency did not deteriorate mechanical integrity of jaw bone tissues.

A potential limitation of the current study may be that a period of 2 months after OVX of a 6-month-old rat is not enough to fully induce osteoporosis. However, it has been observed that rats at 6 months of age are not fast growing and have reached social maturity (Adams and Boice, 1983; Johnston and Ward, 2015), show the best osteoporotic response by OVX (Francisco et al., 2011), and demonstrate changes in bone by 2 months following OVX (Lelovas et al., 2008; Wronski et al., 1988). The most convincing evidence of osteoporosis was that the rats used in the current study were the same as those examined in a previous study showing clear symptoms of vertebral osteoporosis (Kim et al., 2012). Further studies to confirm the effects of longer post-OVX periods on the detailed characteristics of jaw bone are needed. Another limitation is that the current study did not include cell and molecular analyses. Mastication might play an important role in stimulating bone cell activities in various regions of jaw bone (Inoue et al., 2019). The underlying mechanism of mechanobiological osteogenesis in jaw bone remains to be clarified.

In conclusion, estrogen deficiency induced by OVX did not deteriorate bone characteristics including mineral density, morphology, and nanoindentation parameters in rat mandibles. These findings are consistent with previous studies that showed less sensitivity of jaw bone to OVX (Chen et al., 2018; Gallina et al., 2009; Johnston and Ward, 2015; Liu et al., 2015; Mavropoulos et al., 2007). Further, we also found that OVX increased tissue mineral density (TMD) in the cortical bone (CB) region. These results provide insight into why osteoporosis-associated jaw bone fractures are extremely rare. Further studies are needed to elucidate why the jaw bone is less influenced by postmenopausal osteoporosis. The current findings can provide baseline information to help understand the process of mineralization in association with mechanical integrity of AB altered by bisphosphonate-related osteonecrosis of the jaw (BRONJ), periodontal bone disease, and orthodontic tooth movement.

#### Author statement

Keiichiro Watanabe: Investigation, Data curation, Writing - original draft, Writing - review & editing, Visualization. Samantha Lewis: Investigation, Data curation, Writing - original draft. Xiaohan Guo:

Formal analysis, Writing - original draft. Ai Ni: Validation, Formal analysis, Writing - original draft. Beth S. Lee: Conceptualization, Writing - original draft, Writing - review & editing. Toru Deguchi: Resources, Writing - original draft, Funding acquisition. Do-Gyoon Kim: Conceptualization, Methodology, Validation, Formal analysis, Investigation, Resources, Data curation, Writing - original draft, Writing - review & editing, Visualization, Supervision, Project administration, Funding acquisition

#### Declaration of competing interest

There are no conflicts of interest for any author.

#### Acknowledgements

The project described here was supported by Grant Number AG033714 from the National Institute on Aging (Kim, D-G) and an American Association of Orthodontists Foundation Award (Kim, D-G). Its contents are solely the responsibility of the authors and do not necessarily represent the official views of the National Institute on Aging. We thank Caitlin Kiracofe for helping data collection.

#### References

- Adams, N., Boice, R., 1983. A longitudinal study of dominance in an outdoor colony of domestic rats. *J. Comp. Psychol.* 97 (1), 24–33.
- Aghaloo, T.L., Chaichanasakul, T., Bezouglaia, O., Kang, B., Franco, R., Dry, S.M., Atti, E., Tetradis, S., 2010. Osteogenic potential of mandibular vs. Long-bone marrow stromal cells. *J. Dent. Res.* 89 (11), 1293–1298.
- Akintoye, S.O., Lam, T., Shi, S., Brahim, J., Collins, M.T., Robey, P.G., 2006. Skeletal site-specific characterization of orofacial and iliac crest human bone marrow stromal cells in same individuals. *Bone* 38 (6), 758–768.
- Buenacamino, M.C., Palomo, L., Thacker, H.L., 2009. How menopause affects oral health, and what we can do about it. *Cleve. Clin. J. Med.* 76 (8), 467–475.
- Buie, H.R., Campbell, G.M., Klinck, R.J., MacNeil, J.A., Boyd, S.K., 2007. Automatic segmentation of cortical and trabecular compartments based on a dual threshold technique for in vivo micro-ct bone analysis. *Bone* 41 (4), 505–515.
- Busse, B., Hahn, M., Soltan, M., Zustin, J., Puschel, K., Duda, G.N., Amling, M., 2009. Increased calcium content and inhomogeneity of mineralization render bone toughness in osteoporosis: mineralization, morphology and biomechanics of human single trabeculae. *Bone* 45 (6), 1034–1043.
- Chen, C.H., Wang, L., Serdar Tulu, U., Arioka, M., Moghim, M.M., Salmon, B., Chen, C.T., Hoffmann, W., Gilgenbach, J., Brunski, J.B., et al., 2018. An osteopenic/osteoporotic phenotype delays alveolar bone repair. *Bone* 112, 212–219.
- Cheung, W.H., Miclau, T., Chow, S.K., Yang, F.F., Alt, V., 2016. Fracture healing in osteoporotic bone. *Injury* 47 (Suppl. 2), S21–S26.
- Daegling, D.J., Hylander, W.L., 1997. Occlusal forces and mandibular bone strain: is the primate jaw "overdesigned"? *J. Hum. Evol.* 33 (6), 705–717.
- Dallas, S.L., Prideaux, M., Bonewald, L.F., 2013. The osteocyte: an endocrine cell ... And more. *Endocr. Rev.* 34 (5), 658–690.
- Earnshaw, S.A., Keating, N., Hosking, D.J., Chilvers, C.E., Ravn, P., McClung, M., Wasnich, R.D., 1998. Tooth counts do not predict bone mineral density in early postmenopausal caucasian women. Epic study group. *Int. J. Epidemiol.* 27 (3), 479–483.
- Eastell, R., O'Neill, T.W., Hofbauer, L.C., Langdahl, B., Reid, I.R., Gold, D.T., Cummings, S.R., 2016. Postmenopausal osteoporosis. *Nat. Rev. Dis. Prim.* 2, 16069.
- Ejiri, S., Toyooka, E., Tanaka, M., Anwar, R.B., Kohno, S., 2006. Histological and histomorphometrical changes in rat alveolar bone following antagonistic tooth extraction and/or ovariectomy. *Arch. Oral Biol.* 51 (11), 941–950.
- Elders, P.J., Habets, L.L., Netelenbos, J.C., van der Linden, L.W., van der Stelt, P.F., 1992. The relation between periodontitis and systemic bone mass in women between 46 and 55 years of age. *J. Clin. Periodontol.* 19 (7), 492–496.
- Famili, P., Cauley, J., Suzuki, J.B., Weyant, R., 2005. Longitudinal study of periodontal disease and edentulism with rates of bone loss in older women. *J. Periodontol.* 76 (1), 11–15.
- Fan, Z., Rho, J.Y., 2003. Effects of viscoelasticity and time-dependent plasticity on nanoindentation measurements of human cortical bone. *J. Biomed. Mater. Res.* 67A (1), 208–214.
- Ferguson, V.L., Bushby, A.J., Boyde, A., 2003. Nanomechanical properties and mineral concentration in articular calcified cartilage and subchondral bone. *J. Anat.* 203 (2), 191–202.
- Fischer-Cripps, A.C., 2004. A simple phenomenological approach to nanoindentation creep. *Mater. Sci. Eng., A Struct. Mater. Prop. Microstruct. Process.* 385 (1–2), 74–82.
- Francisco, J.L., Yu, Y., Oliver, R.A., Walsh, W.R., 2011. Relationship between age, skeletal site, and time post-ovariectomy on bone mineral and trabecular microarchitecture in rats. *J. Orthop. Res.* 29 (2), 189–196.
- Gallina, S., Barranco-Piedra, S., Torres-Lagares, D., Baroukh, B., Llorens, A., Gutierrez-Perez, J.L., Saffar, J.L., Cherruau, M., Lesclous, P., 2009. Estrogen withdrawal

- transiently increased bone turnover without affecting the bone balance along the tooth socket in rats. *J. Periodontol.* 80 (12), 2035–2044.
- Garnero, P., Sornay-Rendu, E., Chapuy, M.C., Delmas, P.D., 1996. Increased bone turnover in late postmenopausal women is a major determinant of osteoporosis. *J. Bone Miner. Res.* 11 (3), 337–349.
- Gong, X., Yu, W., Zhao, H., Su, J., Sheng, Q., 2017. Skeletal site-specific effects of zoledronate on *in vivo* bone remodeling and *in vitro* bmscs osteogenic activity. *Sci. Rep.* 7, 36129.
- Hadjiargyrou, M., O'Keefe, R.J., 2014. The convergence of fracture repair and stem cells: interplay of genes, aging, environmental factors and disease. *J. Bone Miner. Res.* 29 (11), 2307–2322.
- Herbert, E.G., Johanns, K.E., Singleton, R.S., Pharr, G.M., 2013. On the measurement of energy dissipation using nanoindentation and the continuous stiffness measurement technique. *J. Mater. Res.* 28 (21), 3029–3042.
- Hoffler, C.E., Guo, X.E., Zysset, P.K., Goldstein, S.A., 2005. An application of nanoindentation technique to measure bone tissue lamellae properties. *J. Biomech. Eng.* 127 (7), 1046–1053.
- Huja, S.S., Beck, F.M., Thurman, D.T., 2006. Indentation properties of young and old osteons. *Calcif. Tissue Int.* 78, 392–397. Journal Article.
- Huja, S.S., Fernandez, S.A., Hill, K.J., Gulati, P., 2007. Indentation modulus of the alveolar process in dogs. *J. Dent. Res.* 86 (3), 237–241.
- Inoue, M., Ono, T., Kameo, Y., Sasaki, F., Ono, T., Adachi, T., Nakashima, T., 2019. Forceful mastication activates osteocytes and builds a stout jawbone. *Sci. Rep.* 9 (1), 4404.
- Jiang, G.Z., Matsumoto, H., Hori, M., Gunji, A., Hakozi, K., Akimoto, Y., Fujii, A., 2008. Correlation among geometric, densitometric, and mechanical properties in mandible and femur of osteoporotic rats. *J. Bone Miner. Metabol.* 26 (2), 130–137.
- Johnston, B.D., Ward, W.E., 2015. The ovariectomized rat as a model for studying alveolar bone loss in postmenopausal women. *BioMed Res. Int.* 2015, 635023.
- Kaye, E.K., 2007. Bone health and oral health. *JADA (J. Am. Dent. Assoc.)* 138 (5), 616–619.
- Kim, D.G., Haghighi, A., Kwon, H.J., Coogan, J.S., Nicoletta, D.P., Johnson, T.B., Kim, H. D., Kim, N., Agnew, A.M., 2017. Sex dependent mechanical properties of the human mandibular condyle. *J. Mech. Behav. Biomed. Mater.* 71, 184–191.
- Kim, D.G., Huja, S.S., Lee, H.R., Tee, B.C., Hueni, S., 2010. Relationships of viscosity with contact hardness and modulus of bone matrix measured by nanoindentation. *J. Biomech. Eng.* 132 (2), 024502.
- Kim, D.G., Huja, S.S., Navalgund, A., D'Atri, A., Tee, B., Reeder, S., Ri Lee, H., 2013. Effect of estrogen deficiency on regional variation of a viscoelastic tissue property of bone. *J. Biomech.* 46, 110–115.
- Kim, D.G., Jeong, Y.H., Kosel, E., Agnew, A.M., McComb, D.W., Bodnyk, K., Hart, R.T., Kim, M.K., Han, S.Y., Johnston, W.M., 2015. Regional variation of bone tissue properties at the human mandibular condyle. *Bone* 77, 98–106.
- Kim, D.G., Jeong, Y.H., McMichael, B.K., Bahler, M., Bodnyk, K., Sedlar, R., Lee, B.S., 2018. Relationships of bone characteristics in myo9b deficient femurs. *J. Mech. Behav. Biomed. Mater.* 84, 99–107.
- Kim, D.G., Navalgund, A.R., Tee, B.C., Noble, G.J., Hart, R.T., Lee, H.R., 2012. Increased variability of bone tissue mineral density resulting from estrogen deficiency influences creep behavior in a rat vertebral body. *Bone* 51 (5), 868–875.
- Klemetti, E., Vainio, P., Lassila, V., Alhava, E., 1993. Trabecular bone mineral density of mandible and alveolar height in postmenopausal women. *Scand. J. Dent. Res.* 101 (3), 166–170.
- Kribbs, P.J., Chesnut, C.H.R., Ott, S.M., Kilcoyne, R.F., 1990. Relationships between mandibular and skeletal bone in a population of normal women. *J. Periodontol.* 63, 218–222.
- Lee, D.J., Kwon, J., Current, L., Yoon, K., Zalal, R., Hu, X., Xue, P., Ko, C.C., 2019. Osteogenic potential of mesenchymal stem cells from rat mandible to regenerate critical sized calvarial defect. *J. Tissue Eng.* 10, 2041731419830427.
- Lee, K., Jessop, H., Suswillo, R., Zaman, G., Lanyon, L., 2003. Bone adaptation requires oestrogen receptor- $\alpha$ . *Nature* 424, 389.
- Lelovas, P.P., Xanthos, T.T., Thoma, S.E., Lyritis, G.P., Dontas, I.A., 2008. The laboratory rat as an animal model for osteoporosis research. *Comp. Med.* 58 (5), 424–430.
- Liu, X.L., Li, C.L., Lu, W.W., Cai, W.X., Zheng, L.W., 2015. Skeletal site-specific response to ovariectomy in a rat model: change in bone density and microarchitecture. *Clin. Oral Implants Res.* 26 (4), 392–398.
- Mattson, J.S., Cerutti, D.R., Parrish, L.C., 2002. Osteoporosis: a review and its dental implications. *Comp. Cont. Educ. Dent.* 23 (11), 1001–1004, 1006, 1008 passim; quiz 1014.
- Mavropoulos, A., Kiliaridis, S., Bresin, A., Ammann, P., 2004. Effect of different masticatory functional and mechanical demands on the structural adaptation of the mandibular alveolar bone in young growing rats. *Bone* 35 (1), 191–197.
- Mavropoulos, A., Rizzoli, R., Ammann, P., 2007. Different responsiveness of alveolar and tibial bone to bone loss stimuli. *J. Bone Miner. Res.* 22 (3), 403–410.
- Meta, I.F., Fernandez, S.A., Gulati, P., Huja, S.S., 2008. Alveolar process anabolic activity in c3h/HeJ and c57Bl/6J inbred mice. *J. Periodontol.* 79 (7), 1255–1262.
- Mulder, L., Koolstra, J.H., den Toonder, J.M.J., van Eijden, T.M.G.J., 2007. Intrabuccal distribution of tissues stiffness and mineralization in developing trabecular bone. *Bone* 41, 256–265. Journal Article.
- Naitoh, M., Kurosu, Y., Inagaki, K., Katsumata, A., Noguchi, T., Ariji, E., 2007. Assessment of mandibular buccal and lingual cortical bones in postmenopausal women. *Oral Surg. Oral Med. Oral Pathol. Oral Radiol. Endod.* 104 (4), 545–550.
- Naveh, G.R., Lev-Tov Chattah, N., Zaslansky, P., Shahar, R., Weiner, S., 2012. Tooth-pdl-bone complex: response to compressive loads encountered during mastication - a review. *Arch. Oral Biol.* 57 (12), 1575–1584.
- NIH Consensus Development Panel on Osteoporosis Prevention D, Therapy, 2001. Osteoporosis prevention, diagnosis, and therapy. *JAMA, J. Am. Med. Assoc.* 285 (6), 785–795.
- Oliver, W.C., Pharr, G.M., 1992. An improved technique for determining hardness and elastic modulus using load and displacement-sensing indentation systems. *J. Mater. Res.* 7, 1564–1583. Journal Article.
- Pilgram, T.K., Hildebolt, C.F., Yokoyama-Crothers, N., Dotson, M., Cohen, S.C., Hauser, J.F., Kardaris, E., 1999. Relationships between longitudinal changes in radiographic alveolar bone height and probing depth measurements: data from postmenopausal women. *J. Periodontol.* 70 (8), 829–833.
- Riggs, B.L., Khosla, S., Melton 3rd, L.J., 2002. Sex steroids and the construction and conservation of the adult skeleton. *Endocr. Rev.* 23 (3), 279–302.
- Roy, M.E., Rho, J.Y., Tsui, T.Y., Evans, N.D., Pharr, G.M., 1999. Mechanical and morphological variation of the human lumbar vertebral cortical and trabecular bone. *J. Biomed. Mater. Res.* 44 (2), 191–197.
- Sebaoun, J.D., Kantarci, A., Turner, J.W., Carvalho, R.S., Van Dyke, T.E., Ferguson, D.J., 2008. Modeling of trabecular bone and lamina dura following selective alveolar decortication in rats. *J. Periodontol.* 79 (9), 1679–1688.
- Seeman, E., 2003. Pathogenesis of osteoporosis. *J. Appl. Physiol.* 95, 2142–2151. Journal Article.
- Seeman, E., 2013. Age- and menopause-related bone loss compromise cortical and trabecular microstructure. *J. Gerontol. Biol. Med. Sci.* 68 (10), 1218–1225.
- Sims, N.A., Civitelli, R., 2014. Cell-cell signaling: broadening our view of the basic multicellular unit. *Calcif. Tissue Int.* 94 (1), 2–3.
- Thompson, D.D., Simmons, H.A., Pirie, C.M., Ke, H.Z., 1995. Fda guidelines and animal models for osteoporosis. *Bone* 17 (4), S125–S133. Supplement.
- Turner, R.T., Maran, A., Lotinun, S., Hefferan, T., Evans, G.L., Zhang, M., Sibonga, J.D., 2001. Animal models for osteoporosis. *Rev. Endocr. Metab. Disord.* 2 (1), 117–127.
- Wronski, T.J., Cintron, M., Dann, L.M., 1988. Temporal relationship between bone loss and increased bone turnover in ovariectomized rats. *Calcif. Tissue Int.* 43 (3), 179–183.
- Yamaza, T., Ren, G., Akiyama, K., Chen, C., Shi, Y., Shi, S., 2011. Mouse mandible contains distinctive mesenchymal stem cells. *J. Dent. Res.* 90 (3), 317–324.
- Zael, R., Yeni, Y.N., Christopherson, G.T., Cody, D.D., Fyhr, D.P., 2004. Segmentation algorithm for accurate 3d representation of microcomputed tomographic images of human vertebral bodies. *Trans. Orthop. Res. Soc.* 29, 1018, 2004.